

Delft University of Technology (TU Delft)  
Faculty of Mechanical, Maritime and Materials Engineering (3ME)  
Department of BioMechanical Engineering, Section Biomaterials Technology

# **The response of SV-HFO cells to Ti6Al7Nb surfaces modified by Plasma Electrolytic Oxidation**

by

Nicole de Groot

in partial fulfilment of the requirements for the degree of  
MASTER OF SCIENCE

22<sup>nd</sup> of August 2012

Supervisor(s):

Technical:

Dr.ir. L.E. Fratila-Apachitei (TU Delft)  
Assoc. Prof. Dr.ir. J. Duszczyk (TU Delft)

Clinical:

Prof. dr. J.P.T.M. Van Leeuwen (Erasmuc MC)

## Preface

This master thesis is comprised of two different parts. In the first part the reader will find an article with the most important results obtained during the research. The second part contains the thesis report with detailed information on all the findings and the experimental work performed.

Enjoy reading,

Nicole

## Contents

Preface.....	2
Contents .....	3
PART I: Article	
PART II: Report	
List of Figures.....	6
List of Tables.....	7
Acknowledgments.....	8
Chapter 1 Introduction.....	9
1.1 Background.....	9
1.2 Osseointegration of titanium implants .....	10
1.3 Plasma Electrolytic Oxidation for surface modification of titanium implants .....	10
1.4 Research goal.....	12
Chapter 2 Materials and Methods .....	13
2.1 Preparation of metallic samples and oxidation by PEO .....	13
2.1.1 Reuse of oxidized samples .....	13
2.1.2 PEO process.....	13
2.2 Surface characterization of the oxidized samples.....	14
2.2.1 Surface morphology .....	14
2.2.2 Surface roughness .....	14
2.2.3 Surface porosity .....	16
2.2.4 Elemental composition .....	16
2.2.5 Oxide phase composition.....	16
2.2.6 Surface wettability and free energy.....	16
2.3 <i>In vitro</i> cellular response to oxidized surfaces .....	18
2.3.1 Cell pre-culturing, seeding and refreshing.....	18
2.3.2 Cellular adhesion and cytoskeletal organization .....	18
2.3.3 Cell morphology .....	19
2.3.4 Metabolic activity.....	19
2.3.5 ExtraCellular Matrix (ECM) synthesis.....	19
2.3.6 ECM mineralization .....	20
2.3.7 Statistics .....	20

Chapter 3	Results and Discussion .....	21
3.1	Synthesis of the oxide layers .....	21
3.2	Oxide surface characteristics .....	22
3.2.1	Topography .....	22
3.2.2	Surface roughness .....	23
3.2.3	Surface porosity .....	24
3.2.4	Surface chemistry .....	26
3.2.5	Surface wettability and surface free energy .....	27
3.2.6	Summary of the main surface characteristics of the different surfaces.....	29
3.3	<i>In vitro</i> response of SV-HFO to oxidized surfaces.....	30
3.3.1	Adhesion of SV-HFO cells (4-48 hours) .....	30
3.3.2	Metabolic activity of SV-HFO cells cultured on the two surfaces (1-7 days).....	35
3.3.3	Extracellular Matrix synthesis (7-21 days) .....	38
3.3.4	ECM mineralization (7-21 days) .....	42
3.3.5	Summary of the <i>in vitro</i> cellular response .....	46
Chapter 4	Conclusions.....	47
Chapter 5	Recommendations and future research .....	49
Chapter 6	References.....	50
Chapter 7	Appendix 1: Additional calculations.....	53
7.1	Surface roughness .....	53
7.2	Surface porosity.....	54
7.3	Surface Chemistry.....	56
7.4	Surface wettability and surface free energy .....	57
7.5	Metabolic activity day 1 and day 2.....	58
7.6	Metabolic activity day 5 and day 7.....	59
7.7	ECM mineralization .....	60

# The response of SV-HFO cells to Ti6Al7Nb surfaces modified by Plasma Electrolytic Oxidation

---

## Abstract

The aim of this study was to assess the response of preosteoblasts (SV-HFO), from adhesion to matrix mineralization, on Ti6Al7Nb surfaces modified by plasma electrolytic oxidation (PEO). Two different surfaces have been generated by changing the oxidation duration from 1 to 5 minutes. The resultant (PEO1 and PEO5) surfaces showed uniform porous topographies with pores mostly in the submicron range and a mixture of anatase and rutile TiO<sub>2</sub> phases. However, the average surface roughness, maximum peak-to-valley height, pore size and Ca/P ratio increased with oxidation time whereas pore density and surface porosity decreased. On the PEO1 surface SV-HFO cells attached and spread easily using the pores as anchoring sites for their extensions and showing cell-cell contact after 48 hours. The larger pores protruding from the PEO5 surface suppressed cell adhesion. Deposition of extracellular matrix started earlier on the PEO1 surface and after 21 incubation days a net-like structure well integrated with the porous surface was visible. Matrix mineralization was evidenced on both surfaces after 21 days. However, more uniform mineralized areas were observed on the PEO1 surface whereas an accelerated mineralization was noticed after 14 days on the PEO5 surface. In conclusion, by varying only one PEO process condition, significant changes occurred on the surface of Ti6Al7Nb alloy, which influenced both the early and late response of SV-HFO cells. The observed surface-induced effects indicated that surfaces produced at shorter oxidation time may be more beneficial for early osteogenesis.

*Keywords:* Ti6Al7Nb, SV-HFO, adhesion, metabolic activity, ECM mineralization

---

## 1. Introduction

Osseointegration of titanium-based implants is essential for the clinical success of cementless total joint replacements used for treatment of osteoarthritis. The increasing number of patients, including both elderly and young population, imposes higher demands for these implants which include an extended safety and biofunctionality over few decades.

The stability of these implants is ensured through osseointegration which involves growth and maintenance of bone in direct contact with the implant under loading with no interfering fibrous tissue [1]. The process is the result of complex and interrelated interactions at the bio-implant interface, which involves several cell types and which are influenced by the surface characteristics of the implant. To achieve osseointegration, rough and/or macroporous surfaces are generated by processes such as plasma spraying or fiber-mesh sintering in order to favor bone in-growth. In addition, hydroxyapatite coatings are used as osteoconductive surfaces to enable direct bone apposition on the surface of the implant [2]. More recently, titanium surfaces with

micro- and nanoscale topographies are developed in an attempt to stimulate bone formation at cellular and molecular level [3-6].

One process able to generate porous titanium surfaces in the micron/submicron scale is Plasma Electrolytic Oxidation (PEO). The protective native oxide layers are artificially thickened from nanometers up to few tens of microns and a porous, well adherent structure is developed due to the in-depth growth mechanism in the presence of sparks [7]. By adjusting the parameters during the anodic oxidation process, oxide layers with different pore size, thickness and structure may be achieved. Further, during the PEO process, species from the electrolyte can be incorporated into the thickening oxide layer. When using electrolytes that contain calcium and phosphorus species, calcium phosphates can be integrated into the oxide layers, which resemble the bone mineral (hydroxyapatite), thereby favoring osseointegration.

The biocompatibility of PEO surfaces for bone implants was evidenced *in vivo* by enhanced bone contact and higher removal torques relative to non-oxidized titanium [3-6, 8]. Further, these layers may provide new

biofunctionalities, such as antibacterial activity [9].

The effects of PEO oxides on the cellular processes involved in osseointegration are under intense research focus [10-14]. However, the results are by far not yet conclusive impeding significantly the development of optimum layers for orthopedic titanium-based devices. Reasons include the large variability in the oxidation conditions used to create the surfaces, the resultant surface characteristics, cell type used, incubation and testing conditions. As an example, Zhu et al. [10], stated that adhesion of SaOS-2 cells to PEO-treated surfaces increased with higher voltages (140 – 350V) and was independent of the type of electrolyte, while Li et al. [11] reported a decrease in the number of adhering MG63 cells when voltages exceeded 300 V. Most of the *in vitro* studies are focused on the early cell responses and on oxide layers formed on commercially pure titanium surfaces [12-14].

In this study, the *in vitro* response of preosteoblast cells to Ti6Al7Nb alloy oxidized by PEO was systematically assessed. Therefore, Simian Virus 40 – Human Fetal Osteoblasts (SV-HFO) have been used. This cell line is attractive for research because the cells do not alter after several passages, they keep their proliferative activity and they do not spontaneously transform [15]. The Ti6Al7Nb alloy is the first titanium composition specifically designed for biomedical applications and is used in orthopedic implants starting from 1985 [16].

Two different PEO surfaces have been generated by changing one PEO process parameter, i.e. oxidation duration from 1 to 5 minutes. The resultant oxides have been examined for morphology, chemical and phase composition. The *in vitro* cellular response, from adhesion to matrix mineralization, was evaluated on both oxidized surfaces over a culture period of 21 days.

## 2. Material and Methods

### 2.1 Materials

Cylindrical samples ( $\varnothing$ : 21 mm, 7.5 mm thickness) were machined from bars of

Ti6Al7Nb. The discs were successively ground with 320, 800 and 1200 grit paper, followed by thorough cleaning in 99% acetone, 96% ethanol and deionized water in an ultrasonic bath.

### 2.2 PEO process

PEO was carried out in an aqueous solution of 0.02 M calcium acetate (CaAc) and 0.15 M calcium glycerophosphate (CaGly), under galvanostatic conditions using a current density of 20 A dm<sup>-2</sup> for 1 (PEO1) or 5 (PEO5) minutes. During the process, the electrolyte was stirred at 500 r.p.m with a magnetic stirrer and cooled by an external bath to 10 °C  $\pm$  1 °C. The samples were made anode in the electrolytic cell and a cylindrical steel cathode was used as counter electrode. The current and voltage transients were recorded during the process at 1 s intervals by a National Instruments SCXI data acquisition system.

After oxidation, the samples were rinsed under running tap water, followed by ultrasonic cleaning in 70% ethanol, rinsing in deionized water and ultrasonic cleaning in deionized water. Finally, the samples were dried and sterilized for 1 h at 110 °C using a Nabertherm oven.

### 2.3 Surface characterization after oxidation

#### 2.3.1 Surface topography

The topography of the specimens was investigated by Scanning Electron Microscopy (SEM) on a JEOL JSM-6500F microscope, using an accelerating voltage of 10 kV and a working distance between 8 and 10 mm. Before imaging the samples were coated with a uniform carbon layer using an Auto Carbon Coater type JEC-530.

#### 2.3.2 Surface roughness

The surface roughness of the oxidized specimens was determined by Micro Surface Profilometry (MSP), using a SURTRONIC3+ Surface Texture meter. Triplicates for each surface were analyzed and three parameters evaluated: average roughness (Ra), maximum peak-to-valley height (Ry) and mean spacing between the profile peaks (Sm).

### 2.3.3 Surface porosity

The surface porosity was evaluated based on SEM images acquired at 2,000x magnification for PEO1 and 1,000x for PEO5 surfaces. The SEM images were uploaded in Adobe Photoshop CS 5 and the open pores were identified using the software. For each oxidized surface three images were analyzed based on which pore size distribution, pore density and surface porosity were determined.

### 2.3.4 Elemental composition

The elemental composition of the samples was estimated by Energy Dispersive Spectroscopy (EDS) in combination with SEM. Using the Noran System Six (NSS) software, the elemental composition was determined from SEM images taken at a magnification of 3,000x. Triplicates of the oxidized surfaces were analyzed by measuring the composition at 6 different locations on each sample.

### 2.3.5 Oxide phase composition

The formation of crystalline oxide phases was evaluated by X-Ray Diffraction analysis (XRD) and compared to the non-oxidized surface. The measurements were carried out on a Bruker-AAXS type DX Advance Series 2 diffractometer using Co K $\alpha$  radiation and a 2 $\theta$  angle ranging from 20 to 120 degrees.

## 2.4 In vitro response of SV-HFO cells

### 2.4.1 Cell seeding

The SV-HFO cells were pre-cultured in  $\alpha$ -Minimum Essential Medium ( $\alpha$ MEM) without phenol red, supplemented with 20 mM HEPES, 2% streptomycin/penicillin, 1.8 mM CaCl<sub>2</sub> and 10% heat-inactivated Fetal Calve Serum (HT-FCS) with pH 7.5, at 37 °C and 5% CO<sub>2</sub> in a humidified atmosphere for one week. Prior to seeding, the oxidized titanium samples were placed in 12-wells culture plates (Costar, Sigma Aldrich) and  $\alpha$ MEM without phenol red, supplemented with 20 mM HEPES, 2% Streptomycin/ Penicillin, 1.8 mM CaCl<sub>2</sub> and 2% Charcoal-Treated Fetal Calve Serum (CT-FCS) was added. This medium was used for the refreshments as well.

The cells (35,000 cells per well) were inoculated onto the oxidized samples or on

the plastic of the well plate (positive control). Negative controls included only the culture medium with the titanium discs. The culture medium was refreshed every 2 days. To trigger differentiation of the SV-HFO cells, the culture medium was supplemented with osteogenic factors: 1 $\mu$ M dexamethasone (DEX) and 10 mM  $\beta$ -glycerophosphate, starting at day 2. Culturing time ranged from 4 hours to 21 days depending on the specific cellular function assessed. For all experiments triplicates have been used and each experiment was repeated at least twice.

### 2.4.2 Cell adhesion and cytoskeletal organization

After 4h, 24h, 2, 5 and 7 days of incubation, the medium was removed from the samples and they were washed with Phosphate Buffered Saline (PBS, 1X solution). The cells were fixed using 4% paraformaldehyde, washed three times with PBS and permeabilized by incubation with PBS containing 0.15% Triton X-100. The actin filaments were stained with a 1:100 dilution of Phalloidin-Rhodamine in PBS containing 1% Bovine Serum Albumin (BSA). Three consecutive washes with PBS were followed by dehydration with ethanol: 70 % and 100% ethanol. The cell nuclei were stained with 1:50000 solution DAPI in PBS after which the cells were left to air dry.

Examination by fluorescence microscopy (FM) was performed at a 10 x magnification by imaging the stained nuclei and actin filaments. These images were analyzed by Cell Profiler Software to determine the number of nuclei.

### 2.4.3 Cell morphology

The investigations of cell morphology and cell-surface interface during 21 incubation days were performed by SEM. Prior to imaging the samples were washed with PBS three times, followed by fixation with 4% formaldehyde and 2% glutaraldehyde in 0.1 M sodium cacodylate buffer for 2 hours at 4 °C. Thereafter, the cells were washed three times with 0.1 M cacodylate buffer, followed by dehydration with ethanol (50%, 70% and 100% for 1 min) and left to air dry. The samples were coated with a uniform carbon/gold layer and examined on the

JEOLJSM-6500F microscope. Magnifications ranged from 50 to 4,000x.

#### 2.4.4 Metabolic activity

The metabolic activity of the cells was determined by Alamar Blue Test (ABT) after 1, 2, 5 and 7 incubation days. Alamar Blue dye (37°C) was added to each well in an amount equal to 10% of the total well volume and further incubated for 3 hours at 37 °C. The fluorescence was measured at an excitation length of 530 nm using the Wallac 142 Victor 2 plate reader.

#### 2.4.5 ExtraCellular Matrix (ECM) synthesis and mineralization

ECM mineralization was monitored by SEM. For mineralization, two days after seeding Xylenol Orange ( $C_{31}H_{28}N_2O_{13}SNa_4$ ) was added to the refreshment medium, in a final concentration of 20  $\mu$ M. After 7, 14 and 21 days of incubation the mineralization was qualitatively assessed by fluorescent microscopy at a 10x magnification. The number of mineralized nodules was determined using Cell Profiler software on 5 images per surface. Triplicates of each surface have been used and the experiment was repeated three times.

#### 2.4.6 Statistics

Pore size values are median values  $\pm$  the standard deviation. All other values presented are the average  $\pm$  the standard deviation. Statistical analysis of the results was performed using the Student's *t*-test ( $p < 0.01$ ).

### 3. Results and Discussion

#### 3.1 Voltage transients

Typical voltage transients recorded during the PEO process are presented in Fig.1. The average end-voltage after 1 minute oxidation (PEO1) was  $153 \pm 4.29$  V and after 5 minutes (PEO5) it reached  $242 \pm 4.47$  V. The voltage transients showed two distinctive regions, based on the rate of voltage rise. In the first region, the voltage increased rapidly to  $\sim 120$  V due to formation of a dense oxide layer. In the second region of lower increase rate, visible sparking was observed indicating the growth of a porous oxide.

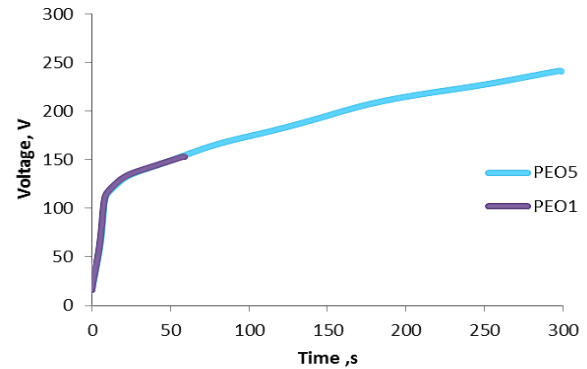


**Fig. 1:** Voltage transients for the 1 and 5 minute oxidation process ( $20 \text{ A/dm}^2$ , 0.15 M CaGly and 0.02 M CaAc).

#### 3.2 Oxide surface characteristics

##### 3.2.1 Surface topography

SEM images of the two surfaces at different magnifications are included in Fig.2. Uniform porous topographies were revealed on both surfaces with some residual grinding lines still visible on the PEO1 surface. Further, relatively small, but more numerous pores with irregular shapes were observed on the PEO1 surface whereas the PEO5 surface showed some larger pores protruding from the surface.

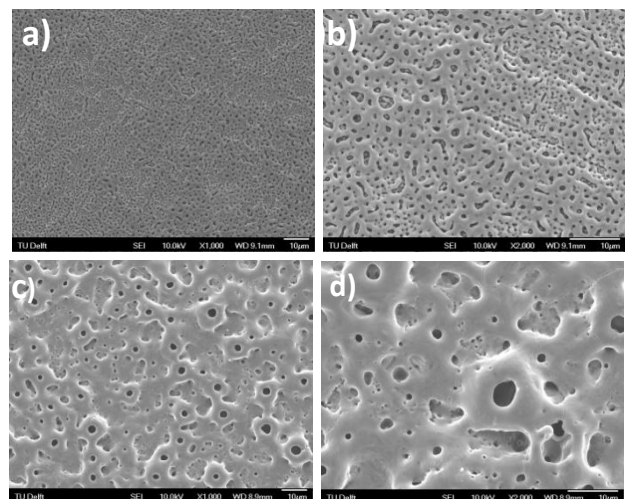


**Fig. 2:** SEM images of PEO1 (a,b) and PEO5 (c,d) surfaces at increased magnifications.

For a certain substrate and electrolyte, the morphology of the PEO oxides formed under galvanostatic conditions is influenced by the evolution of sparks on the surface and the associated processes, such as gas evolution and local heating [11, 17, 18]. Usually, very fine and rapidly moving sparks accompanied by gas evolution are generated at the onset of



porous layer growth, which become larger, less mobile and more intense with extended oxidation duration. Therefore, a fine porous surface develops into a relatively coarser structure in time with larger pores and a crater-like morphology, as observed by SEM investigations in the present study.

### 3.2.2 Surface roughness

By extending oxidation time from 1 to 5 minutes, average roughness (Ra) increased from  $0.19 \pm 0.03 \mu\text{m}$  to  $1.43 \pm 0.08 \mu\text{m}$ . In addition, the average peak-to-valley height (Ry) increased from  $1.64 \pm 0.27 \mu\text{m}$  to  $10.32 \pm 0.80 \mu\text{m}$ . These findings suggest that the PEO5 surface is relatively rough, most probably due to the presence of larger pores protruding from the surface. This topography is the result of a thicker layer formed by local growth at the breakdown sites in the presence of relatively large and more intense sparks occurring at extended oxidation times [11].

### 3.2.3 Surface porosity

Further characterization of the pores was performed using selected SEM images. The results on pore size distribution are presented in Fig.3.

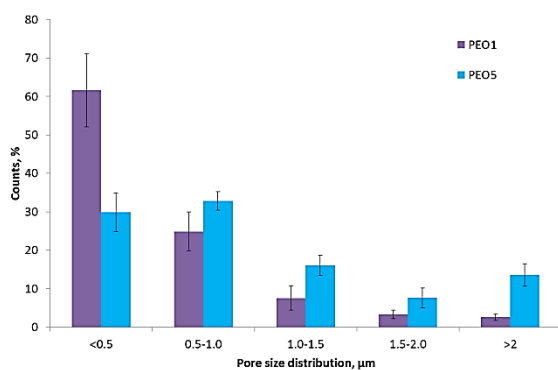


**Fig.3.** Pore size distribution for the two surfaces.

About 62% of the pores on the PEO1 surface were smaller than  $0.5 \mu\text{m}$ , while the majority of the pores on the PEO5 surface were smaller than  $1.0 \mu\text{m}$ . In addition, on the PEO5 surface more pores larger than  $1.5 \mu\text{m}$  were observed. Pore density calculations confirmed the SEM observations, indicating the presence of significantly more pores on the PEO1 surface ( $6.05 \times 10^5$ ), relative to the PEO5 surface ( $3.8 \times$

$10^4$ ). The PEO1 surface with smaller, but more numerous pores, revealed the highest surface porosity. Thus, in addition to surface roughness, the pore morphology and density changed with treatment time.

### 3.2.4 Surface chemistry

The elemental and phase composition of the PEO1 and PEO5 surfaces was assessed by SEM/EDS and XRD, respectively. Typical EDS spectra for each surface are included in Fig.4.

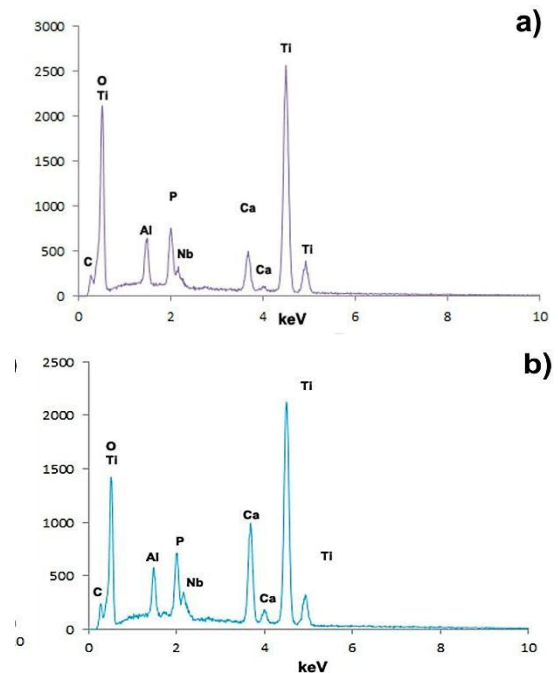


**Fig. 4:** Typical EDS spectra for (a) PEO1 and (b) PEO5 surfaces.

Next to the elements from the Ti6Al7Nb alloy, Ca and P peaks were visible on the two surfaces. Further, larger Ca and P concentrations were measured on the PEO5 surface. The Ca/P ratio increased from almost 1.0 on the PEO1 surface to about 2.0 on the PEO5 surface. These findings suggest incorporation of Ca and P species from the electrolyte during the oxidation process. The XRD analysis (see Fig.3-8 in the report) indicated formation of crystalline  $\text{TiO}_2$  phases (anatase and rutile) on both surfaces. Below sparking, P species enter the oxide layer by inward migration from the oxide/electrolyte interface, whereas Ca species, which are found mainly in the outer layer regions, suggests possible local surface deposits and/or outward migration [19]. The start of sparking

is associated with increased P and Ca incorporation and the mechanism may involve plasma and thermal processes.

As a result of changes in surface morphology and chemistry following PEO, wettability and surface free energy of PEO1 and PEO5 surfaces increased (see Table 3-3 and Fig. 3.9 in the report).

### 3.3 In vitro response of SV-HFO cells

#### 3.3.1 Adhesion

Adhesion of cells was assessed after 4, 24 and 48 hours by Fluorescence Microscopy (FM) and SEM. The main results are included in Fig.5 and Fig.6, respectively. After 4 hours of incubation (Fig.5a-c) fewer cells have been found on the oxidized surfaces than on the positive control (PC). With increasing incubation time from 4 to 24 hours (Fig.5d-f), the number of adhering cells increased on all surfaces. However, more cells were visible on the PEO1 surface than on the PEO5 surface.

Cells that adhered to the oxidized surfaces started to spread, more pronounced on the PEO1 surface. After 48 hours of incubation (Fig. 5g-i) cells on the PEO1 surface had similar morphology to those on the PC. The cells on the PEO5 surface showed a thin, small cytoskeleton and some filopodia.

SEM investigations performed after 24 and 48 hours provided additional information on surface-cell interactions. The results after 24 hours are included in Fig.6. The findings confirmed that the number of cells adhering to the PEO5 surface was lower than on the PEO1 surface. Furthermore, the high magnification images (Fig.6c-f) revealed that the cells on the PEO1 surface followed closely the topography of the oxide layer and developed protrusion that entered the pores as opposed to the cells on the PEO5 surface, which were mostly confined in the areas between the large pores and showed fewer filopodia.

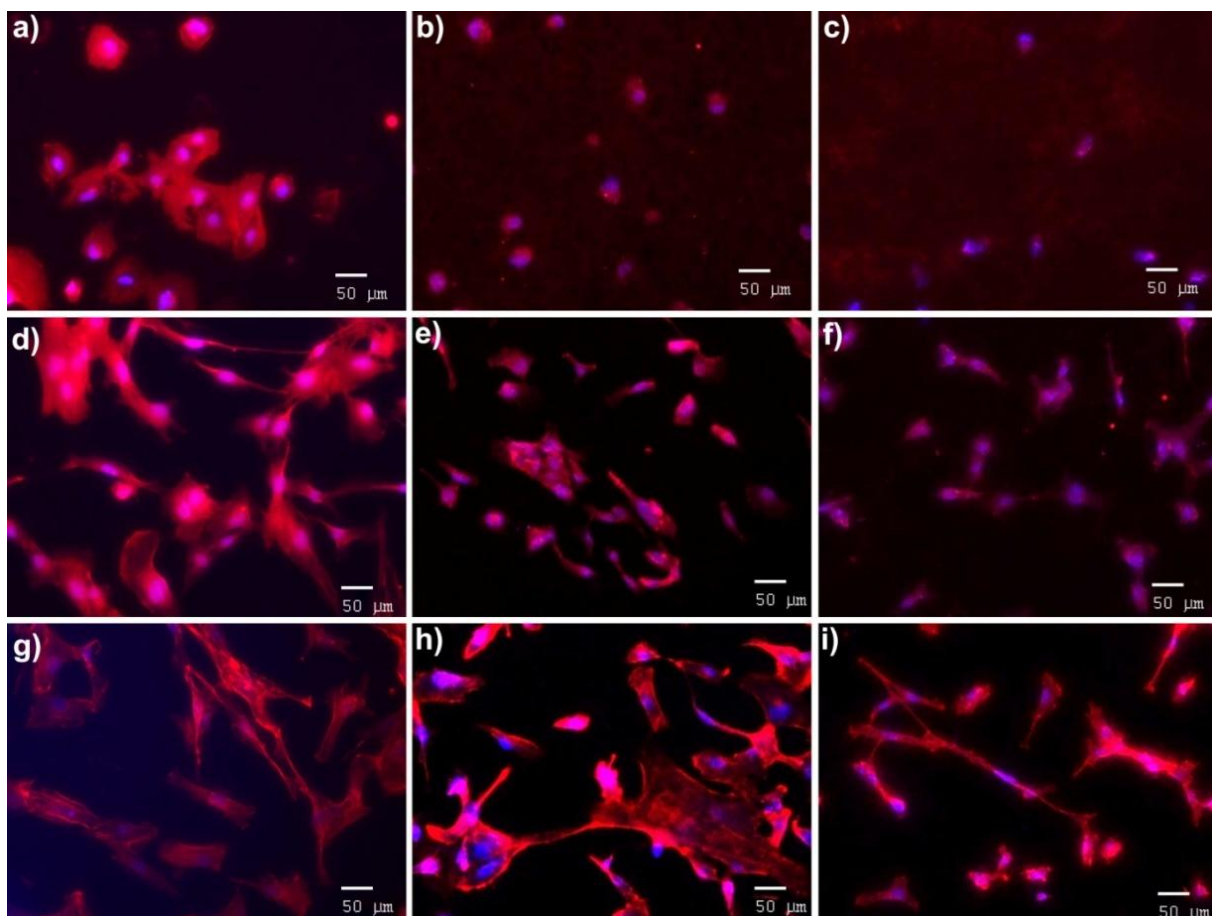


**Fig.5:** FM images of SV-HFO cells on: PC (a,d,g), PEO1(b,e,h) and PEO5(c,f,i) after 4h (a-c), 24h (d-f) and 48h (g-i) of incubation

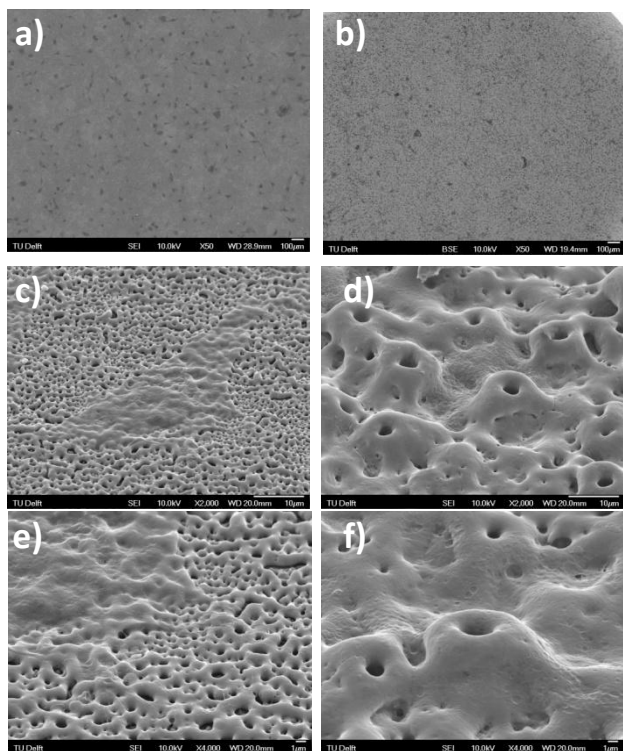


**Fig. 6:** SEM images of the SV-HFO cells after 24 hours on PEO1 (a,c,e) and PEO5 (b,d,f) surfaces.

Adhesion represents the first phase in cell-material interactions with impact on the subsequent proliferation and differentiation stages [20]. It involves specific proteins that are expressed by the cells and are influenced by the surface characteristics. It is known that osteoblasts are anchorage dependent cells, preferring rough surfaces for attachment [21]. Previous studies showed that the number of SaOS-2 cells adhering to PEO-treated titanium surfaces after 1 hour of incubation increased with surface roughness in the range 0.25-0.4  $\mu\text{m}$  [10]. However, Li et al. [11] reported a decreased number of MG63 after 3 incubation days on titanium surfaces oxidized by PEO above 300V, corresponding to surface roughness larger than 0.4  $\mu\text{m}$ . Further, Verrier et al. [22] examined the morphology of two different cell lines (hFOB and hBMSC) on anodized titanium (porous and dense surfaces with an average roughness between 0.9 – 1.2  $\mu\text{m}$ ). After 2 days of culturing both type of cells revealed a well spread morphology with long and thin pseudopodia and cell-cell contacts on the porous PEO-treated surfaces, while this morphology was only visible for the hBMSC on the dense oxidized surfaces,

suggesting a higher sensitivity of hFOB1.19 to surface morphology.

The optimum topographies of titanium anodic oxides for osteoblast-like cell adhesion is not yet established due to the different conditions of oxidation used in different studies, cell type, incubation durations and evaluation methods, all possibly affecting the adhesion results.

In the present study, after 2 days of incubation on PEO-treated Ti6Al7Nb alloy, SV-HFO cells preferred the surface showing a finer porous structure with a larger pore density and a lower average roughness ( $0.19 \pm 0.03 \mu\text{m}$ ) for adhesion. On this surface the cells could spread and migrate easily using the pores as anchorage sites for their protrusions and showing cell-cell contacts after 48 hours. Despite the higher average roughness of PEO5 surfaces ( $1.43 \pm 0.08 \mu\text{m}$ ), the organization of roughness, namely the presence of local high pores contributing to the larger  $R_y$  value (ca. 10  $\mu\text{m}$ ), suppressed cell adhesion. The larger pores protruding from the surface acted rather as obstacles for adhesion, migration and cell-surface interactions in the first 48 hours of incubation. These findings indicate that the detailed analysis of oxides surface morphology is important in understanding surface-cell interactions during the adhesion phase. This aspect is however largely neglected in literature and may be one factor contributing to the non-conclusive results so far on roughness effects.

### 3.3.2 Metabolic activity

The metabolic activity of the SV-HFO cells was measured by ABT after 1, 2, 5 and 7 days of incubation (Fig.7). The results were complemented with FM and SEM investigations (see Fig 3.15 and Fig.3.16 in the report).

The ABT results indicated an increase in the metabolic activity of the cells on all surfaces during 7 days of culturing. Further, after 2 days of incubation the rate of increase was higher. This could be due to the proliferative activity expected in this period and the addition of dexamethasone to the medium to stimulate osteogenic differentiation. The lower metabolic activity of the cells on the

PEO5 surface may be related to the lower number of cells adhered on this surface.

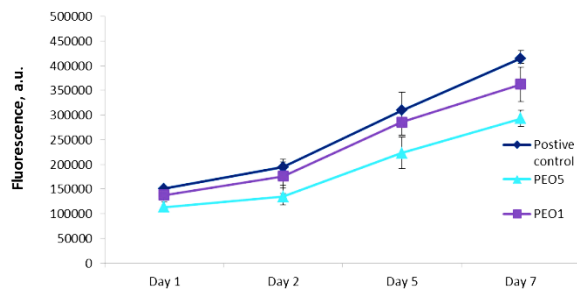


**Fig. 7:** Metabolic activity obtained with ABT for PC, PEO1 and PEO5 after 1, 2, 5 and 7 days of incubation.

Between day 2 and day 7, SV-HFO cells are expected to proliferate and start differentiation [23]. It was previously shown that an increase in the average roughness of titanium surfaces by mechanical treatments from less than 0.2  $\mu\text{m}$  to  $\sim 0.6 \mu\text{m}$ , decreased the proliferation rates of osteoblasts by almost 40% [24]. In the case of PEO surfaces, Zhu et al. [10], observed a slightly larger number of SaOS-2 cells after 4 days on the PEO surfaces with lower Ra (0.25 vs. 0.4  $\mu\text{m}$ ) and Ca/P ratio (0.4 vs. 1.0). More recently, Whiteside et al. [25], found the highest proliferation rate of primary human osteoblast after 7 days on titanium oxide layers with a roughness of 1.29  $\mu\text{m}$  and Ca/P ratio of 0.27. The proliferation rates were relatively low on the rougher (Ra=1.67  $\mu\text{m}$ ; Ca/P=0.27), but also on the smoother (Ra=0.78  $\mu\text{m}$ , Ca/P=0.14) surfaces produced in different Ca/P based electrolytes.

When rat osteoblasts have been cultured on PEO-treated TiZrSnMoNb alloy [26], a higher metabolic activity was found after 7 days on the rougher surfaces (2.3 vs. 0.7  $\mu\text{m}$ ) with a higher Ca/P ratio (2.1 vs. 1.26). These findings suggest that proliferation of osteoblast-like cells on PEO-treated surfaces may be affected by surface roughness, surface chemistry as well as cell type. More systematic research is needed to further elucidate the effect of each factor on the growth phase of osteoblast(-like) cells. In our study, SV-HFO cells showed similar rates of metabolic activity increase on the two surfaces during 7 days of incubation.

### 3.3.3 Matrix formation and mineralization

Formation and mineralization of the ECM were assessed by SEM/EDS (Figs.8-9) and Xylenol Orange (XO) staining (Figs.10-11)

After 7 days of culturing we observed the start of ECM synthesis on the PEO1 surface (Fig.8a-b), which was not yet visible on the PEO5 surface (Fig.9a-b). On the PEO1 surface the amount of ECM increased with time from day 7 to day 21 (Fig.8c-h). In addition, the morphology changed from a monolayer structure to appearance of deposits protruding from the surface and formation of net-like structures which were well integrated with the porous surface. On the PEO5 surface we observed the formation of a monolayer covering all the pores during 14 days (Fig. 9c-d) and at day 21 a thick cell layer with white deposits was visible (Fig.9e-f).

These findings indicate that both PEO surface provided a suitable support for ECM formation. However, the cells on the PEO1 surface started matrix deposition earlier than those on the PEO5 surface.

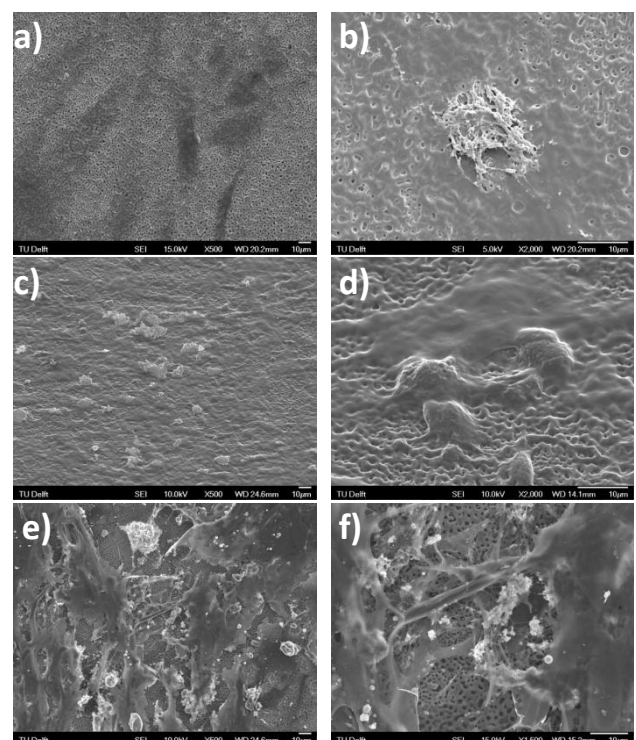


**Fig 8:** SEM images of PEO1 surface after: 7 days, (a-b), 14 days (c-d) and 21 days (e-f) of incubation.

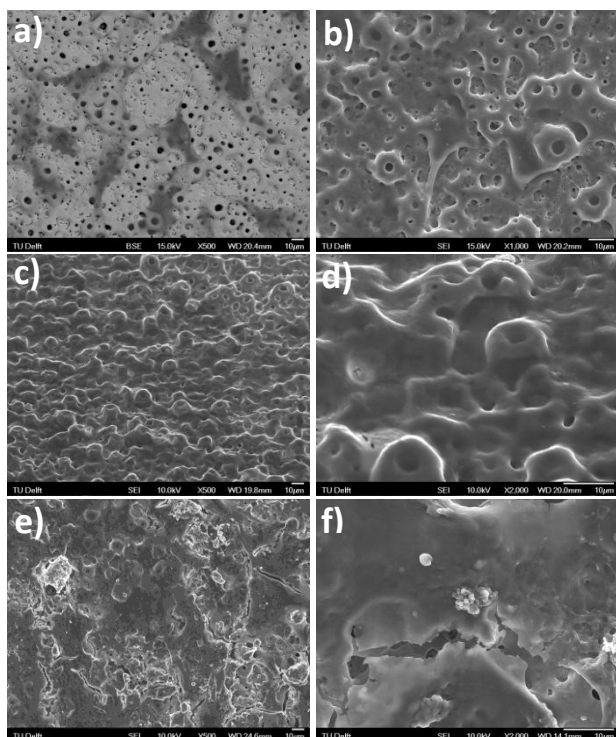


**Fig 9:** SEM images of PEO5 surface after: 7 days (a-b), 14 days (c-d) and 21 days (e-f) of incubation.

When cultured on plastic, SV-HFO cells start synthesizing their matrix between day 12 and 14 of incubation [23]. Only one reference was found on collagen synthesis by human osteoblast cells seeded on PEO surfaces [25]. The surfaces were produced on cp-titanium in four different Ca/P based electrolytes and the resultant surfaces differed significantly with regard to their morphology, structure and chemistry. The findings of this study showed that cells on the PEO surfaces produced more collagen after 28 days when compared to those on uncoated surfaces. This was due to an accelerated rate of synthesis after 14 incubation days on the PEO surfaces. Further, surfaces with the highest Ca/P ratio (0.46) having also the smallest average pore size (4  $\mu\text{m}$ ), highest pores density and highest roughness (2.28  $\mu\text{m}$ ) promoted collagen formation. These results suggest that collagen synthesis may be favored by incorporation of Ca/P species in the oxide layer. Nevertheless, the effects of the other surface characteristics on collagen synthesis cannot be excluded.

For our study, it could be hypothesized that the coarser topography of the PEO5 surface, which led to lower cell adhesion and lower cell number, delayed formation of the ECM, but

when the cell number is high enough, the higher Ca/P ratio may stimulate ECM synthesis. To prove this hypothesis, further research at longer incubation times with the PEO5 surface is required. In addition, the effect of Ca and P released from these surfaces on each cellular function need to be established and corroborated with the effects of the other surface features.

The XO results indicated that after 7 days of incubation (see Fig.3.21 in the report), very few orange dots were observed on all three surfaces, but these were not numerous enough to conclude that the surfaces started to mineralize. After 14 days of incubation (Fig. 10) an increased number of nodules was found on the three different surfaces. The trend indicated the lowest number on the PEO5 surface. In addition, EDS analysis confirmed the existence of calcium in the deposits on the PEO1 surface.

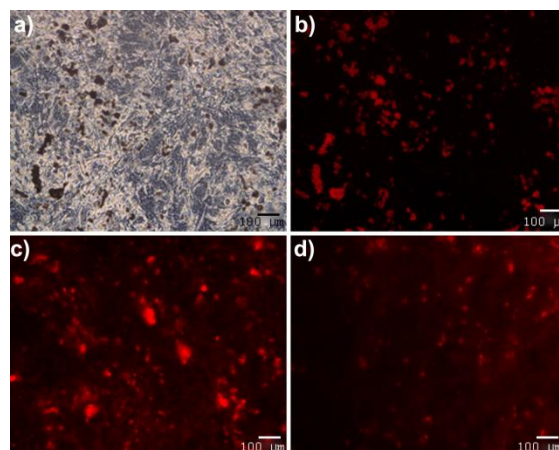


**Fig.10:** XO images at day 14 of SV-HFO on: PC (a,b), PEO1 (c) and PEO 5 (d) surfaces.

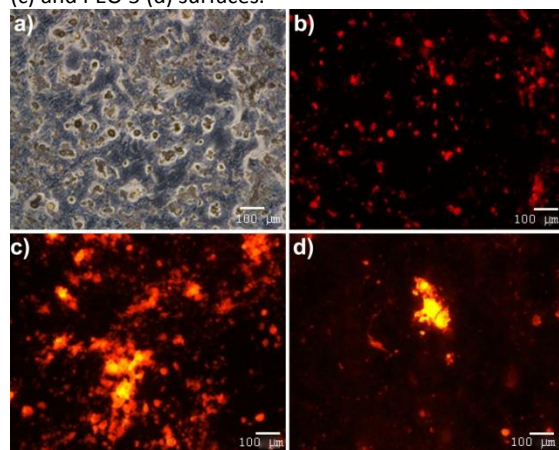


**Fig.11:** XO images at day 21 of SV-HFO on: PC (a,b), PEO1 (c) and PEO 5 (d) surfaces.

Between day 14 and 21 (Fig.11), the largest increase in the number of nodules was observed for the three surfaces. Interestingly, the rate of increase was higher on the PEO5 surface than on the PEO1 surface (Fig.12), suggesting that in this time interval matrix mineralization was faster on this surface.

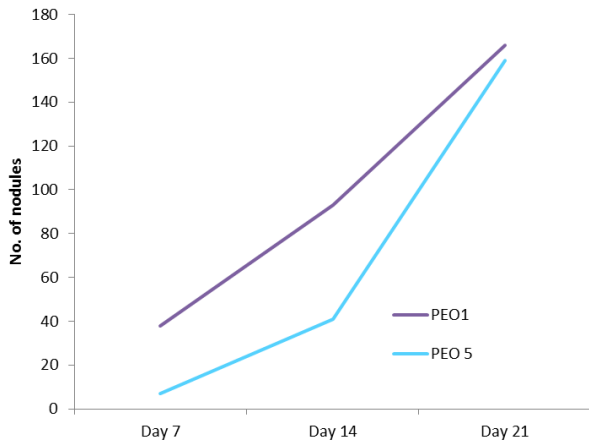


**Fig. 12.** Number of calcified nodules determined from XO images at day 7, 14 and 21.

However, the mineralized area was more uniform on the PEO1 surface, relative to the more patchy appearance on the PEO5 surface. EDS analysis of the deposits found on the two surfaces after 21 days (Fig.13) revealed high peaks of Ca.

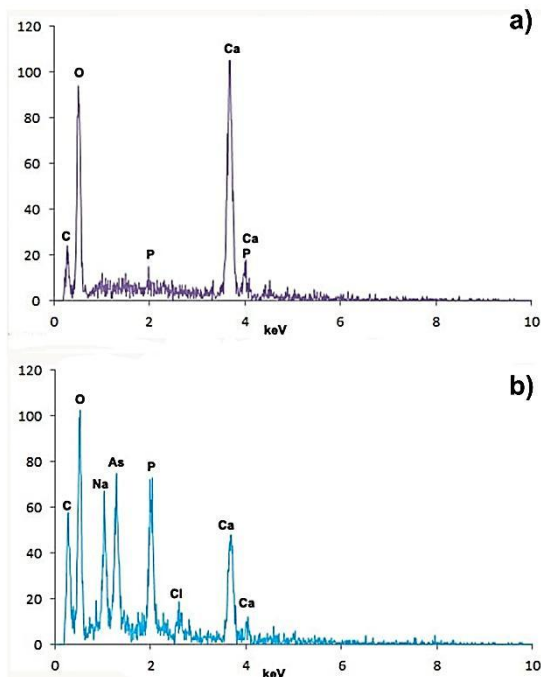


**Fig.13:** EDS spectra of (a) PEO1 and (b) PEO5 surfaces after 21 days of incubation with SV-HFO cells.

These findings indicate that SV-HFO cells cultured on these two PEO surfaces could differentiate into osteoblasts which were then able to produce and mineralize the ECM. The mineralization results show a slower matrix mineralization on the PEO5 surface up to 14 days of incubation. This could be the effect of the suppressed earlier cell adhesion on this surface, combined with the similar growth rates observed on the two surfaces which may result in more time needed for growth and differentiation of cells on this surface. Nevertheless, the enhanced mineralization rate observed after 14 days of incubation suggest a possible favorable effect of surface chemistry (higher Ca/P ratio of this surface) on mineralization. Further research is needed to delineate the effects of topography and chemistry of these PEO surfaces on the late cellular functions and to further understand the relationship between the short and long term cellular responses on a similar surface.

No results were found in literature on the effects of PEO oxide characteristics on matrix mineralization. Verrier et al. [22] compared hFOB1.19 and hBMSC cell response to three different titanium surfaces produced by vacuum plasma spraying, conventional anodizing and PEO (Ca/P electrolyte). Their findings showed enhanced mineralization on the PEO-treated surface after 10 and 15 incubation days, relative to the other two surfaces. However, the surfaces studied were very different and difficult to compare with regard to surface-induced effects. In addition, matrix mineralization was assessed by Alizarin Red staining, which in our previous trials showed interference from the calcium incorporated in the oxide layer during the PEO process.

The results of the present study showed that both early and late cellular responses have been influenced by the two surfaces. The PEO1 surface followed more closely the PC, suggesting that this surface may be more beneficial in assisting surface-cell interactions leading to osteogenesis. It is believed that further studies on the effects of Ca/P on the investigated cellular functions will enable further tailoring of PEO1 surface characteristics for orthopedic implants.

## 5. Conclusions

In this study, the *in vitro* response of SV-HFO cells to Ti6Al7Nb alloy oxidized by plasma electrolytic oxidation (PEO) was systematically assessed. Two different surfaces have been generated by changing one process parameter, i.e. oxidation duration from 1 to 5 minutes. The cellular response, from adhesion to matrix mineralization was evaluated on both oxidized surfaces and on positive controls over a culture period of 21 days.

By extending the oxidation time from 1 to 5 minutes, the average surface roughness, maximum peak-to-valley height, pore size and Ca/P ratio of the oxide layers increased, while surface porosity and pore density decreased. Both surfaces (PEO1 and PEO5) had most of the pores in the submicron range and a mixture of anatase and rutile oxide phases.

During the adhesion phase SV-HFO cells preferred the smoother surface with finer pores and higher pore density. On this surface the cells could attach and spread easily using the pores as anchorage sites for their protrusions and showing cell-cell contacts after 48 hours. The protruding pores on the PEO5 surface acted as obstacles for cell adhesion. These findings highlighted the importance of detailed morphological investigations of the PEO surfaces with respect to cellular response and showed that average roughness is not sufficient to understand the surface-cell interactions during the early adhesion phase.

Metabolic activity of the cells increased at similar rates on the two surfaces during 7 incubation days. Further, SEM analyses showed that both PEO surfaces provided a suitable substrate for extracellular matrix formation. However, the cells on the PEO1 surface started matrix deposition earlier than those on the PEO5 surface suggesting that the surface-induced effects during cell adhesion and growth on this surface may have influenced subsequent matrix formation.

After 21 days of incubation mineralization of the matrix was evidenced on both PEO surfaces by XO staining and SEM/EDS analyses of the Ca-rich deposits. Nevertheless, larger and more uniform mineralized areas were visible on the PEO1 surface, whereas an

accelerated matrix mineralization above 14 incubation days and a more patchy appearance were observed on the PEO5 surface.

The PEO surfaces generated on the Ti6Al7Nb alloy under the conditions used in this study provided positive guidance for SV-HFO cells enabling them to fulfil their functions from adhesion to matrix synthesis and mineralization. The observed surface-induced effects indicated that PEO1 surface may be more beneficial for early osteogenesis.

## 6. References

1. Dorland, W.A., Dorland, D., *Dorland's Illustrated Medical Dictionary*. Vol. 29. 2010: Elsevier Health Sciences. 2087.
2. Le Guehennec, L., Soueidan, A., Layrolle, P., Amouriq, Y., *Surface treatments of titanium dental implants for rapid osseointegration*. Dental Materials, 2007. **23**: p. 11.
3. Schlegel, P., Hayes, J.S., Frauchiger, V.M., Gasser, B., Wieling, R., Textor, M., Richards, R.G., *An in vivo evaluation of the biocompatibility of anodic plasma chemical (APC) treatment of titanium with calcium phosphate*. Journal of Biomedical Materials Research Part B: Applied Biomaterials, 2008. **90B**(1): p. 26-34.
4. Sul, Y.T., Johansson, C.B., Röser, K., Albrektsson, T., *Qualitative and quantitative observations of bone tissue reactions to anodized implants*. Biomaterials, 2002. **23**(8): p. 1809-1817.
5. Sul, Y.T., Johansson, C.B., Petronis, S., Krozer, A., Jeong, Y., Wennerberg, A., Albrektsson, T., *Characterization of the surface oxides on turned and electrochemically oxidized pure titanium implants up to dielectric breakdown: the oxide thickness, micropore configurations, surface roughness, crystal structure and chemical composition*. Biomaterials, 2002. **23**(2): p. 491-501.
6. Park, K.H., Heo, S.J., Koak, J.Y., Kim, S.K., Lee, J.B., Kim, S.H., Lim, Y.J., *Osseointegration of anodized titanium*

- implants under different current voltages: a rabbit study.* Journal of Oral Rehabilitation, 2007. **34**(7): p. 517-527.
7. Matykina, E., Montfort, F., Berkani, A., Skeldon, P., Thompson, G.E., Gough, J., *Characterization of Spark-Anodized Titanium for Biomedical Applications.* Journal of The Electrochemical Society, 2007. **154**(6): p. C279-C285.
  8. Jungner, M., Lundqvist, P., Lundgren, S., *Oxidized titanium implants (Nobel Biocare TiUnite) compared with turned titanium implants (Nobel Biocare mark III) with respect to implant failure in a group of consecutive patients treated with early functional loading and two-stage protocols).* Clinical Oral Implants Research, 2005. **16**(3): p. 308-312.
  9. Necula, B.S., Fratila-Apachitei, L.E., Zaat, S.A.J., Apachitei, I., Duszczuk, J., *In vitro antibacterial activity of porous TiO<sub>2</sub>-Ag composite layers against methicilin-resistant Staphylococcus Aureus.* Acta Biomaterialia, 2009. **5**(9): p. 3573-3580.
  10. Zhu, X., *Effects of topography and composition of titanium surface oxides on osteoblast responses.* Biomaterials, 2004. **25**(18): p. 4087-4103.
  11. Li, L.H., Kong, Y.M., Kim, H.W., Kim, Y.W., Kim, H.E., Heo, S.J., Koak, J.Y., *Improved biological performance of Ti implants due to surface modification by micro-arc oxidation.* Biomaterials, 2004. **25**(14): p. 2867-2875.
  12. Matschegewski, C., Staehlke, S., Loeffler, R., Lange, R., Chai, F., Kern, D.P., Beck, U., Nebe, B.J., *Cell architecture–cell function dependencies on titanium arrays with regular geometry.* Biomaterials, 2010. **31**(22): p. 5729-5740.
  13. Le Guehennec, L., Lopez-Heredia, M.-A., Enkel, B., Weiss, P., Amouriq, Y., Layrolle, P., *Osteoblastic cell behaviour on different titanium implant surfaces.* Acta Biomaterialia, 2008. **4**(3): p. 535-543.
  14. Takebe, J., Ito, S., Champagne, C. M., Cooper, L. F., Ishibashi, K., *Anodic oxidation and hydrothermal treatment of commercially pure titanium surfaces increases expression of bone morphogenetic protein-2 in the adherent macrophage cell line J774A.1.* Journal of Biomedical Materials Research Part A, 2007. **80A**(3): p. 711-718.
  15. Seriwatanachai, D., Krishnamra, N., Van Leeuwen, J.P.T.M., *Evidence for direct effects of prolactin on human osteoblasts: inhibition of cell growth and mineralization.* Journal of Cellular Biochemistry, 2009. **107**(4): p. 677-685.
  16. Semlitsch, M., Staub, F., Weber, H., *Titanium-Aluminium-Niobium alloy, development for biocompatible, high strength surgical implants.* Biomed Technik, 1985. **30**: p. 5.
  17. Ishizawa, H., Fujino, M., Ogino, M., *Mechanical and histological investigation of hydrothermally treated und untreated anodic titanium oxide films containing Ca and P.* Journal of Biomedical Materials Research, 1995. **29**(11): p. 1459-1468.
  18. Teh, T.H., Berkani, A., Mato, S., Skeldon, P., Thompson, G.E., Habazaki, H., Shimizu, K., *Initial stages of plasma electrolytic oxidation of titanium.* Corrosion Science, 2003. **45**: p. 2752-2768.
  19. Matykina, E., Arrabal, R., Skeldon, P., Thompson, G.E., *Transmission electron microscopy of coatings formed by plasma electrolytic oxidation of titanium.* Acta Biomaterialia, 2009. **5**(4): p. 1356-1366.
  20. Anselme, K., *Osteoblast adhesion on biomaterials (review).* Biomaterials, 2000. **21**(7): p. 667-681.
  21. Das, K., Bose, S., Bandyopadhyay, A., *Surface modifications and cell–materials interactions with anodized Ti.* Acta Biomaterialia, 2007. **3**(4): p. 573-585.
  22. Verrier, S., Peroglio, M., Voisard, C., Lechmann, B., Alini, M., *The osteogenic differentiation of human osteoprogenitor cells on Anodic-Plasma-Chemical treated Ti6Al7Nb.* Biomaterials, 2011. **32**(3): p. 672-680.



23. Eijken, H.J.M., *Human osteoblast differentiation and bone formation: growth factors, hormones and regulatory networks*. 2007, Erasmus University: Rotterdam. p. 157.
24. Linez-Bataillon, P., Monchau, F., Bigerelle, M., Hildebrand, H.F., *In vitro MCT3 osteoblast adhesion with respect to surface roughness of Ti6Al4V substrates*. *Biomoléculaire Engineering*, 2002. **19**: p. 133-141.
25. Whiteside, P., Matykina, E., Gough, J.E., Skeldon, P., Thompson, G.E., *In vitro evaluation of cell proliferation and collagen synthesis on titanium following plasma electrolytic oxidation*. *Journal of Biomedical Materials Research Part A*, 2010. **94A**(1): p. 38-46.
26. Zhao, L., Wei, Y., Li, J., Han, Y., Ye, R., Zhang Y., *Initial osteoblast functions on Ti-5Zr-3Sn-5Mo-15Nb titanium alloy surfaces modified by microarc oxidation*. *Journal of Biomedical Materials Research Part A*, 2010. **92A**(2): p. 432-440.

The background of the entire page is a grayscale scanning electron microscope (SEM) image of a porous, textured surface. The surface is characterized by a complex, interconnected network of ridges and valleys, with numerous small, circular pores or voids scattered throughout. The lighting creates strong shadows and highlights, emphasizing the three-dimensional nature of the structure.

PART II: Report

**The response of SV-HFO cells to Ti6Al7Nb  
surfaces modified by Plasma Electrolytic  
Oxidation**

**THESIS REPORT**

by

Nicole de Groot

## List of Figures

Fig. 1.1: Osseointegration. ....	10
Fig. 1.2: Typical morphologies of anodic oxide films of titanium .....	11
Fig. 2.1: PEO set-up at Biomaterials Lab, TU Delft. ....	13
Fig. 2.2: SEM set-up used for examination of PEO layers, at 3ME faculty from TU Delft.....	14
Fig. 2.3: Cartesian coordinate system used to calculate Ra .....	15
Fig. 2.4: Determination of the largest peak to valley height $R_y$ .....	15
Fig. 2.5: Determination of the mean spacing value $S_m$ . ....	15
Fig. 2.6: Drop Shape Analyzer from Kruss available at TU Delft, Biomaterials Lab. ....	17
Fig. 3.1: Non-oxidized and oxidized surfaces created by PEO. ....	21
Fig. 3.2: Voltage transients for the 1 and 5 minute oxidation process .....	21
Fig. 3.3: SEM images of PEO1 surface .....	22
Fig. 3.4: SEM images of PEO5 surface .....	23
Fig. 3.5: SEM images taken at different locations to determine porosity .....	24
Fig. 3.6: Pore size distribution of the two oxidized surfaces. ....	25
Fig. 3.7: EDS spectra for: (a) PEO1 and (b) PEO5 surface, (c) the chemical composition .....	26
Fig. 3.8: Phase composition as determined by XRD .....	27
Fig. 3.9: Surface Free Energy (SFE). ....	28
Fig. 3.10: Fluorescent images of SV-HFO cells on: PC, PEO1 and PEO5 after 4), 24 hours and 48 hours of incubation. ....	31
Fig. 3.11: Number of nuclei of SV-HFO cells after 4 hours of incubation .....	32
Fig. 3.12: SEM images of the cells after 24 hours of incubation on: PEO1 and PEO5 .....	33
Fig. 3.13: SEM images of the cells after 48 hours of incubation on PEO1 and PEO5 .....	34
Fig. 3.14: Metabolic activity obtained with ABT .....	35
Fig. 3.15: FM images after 2, 5 and 7 days of incubation .....	36
Fig. 3.16: SEM images of cells after 2, 5 and 7 days of incubation .....	37
Fig. 3.17: Sirius Red staining after: 7, 14 and 21 days .....	38
Fig. 3.18: Absorbance of Sirius Red staining after 7, 14 and 21 days .....	39
Fig. 3.20: SEM images of PEO5 surface after: 7,14 and 21 days of incubation .....	41
Fig. 3.21: Microscopic images of mineralisation by Xylenol Orange after 7 days .....	43
Fig. 3.22: Microscopic images of mineralisation by Xylenol Orange after 14 days .....	43
Fig. 3.24 EDS spectra after 14 days of ECM on PEO1 and after 21 days on PEO1 and PEO5 .	44
Fig. 3.25: Microscopic images of mineralisation by Xylenol Orange after 21 days .....	45
Fig. 3.26: Time-line of the SV-HFO cells response observed during the 21 incubation days .	46

**List of Tables**

Table 2-1: Surface tension for the wetting liquids used to determine the surface contact angles and surface free energy. .... 17

Table 3-1: Roughness values obtained by profilometry for both surfaces..... 24

Table 3-2: Porosity results for both surfaces ..... 25

Table 3-3: Contact angles and surface free energy for both PEO surfaces and the untreated surface..... 28

Table 4-1: Summary of the main surface characteristics and *in vitro* SV-HFO response to the oxidized surfaces ..... 47

## Acknowledgments

This thesis research and report would not have been possible without the help of several people. I would like to thank my supervisors in Delft: ir. B.S. Necula and Dr.ir. E.L. Fratila-Apachitei. Bogdan, thank you for showing me all the surface characteristics techniques and for getting me started in Rotterdam. Lidy, a very special thanks to you for helping me to interpret results and giving me the tools to present and report the results in the best manner.

Furthermore I would like to thank the entire Department of Internal Medicine at the Erasmus University in Rotterdam. You were great to work with and I learned a lot from discussing my results with you. A special thanks goes out to M. Koedam for preparing the pre-cultures and teaching me several assays. For all the help with the mineralization experiments, I would like to thank R. Koster. Ruben, thank you very much!

Of course I would like to thank my friends and family. They have helped me through writer's blocks, supported me through the ups and downs and gave me the feedback I required. Thank you very much.

## Chapter 1 Introduction

### 1.1 Background

With an increasingly aging population, more people are in need of implants to replace one or more of their joints. In addition, young people and athletes often have injuries that require replacement of their own joint with an implant. In the Netherlands, about 40,000 total joint arthroplasties are performed yearly [1]. The success rate of total joint replacements is approximately 80-90% after 10-20 years [2]. Causes of implant failure include implant associated infections, particle-induced osteolysis<sup>1</sup>, insufficient implant stability in the host bone due to unsuitable design and/or biomaterials, surgical procedure, implant maintenance and use [3, 4]. Other causes for premature failure of these implants are related to patients affected by osteoporosis, diabetes or obesity, due to their poor bone quality and healing ability.

Failure of an implant is often associated with limited mobility and pain. The patient needs to undergo revision surgery, which brings along its risks, especially for elderly people. Before an implant fails, fibrous tissue is formed around the implant, which replaces the strong bone tissue. Fibrous tissue does not have the strength of bone tissue and it is compressed due to micromovement of the implant, which leads to bone necrosis and results in failure [5, 6]. In the actual societal and demographic context, the costs of treating disease and problems caused by loss of bone tissue around the implant are expected to exceed US \$2 billion in the year 2030 in the United States alone [7]. To minimize the revision surgeries, the lifetime of existing implants needs to be extended and therefore intense research efforts are focused on improving implant stability in the host bone, prevention of aseptic loosening and development of implants with antibacterial surfaces.

Fixation of total joint replacements in the host bone can be achieved by two methods: using bone cements (cemented implants) and through osseointegration (cementless implants). Osseointegration represents the direct contact between bone and implant surface under loading, with no interfering fibrous tissue [8] and relies on bone growth on the surface of the implant. An example of osseointegration is depicted in Fig. 1.1, which shows a removed titanium implant that had been implanted for 4 weeks into the tibia of a rabbit [9]. The enhanced magnification (Fig. 1.1b) shows that bone has indeed grown in direct contact with the implant. The clinical performance of the cementless orthopedic implants is at least as good as that of the cemented ones and they are increasingly used, especially but not exclusively for the younger (<65) patients, since a more appropriate interface with the host bone can be achieved with these implants. To improve the stability of these implants, the bone tissue response to various surfaces (and surface finishes) needs to be investigated down to cellular and molecular level under (patho)physiological conditions. Based on the understanding of the complex interactions involved, surfaces that can stimulate early and enhanced bone formation may be developed.

---

<sup>1</sup> Osteolysis: Dissolution or degeneration of bone tissue resulting from disease

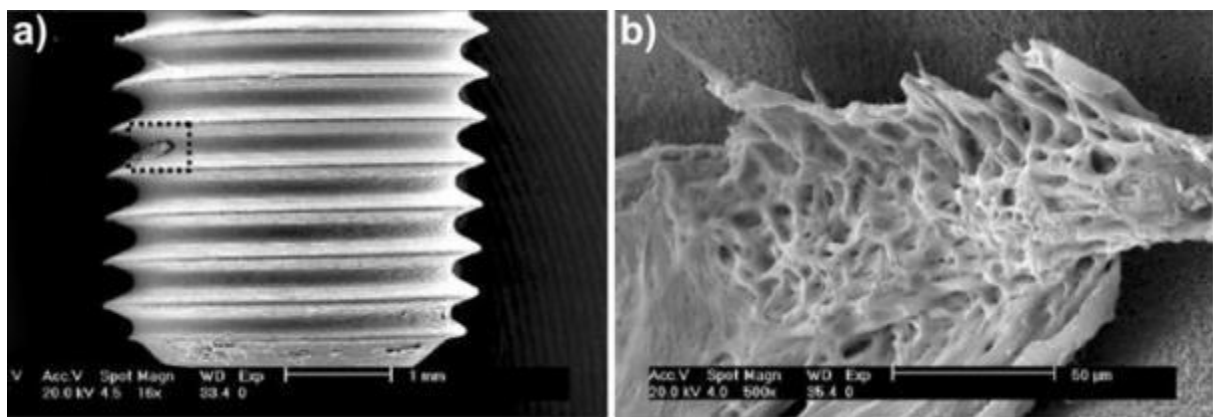


**Fig. 1.1: Osseointegration. (a) Scanning Electron Microscopy (SEM) image of PEO treated Ti implant, removed 4 weeks after implantation from rabbit tibia. (b) High magnification (500x) of the selected area in (a) [9].**

## 1.2 Osseointegration of titanium implants

For cementless implants, titanium based materials are used because, in addition to the favorable mechanical properties e.g. corrosion resistance and light weight [10-12], they have the lowest Young modulus among metallic biomaterials suitable for these devices, thereby ensuring a minimum stress shielding effect. Several different types of titanium alloys are used for dental and orthopedic implants, such as Ti6Al4V, Ti13Cr3Al1Fe and Ti6Al7Nb.

Many factors are important to achieve and maintain osseointegration of an implant, namely the surgical approach, the condition of the patient, time post-implantation, biocompatibility of the implant material, the design of the implant and the surface finish of the implant [13]. Related to the latter, rough and/or macroporous surfaces are generated by processes such as plasma spraying or fiber-mesh sintering to favour bone in-growth. In addition, hydroxyapatite<sup>2</sup> coatings are used as osteoconductive surfaces to enable direct bone apposition on the surface of the implant. More recently, surfaces with lower scale porosity and roughness are considered in an attempt to stimulate cell activity towards peri-implant osteogenesis<sup>3</sup>, which has beneficial effects on osseointegration [14-17].

## 1.3 Plasma Electrolytic Oxidation for surface modification of titanium implants

One process able to generate porous titanium surfaces in the micron or sub-micron scale is Plasma Electrolytic Oxidation (PEO). The protective native oxide layers which form on titanium surfaces when exposed to oxygen, are artificially thickened from nanometers up to few tens of microns, by applying a positive voltage/current to the titanium surface immersed in an electrolyte. As the voltage increases to certain point, sparking occurs because of dielectric breakdown of the oxide layer. Further increase of the voltage results in a newly formed oxide layer that is both porous and firmly adhered to the substrate [18]. By adjusting

<sup>2</sup> Hydroxyapatite is chemically similar to the mineral component of bone and supports bone ingrowth and osseointegration when used in orthopedic and dental applications.

<sup>3</sup> Osteogenesis is the formation and development of new bone tissue.

the parameters during the oxidation process, porous oxide layers with different pore size, thickness and structure. A typical topography of the PEO oxides is included in Fig.1.2.

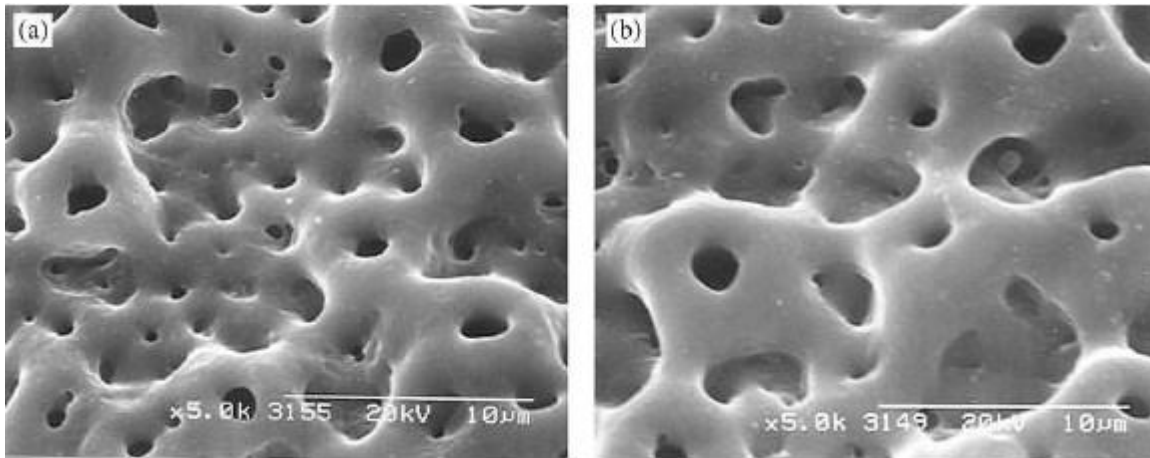


**Fig. 1.2: Typical morphologies of anodic oxide films of titanium created at  $70 \text{ A/m}^2$  and 348 V (final voltage) in: (a) 0.02 M CaGly and 0.15 M CaAc or (b) 0.03 M CaGly and 0.15 M CaAc electrolytes [19].**

During the PEO process, species from the electrolyte can be incorporated into the thickening oxide layer. When using electrolytes that contain calcium and phosphorus species, calcium phosphates can be integrated into the oxide layers, which resemble the bone mineral (hydroxyapatite) thereby favoring osseointegration [20]. This idea has already been developed in the 1960s when Harry Lench, horrified by the Vietnam veterans with amputated limbs, hypothesized that implants containing calcium and phosphorus in proportions similar to bone mineral would not be rejected by the body. He found that such a biomaterial indeed yielded a physiochemical bond with the hosting bone [21].

Several *in vivo* studies [14-17, 22] suggest titanium implants modified by PEO have potential for enhancing implant osseointegration. Park et al. [17], found that anodized implants implanted into the tibia of rabbits had higher removal torques compared to turned commercially pure (cp) titanium implants and to have higher bone-to-implant contact and bone area inside the thread, from which they concluded that the osseointegration improved after anodization. Further, these surfaces may provide additional biofunctionalities to the implants surface, such as antibacterial activity [23].

However, osseointegration involves complex interactions at the bio-implant interface down to cellular and molecular level. To date, the effects of PEO oxide characteristics on the functions of bone cells are not yet clearly established impeding significantly the development of optimum oxides for orthopedic titanium-based devices. Most of the previous studies performed on cp-titanium substrates and early cell response, including adhesion, proliferation and differentiation, with very scarce results on matrix synthesis and/or mineralization [24-26]. In a few studies, cell response is discussed in relation with anodizing voltage and/or the presence of Ca/P on the surfaces [9, 10, 19, 27, 28]. The large variability in anodizing conditions, cell type and analytical methods used makes the



correlation of the results difficult and non-conclusive. Zhu et al.[19], stated that SaOS-2 cell adhesion to PEO-treated increased with higher voltages (140 – 350V) and was independent of the type of electrolyte, while Li et al. [9] reported a decrease in the number of MG63 cells adhering when voltages exceeded 300 V.

#### 1.4 Research goal

The main goal of this MSc study was to assess the response of pre-osteoblast cells, from adhesion to matrix mineralization, on two different PEO surfaces produced on Ti6Al7Nb biomedical alloy.

Therefore, Simian Virus 40 – Human Fetal Osteoblasts (SV-HFO) have been selected. These bone forming cells are derived from fetal tissue and are infected with Simian Virus 40 (SV-40) to create an immortalized cell line. This cell line is attractive for research because the cells do not alter after several passages, they keep their proliferative activity and they do not spontaneously transform [29].

The Ti6Al7Nb alloy is the first titanium composition specifically designed for biomedical applications and is used in orthopedic implants starting from 1985 [30]. The two different PEO surfaces have been produced under similar conditions, except treatment duration. The resultant oxides have been examined for morphology, chemical and phase composition, wettability and surface free energy prior to the *in vitro* cellular studies.

No previous studies have been found on the response of preosteoblast cells (from adhesion to matrix mineralization) to PEO surfaces produced on Ti6Al7Nb alloy under different conditions.

## Chapter 2 Materials and Methods

All chemicals used were purchased from Sigma Aldrich, unless specifically mentioned.

### 2.1 Preparation of metallic samples and oxidation by PEO

Cylindrical samples (diameter 21 mm, 7.5 mm thickness) were machined from bars of Ti6Al7Nb. The discs were successively ground with 320, 800 and 1200 grit paper. After each grinding step the disc was rotated 90 degrees, so that the grinding lines were perpendicular to the previous ones. Grinding was followed by thorough cleaning in 99% acetone (10-15 min), 96% ethanol (10-15 min) and deionized water (10-15 min) in an ultrasonic bath.

#### 2.1.1 Reuse of oxidized samples

During the research, some of the samples have been reused. Therefore, the oxide layer was removed by immersion in sulfuric acid ( $\text{H}_2\text{SO}_4$ , 99 %) at 90°C for 1 – 1.5 hours in an ultrasonic bath. After the layer was dissolved, the samples were rinsed under running tap water and placed in an ultrasonic bath for 10 min, after which they were ready to be ground. The first step of grinding was done with 180 grit paper, which was also used to grind the sides of the discs.

#### 2.1.2 PEO process

The set-up used for Plasma Electrolytic Oxidation (PEO) is shown in Fig. 2.1.

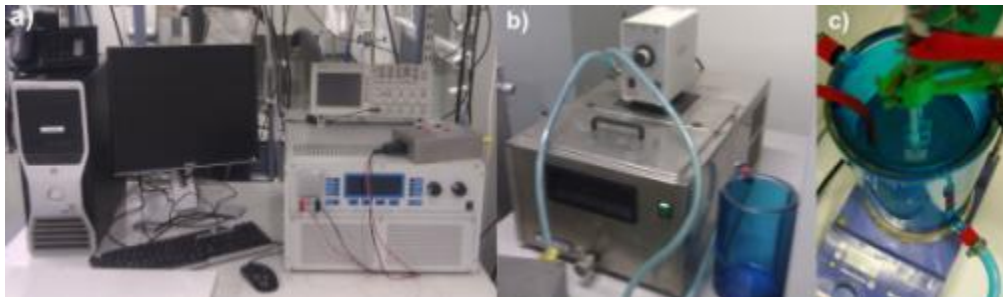


**Fig. 2.1:** PEO set-up at Biomaterials Lab, TU Delft: (a) AC Power Supply and computer; (b) cooling bath; (c) close-up of the electrochemical cell with the steel cathode and sample.

PEO of the specimens was carried out in an aqueous solution of 0.02 M calcium acetate (CaAc) and 0.15 M calcium glycerophosphate (CaGly) [31], under galvanostatic conditions using a current density of  $20 \text{ A dm}^{-2}$  for 1 or 5 min. Samples will be referred to as PEO1 (1 min) and PEO5 (5 min). The current was applied by means of an AC power supply type ACS 1500 (ET Power Systems Ltd., UK) (Fig. 2.1a). The current and voltage transients were recorded during the process at 1 s intervals by a computer interfaced with the power supply through a National Instruments SCXI data acquisition system (Fig. 2.1a).

The oxide layers were produced in the electrolyte which was cooled by an external bath to  $10 \text{ }^\circ\text{C} \pm 1 \text{ }^\circ\text{C}$  (Fig. 2.1b). During the process, the electrolyte was stirred at 500 r.p.m using a magnetic stirrer, to maintain homogeneity. The discs were screwed to an insulated metallic rod and suspended in the centre of the electrolytic cell as anode, surrounded by a cylindrical steel cathode as can be seen in Fig. 2.1c.

After oxidation, the samples were rinsed under running tap water for 5 min, followed by ultrasonic cleaning in 70% ethanol (30 s), rinsing in deionized water for 5 min and ultrasonic cleaning in deionized water (30 s). Finally, the samples were dried and sterilized for 1 h at 110 °C using a Nabertherm oven.

## 2.2 Surface characterization of the oxidized samples

The surface characteristics of the two PEO surfaces were examined for morphology, chemical composition, phase composition, surface wettability and surface free energy.

### 2.2.1 Topography

The surface morphology of the specimens was investigated by Scanning Electron Microscopy (SEM) on a JEOL JSM-6500F microscope attached to a computer, which is shown in Fig. 2.2.

Prior to imaging, the porous samples were coated with a uniform carbon layer to ensure good electrical conductivity, using an Auto Carbon Coater type JEC-530. Images at different magnification have been acquired for each sample using an accelerating voltage of 10 kV and a working distance between 8-10 mm.



Fig. 2.2: SEM set-up used for examination of PEO layers, at 3ME faculty from TU Delft.

### 2.2.2 Surface roughness

The surface roughness of the oxidized specimens was determined by Micro Surface Profilometry (MSP), using a SURTRONIC3+ Surface Texture meter (Taylor/Hobson, UK). Triplicates of each surface were analyzed. Per sample, ten measurements were performed using a cut-off length ( $L_c$ ) of 0.6 mm and an evaluation length ( $L_n$ ) of 4 mm.

The cut-off length ( $L_c$ ) is the length of the reference line used for identifying the irregularities characterizing the surface. The evaluation length ( $L_n$ ) is the length over which the values of the surface parameters are assessed.

The following roughness measurements were recorded: average roughness ( $R_a$ ), the maximum peak-to-valley height ( $R_y$ ) and mean spacing of profile irregularities ( $S_m$ ).

The average roughness,  $R_a$ , is the arithmetic mean of the departures of the profile from the mean line. The mean line is laid on a Cartesian coordinate system as shown in Fig. 2.3, in which the x-axis is the mean line and the y-axis the magnification.  $R_a$  is the arithmetic mean of the departures of the profile from the mean line (Eq. 1).

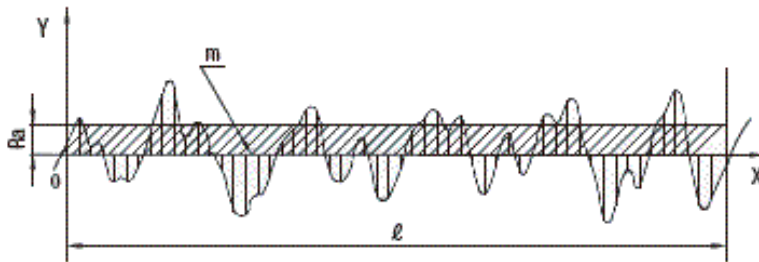


Fig. 2.3: Cartesian coordinate system used to calculate  $R_a$

$$R_a = \frac{1}{L} \int_0^L |y(x)| dx \quad \text{Eq. 1}$$

Within each cut-off length the largest peak to valley heights ( $R_{ti}$ ) are determined as depicted in Fig. 2.4. The largest of these values is the  $R_y$  value.

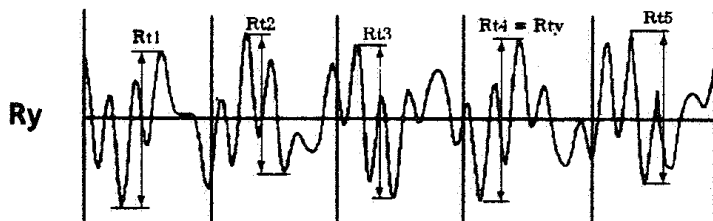


Fig. 2.4: Determination of the largest peak to valley height  $R_y$  [32].

The mean spacing between profile peaks at the mean line ( $S_m$ ) is measured over the assessment length. Fig. 2.5 shows a measured profile and the location of the profile peaks.



Fig. 2.5: Determination of the mean spacing value  $S_m$ .

As can be observed in Fig. 2.5, the distance between each profile peak is numbered and measured.  $S_m$  is the average distance between the measured peaks and is calculated using Eq. 2.

$$Sm = \frac{1}{n} \sum_{i=1}^{i=n} S_i = \frac{(S_1 + S_2 + S_3 + \dots + S_n)}{n} \quad \text{Eq. 2}$$

### 2.2.3 Surface porosity

The surface porosity was evaluated based on SEM images acquired at 2,000x magnification for PEO1 and 1,000x for PEO5 surfaces. The SEM images were uploaded in Adobe Photoshop CS 5 and the open pores were identified using the software. For each oxidized surface three images were analyzed and the values presented are the average with standard deviation. The number of pores used for the analysis was more than 5,000 for the PEO1 surface and more than 1,300 for the PEO5 surface.

Thereafter, pore size, size distribution, pore area, pore density and surface porosity were determined. The pore size was based on the largest length of the pores. The surface porosity was calculated as the ratio between the pore area and image area (Eq. 3) and expressed in %.

$$\text{porosity} = \frac{\text{total area occupied by pores}}{\text{total area of image}} \times 100\% \quad \text{Eq. 3}$$

The pore density was calculated by dividing the total number of pores by the total area of the image (Eq. 4) and expressed in pores/mm<sup>2</sup>.

$$\text{pore density} = \frac{\text{no. of pores}}{\text{total area of image}} \quad \text{Eq. 4}$$

### 2.2.4 Elemental composition

In order to estimate the surface chemistry including the species incorporated from the electrolyte in the porous surface, the elemental composition of the surfaces was estimated by Energy Dispersive Spectroscopy (EDS) in combination with SEM. Using the Noran System Six (NSS) software, the elemental composition was determined from SEM images taken at a magnification of 3,000x. Triplicates for each oxidized surface were analyzed by measuring the composition at 6 different locations on each sample.

### 2.2.5 Oxide phase composition

The formation of crystalline oxide phases was evaluated by X-Ray Diffraction analysis (XRD). The measurement was carried out on a Bruker-AAXS type DX Advance Series 2 diffractometer using Co K $\alpha$  radiation and a 2 $\theta$  angle ranging from 20 to 120 degrees.

### 2.2.6 Surface wettability and free energy

Using the sessile drop technique on a DSA 100 Drop Shape Analyzer (Kruss, Germany), shown in Fig. 2.6, dynamic contact angles were measured, using two different liquids, namely pure water and diiodomethane.

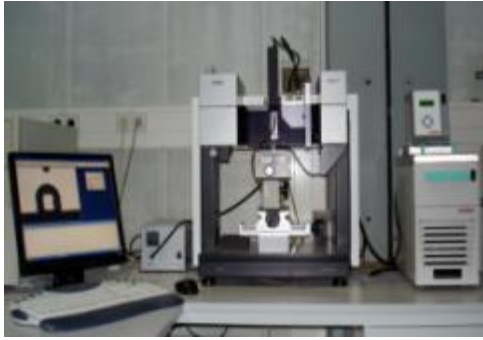


Fig. 2.6: Drop Shape Analyzer from Kruss available at TU Delft, Biomaterials Lab.

Triplicates of the oxidized and non-oxidized surfaces were analyzed with each liquid and three measurements have been performed on each surface.

From the contact angles, the surface free energy was calculated according to the Fowkes theory, which involves the equations presented below.

$$\sigma_s^D = \frac{\sigma_L \times (1 + \cos(\theta))^2}{4} \quad \text{Eq. 5}$$

$$\sqrt{\sigma_L^D} \times \sqrt{\sigma_s^D} + \sqrt{\sigma_L^P} \times \sqrt{\sigma_s^P} = \frac{\sigma_L (1 + \cos(\theta))}{2} \quad \text{Eq. 6}$$

$\sigma_L$  = overall surface tension of liquid, mN/m

$\sigma_s$  = overall surface energy of solid, mN/m

<sup>D</sup>: dispersive component

<sup>P</sup>: polar component

For both liquids the overall surface tension ( $\sigma_L$ ), the polar ( $\sigma_L^P$ ) and dispersive ( $\sigma_L^D$ ) components are known (Table 2-1).

Table 2-1: Surface tension for the wetting liquids used to determine the surface contact angles and surface free energy.

Liquid	$\sigma_L$ , mN/m	$\sigma_L^D$ , mN/m	$\sigma_L^P$ , mN/m
Diiodomethane	50.8	50.8	0
Ultra Pure Water	72.8	21.8	51

The values presented in Table 2-1 for diiodomethane, together with the measured contact angle, were used in Eq. 5 to determine the dispersive component of the surface energy. In Eq. 6 the given values for water and the measured contact angle were filled in to calculate the polar component of surface energy. Adding the polar and dispersive component resulted in the surface free energy.

### 2.3 *In vitro* response of SV-HFO cells to oxidized surfaces

In this study Simian Virus 40 - Human Fetal Osteoblasts (SV-HFO) cells have been used. These cells differentiate following addition of dexamethasone to the medium and in a period of ca. three weeks, they are able to produce and mineralize the extracellular matrix [33].

#### 2.3.1 Cell pre-culturing, seeding and refreshing

The SV-HFO cells were pre-cultured in  $\alpha$ -Minimum Essential Medium ( $\alpha$ MEM) without phenol red, supplemented with 20 mM HEPES, 2% streptomycin/penicillin, 1.8 mM  $\text{CaCl}_2$  and 10% heat-inactivated Fetal Calve Serum (HT-FCS) with pH 7.5, at 37 °C and 5%  $\text{CO}_2$  in a humidified atmosphere for one week. After pre-culturing, the cells were washed with Dulbecco's Phosphate-Buffered Saline (DPBS), detached with trypsin and counted with a haemocytometer.

Prior to seeding, the oxidized titanium samples were placed in 12-wells culture plates (Costar, Sigma Aldrich) and 750  $\mu\text{L}$  of  $\alpha$ MEM without phenol red, supplemented with 20 mM HEPES, 2% Streptomycin/ Penicillin, 1.8 mM  $\text{CaCl}_2$  and 2% Charcoal-Treated Fetal Calve Serum (CT-FCS) was added. This medium was used for the refreshments as well.

The cells in 100  $\mu\text{L}$  volume (yielding a density of 35,000 cells in 850  $\mu\text{L}$ ), were seeded onto the oxidized samples in the 12-well plate and in the well plates without discs (positive control). Depending on the type of experiment, negative controls were included which comprised of culture medium with the titanium discs.

The culture medium was refreshed every 2 days. To trigger differentiation of the SV-HFO cells, the culture medium was supplemented with osteogenic factors: 1  $\mu\text{M}$  dexamethasone (DEX) and 10 mM  $\beta$ -glycerophosphate, starting at day 2.

Culturing time ranged from 4 hours to 21 days depending on the specific cellular function assessed. For all experiments triplicates have been used and each experiment was repeated at least twice.

#### 2.3.2 Cell adhesion and cytoskeletal organization

By fluorescently staining the nuclei and actin filaments of the SV-HFO cells, the cellular adhesion and cytoskeletal organization were assessed on the PEO surfaces and the positive controls.

After 4 hours, 24 hours, 2, 5 and 7 days of incubation, the medium was removed from the samples and they were washed with Phosphate Buffered Saline (PBS). The cells were fixed using 4% paraformaldehyde (15 min, RT), washed three times with PBS and permeabilized by incubation with PBS containing 0.15% Triton X-100 (10 min, RT). The actin filaments were stained with a 1:100 dilution of Phalloidin-Rhodamine in PBS containing 1% Bovine Serum Albumin (BSA) (20 min, RT). Three consecutive washes with PBS were followed by dehydration with ethanol: 70 % ethanol (1 min, RT,) and 100% ethanol (1 min, RT). The cell nuclei were stained with 1:50000 solution DAPI in PBS (2 min, RT), after which the cells were left to air dry.

Examination by fluorescence microscopy was performed at 10x magnification by taking 24 images of the stained nuclei on each surface and 24 images of the actin filaments at the

same location, which are black-and-white images. Multichannel images showing both nuclei (blue) and actin filaments (red) in one color picture were taken randomly on the surfaces at 10x and 20x magnifications. The black-and-white images were analyzed by Cell Profiler Software to determine the number of nuclei and the surface area covered by the cells relative to the surface area of the titanium disc.

### 2.3.3 Cell morphology

The evaluation of cell morphology and cell-surface interface during 21 incubation days was assessed by SEM at low and high magnifications. Prior to imaging, the samples were washed with PBS three times, followed by fixation with 4% formaldehyde and 2% glutaraldehyde in 0.1 M sodium cacodylate buffer for 2 hours at 4 °C. Thereafter, the cells were washed three times with 0.1 M cacodylate buffer, followed by dehydration with ethanol (50%, 70% and 100% for 1 min) and left to air dry. The samples were coated with a uniform carbon layer (Auto Carbon Coater type JEC-530) or with a uniform gold layer and examined on the JEOLJSM-6500F microscope (Fig. 2.2). Magnifications ranged from 50 to 4,000x.

### 2.3.4 Metabolic activity

The metabolic activity of the cells was determined by Alamar Blue Test (ABT) after 1, 2, 5 and 7 incubation days. ABT is used to indicate the metabolic active cells based on the reducing environment these cells create. The reducing environment of the cells is measured through the conversion of resazurin (oxidised) to resorufin (reduced). Metabolically active cells perform this redox reaction, which results in colorimetric changes: resazurin is blue and resofurin is red. By measuring the fluorescence, the metabolic activity of the cells is determined.

For the ABT test, Alamar Blue dye (37°C) was added to each well in an amount equal to 10% of the total well volume and further incubated for 3 hours at 37 °C. Thereafter, the medium was moved to another 12-well plate to stop the above mentioned redox reaction.

Aliquots of 150 µL of the stained medium from each sample were placed in a 96 well plate (Costar, flat bottomed) and the fluorescence was measured at an excitation length of 530 nm using the Wallac 142 Victor 2 (Perkin-Elmer, Wellesley, MA) plate reader. Triplicates for each surface and positive controls were included and the experiment was repeated three times.

### 2.3.5 ExtraCellular Matrix (ECM) synthesis

ECM synthesis was observed in time by SEM imaging and by staining the collagen in the ECM. The SEM protocol has been described in 2.3.3. After the cells have started to differentiate, they produce the extracellular matrix (ECM), which is comprised of different types of collagen and non-collagenous proteins. The synthesis of the extracellular matrix can be visualized by staining the collagen (type I and III) with Sirius Red.

After 7, 14 and 21 days of incubation the medium was removed and the cells were washed with PBS, after which they were fixed with 10% formalin (30 min, RT). The cells were thereafter washed with PBS and with tap water. 1 mL of 0.1% Sirius Red solution was added



to each well and the plate(s) were shaken mildly for 1 hour. After 1 hour, the discs were removed from the culture plate and were washed with 0.01 M hydrochloric acid (HCl) until the solution was clear. The same was done for the positive controls that remained in the plate. Photographic images were taken of the staining at this point.

The discs were placed into a new well-plate and 850  $\mu\text{L}$  of 0.1M NaOH was added to each well in this new plate and to the positive controls in the other plate. The plates were shaken more vigorously for 1 hour at RT, after which 100  $\mu\text{L}$  of liquid from each sample was pipetted into a 96 wells ELISA plate. The absorbance was measured at 531 nm using the Wallac 142 Victor 2 (Perkin-Elmer, Wellesley, MA) plate reader.

Negative controls (oxidized surfaces without cells) have been included. Triplicates have been used for each surface and time point.

### 2.3.6 ECM mineralization

Xylenol Orange ( $\text{C}_{31}\text{H}_{28}\text{N}_2\text{O}_{13}\text{SNa}_4$ ) is a calcium-chelating fluorochrome that labels newly calcified tissues, which can be visualised and analysed by fluorescence microscopy to determine the amount of mineralisation of the ECM.

Two days after seeding and during each medium refreshment, 1  $\mu\text{L}$  Xylenol Orange (XO) was added per mL medium, yielding a final concentration of 20  $\mu\text{M}$ . After 7, 14 and 21 days of incubation the mineralization was qualitatively assessed by fluorescent microscopy at a 10x magnification. The number of mineralized nodules and the area covered by them was estimated using Cell Profiler software on five images per surface.

Triplicates of each surface have been used and the experiment was repeated three times.

### 2.3.7 Statistics

All values presented are the average  $\pm$  the standard deviation, except for the pore size where the median value  $\pm$  the standard deviation is presented. Statistical analysis of the results was performed using the Student's *t*-test ( $p < 0.01$ ).

## Chapter 3 Results and Discussion

### 3.1 Synthesis of the oxide layers

The PEO process was conducted under galvanostatic conditions (constant current density  $20 \text{ A/dm}^2$ ) for 1 and 5 minutes (samples denoted PEO1 and PEO5, respectively). In Fig. 3.1 the non-oxidized and both oxidized surfaces are shown. The non-oxidized surface displayed some grinding lines on the shining surface, while the oxidized surfaces did not, having instead a mat-grey color. The PEO1 surface had a darker grey color compared to PEO5 surface, indicating that the PEO5 surface had a thicker oxide layer with an increased content of calcium [31].

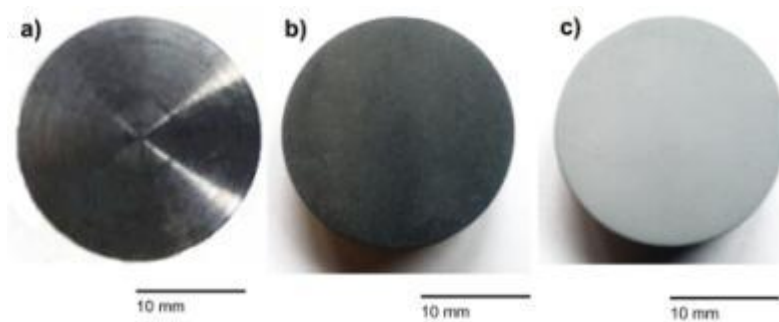


Fig. 3.1: Non-oxidized and oxidized surfaces created by PEO. (a) Ti6Al7Nb, (b) PEO1 and (c) PEO5.

An average of the voltage transients recorded during the PEO process is presented in Fig.3.2. Both lines are the average of 120 surfaces created by PEO. The average end-voltage for the PEO1 samples was  $153 \pm 4.29 \text{ V}$  and for the PEO5 samples the end-voltage reached  $242 \pm 4.47 \text{ V}$ . The PEO response was highly reproducible and no effects of the reuse procedure (acid cleaning) were observed on the voltage transients.

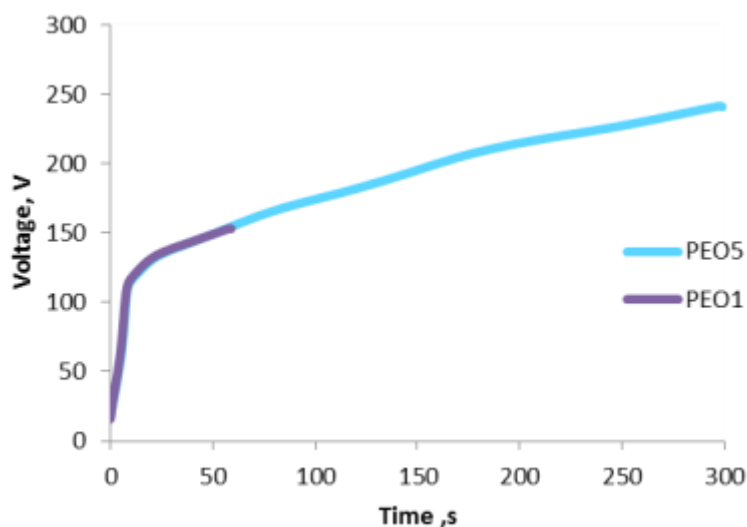


Fig. 3.2: Voltage transients for the 1 and 5 minute oxidation process ( $20 \text{ A/dm}^2$ ,  $0.15 \text{ M CaGly}$  and  $0.02 \text{ M CaAc}$ ).

For both samples the voltage transients showed two distinctive regions based on the rate of voltage rise. In the first region, the voltage increased rapidly to about 120 V due to formation of a dense oxide layer. In the second region of lower increase rate, visible sparking was observed indicating the growth of a porous oxide. During this stage, incorporation of species from the electrolyte is greatly enhanced [34, 35].

## 3.2 Oxide surface characteristics

### 3.2.1 Topography

The two different surfaces created by PEO have been imaged by SEM and the results, at different magnifications, are depicted in Fig. 3.3 and Fig.3.4. Uniform porous topographies were revealed on both surfaces. However, comparison of the two figures indicates that the morphology of the two surfaces differs significantly. The PEO1 surface (Fig. 3.3) showed some residual grinding lines and relatively small, but more numerous pores with irregular shape. The PEO5 surface (Fig.3.4) did not show any grinding lines and larger pores having a more uniform shape are visible, with some of them protruding from the surface.

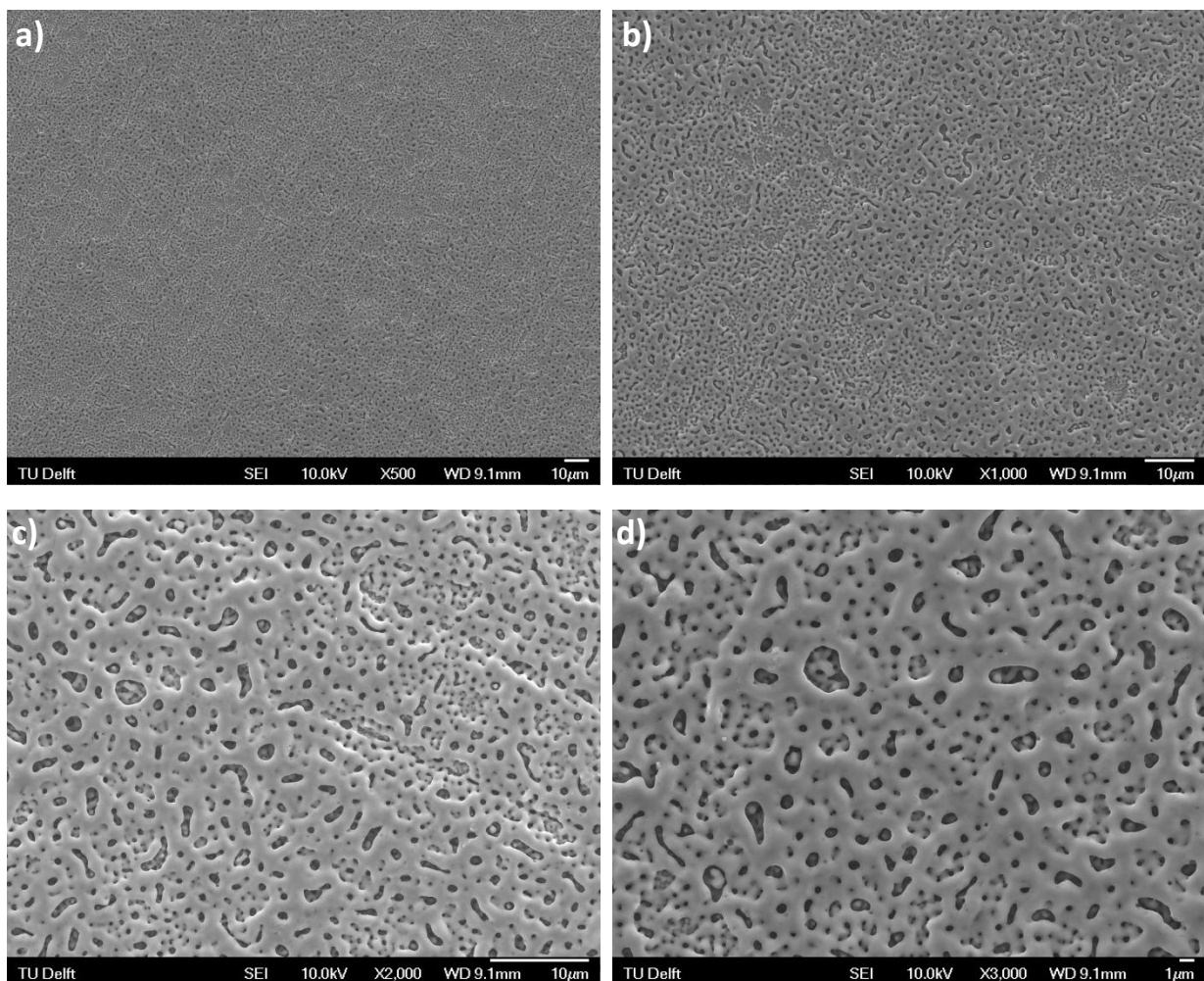
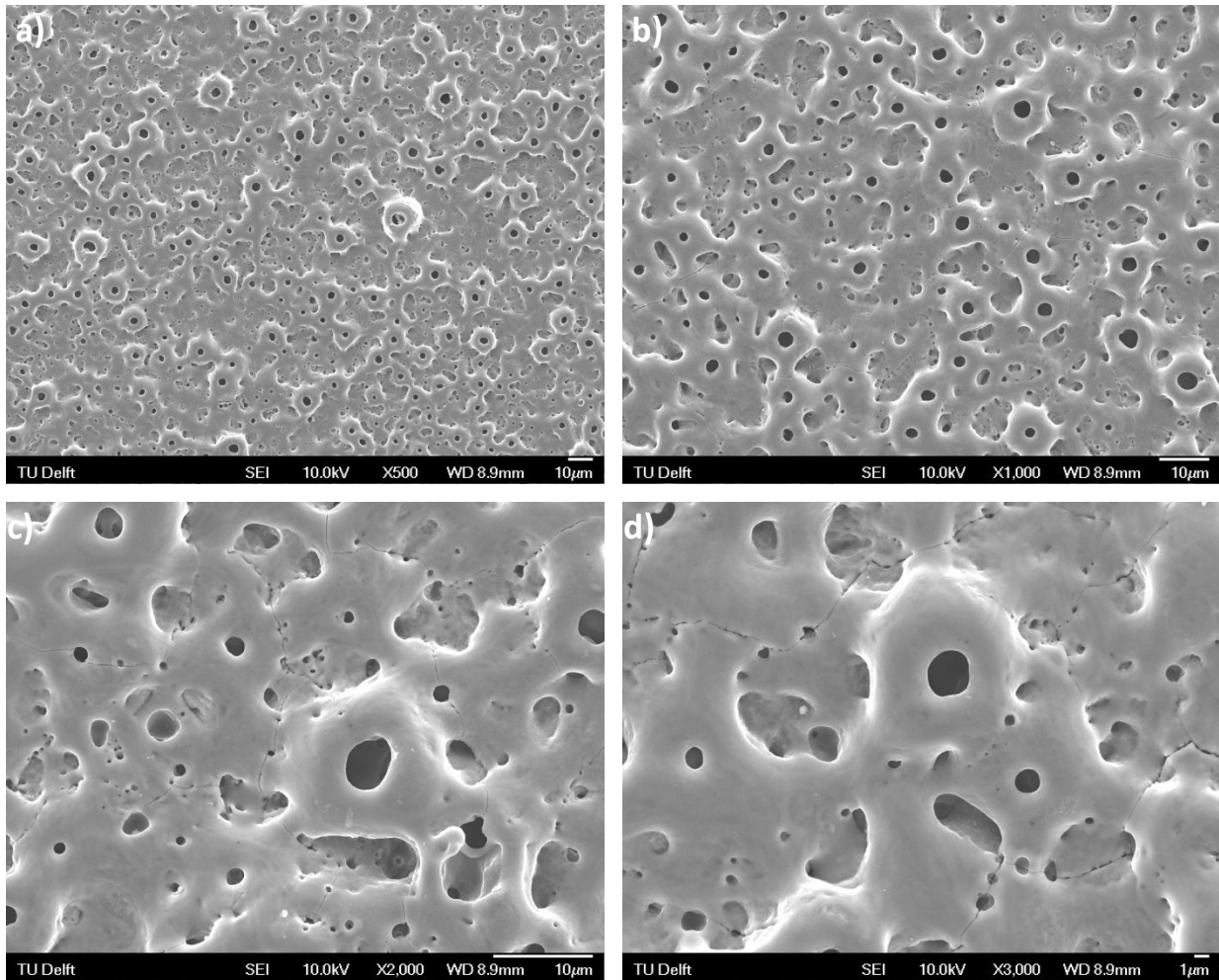


Fig. 3.3: SEM images of PEO1 surface at: (a) 500x, (b) 1,000x, (c) 2,000x and (d) 3,000x magnification.



**Fig. 3.4:** SEM images of PEO5 surface at (a) 500x, (b) 1,000x, (c) 2,000x and (d) 3,000x magnification.

For a certain substrate and electrolyte, the morphology of the PEO oxides formed under galvanostatic conditions is influenced by the evolution of sparks on the surface and the associated processes, such as gas evolution and local heating. Usually, very fine and rapidly moving sparks accompanied by gas evolution are generated at the onset of porous layer growth, which become larger, less mobile and more intense with extended oxidation duration (larger voltages) [9, 34, 36]. Therefore, a fine porous surface develops into a relatively coarser structure in time with larger pores and a crater-like morphology, as observed by SEM investigations in the present study.

### 3.2.2 Surface roughness

In order to obtain quantitative morphological information, surface roughness was evaluated by Micro Surface Profilometry (MSP). Three different parameters have been measured: average roughness ( $R_a$ ), the largest peak-to-valley height ( $R_y$ ) and the mean spacing between the profile peaks at the mean line ( $S_m$ ). These parameters provide information about the amplitude and spatial organization of roughness. The results presented in Table 3-1 are the average and standard deviation of 30 measurements made on three different samples for each surface.

**Table 3-1: Roughness values obtained by profilometry for both surfaces.**

Surface	Ra, $\mu\text{m}$	Ry, $\mu\text{m}$	Sm, $\mu\text{m}$
PEO1	$0.19 \pm 0.03$	$1.64 \pm 0.27$	$41.13 \pm 4.42$
PEO5	$1.43 \pm 0.08$	$10.32 \pm 0.80$	$38.20 \pm 2.28$

From the results in Table 3-1, it can be observed that extending the PEO processing time from 1 to 5 minutes determined a significant increase in Ra (7.5x) and Ry (6.3x). This indicates that the PEO5 surface is relatively rough, mainly due to the presence of larger pores protruding from the surface, as shown by the SEM analysis (Fig.3.4). This topography is the result of a thicker layer formed by local growth at the breakdown sites in the presence of relatively large and more intense sparks occurring at higher voltages (extended oxidation times) [9]. The mean spacing between the profile peaks (Sm) for the two surfaces suggests formation of uniform porous structures on both surfaces. The roughness measurements are in line with the SEM observations, confirming that the PEO5 surface is relatively rough and that uniform porous structures are developed on both surfaces.

### 3.2.3 Surface porosity

The morphological investigation continued with assessment of pore size, pore density and surface porosity, based on selected SEM images (Fig.3.5). Different magnifications have been used for the two surfaces i.e. 2,000x for the PEO1 and 1,000x for the PEO5 surface, to ensure the selection accuracy of open pores. Based on the data acquired from the images presented in Fig.3.5 surface porosity (%) and pore density (pores/mm<sup>2</sup>) have been calculated (see 2.2.3). The raw data is presented in Appendix 1 and the results are presented in Fig. 3.6 and Table 3-2.

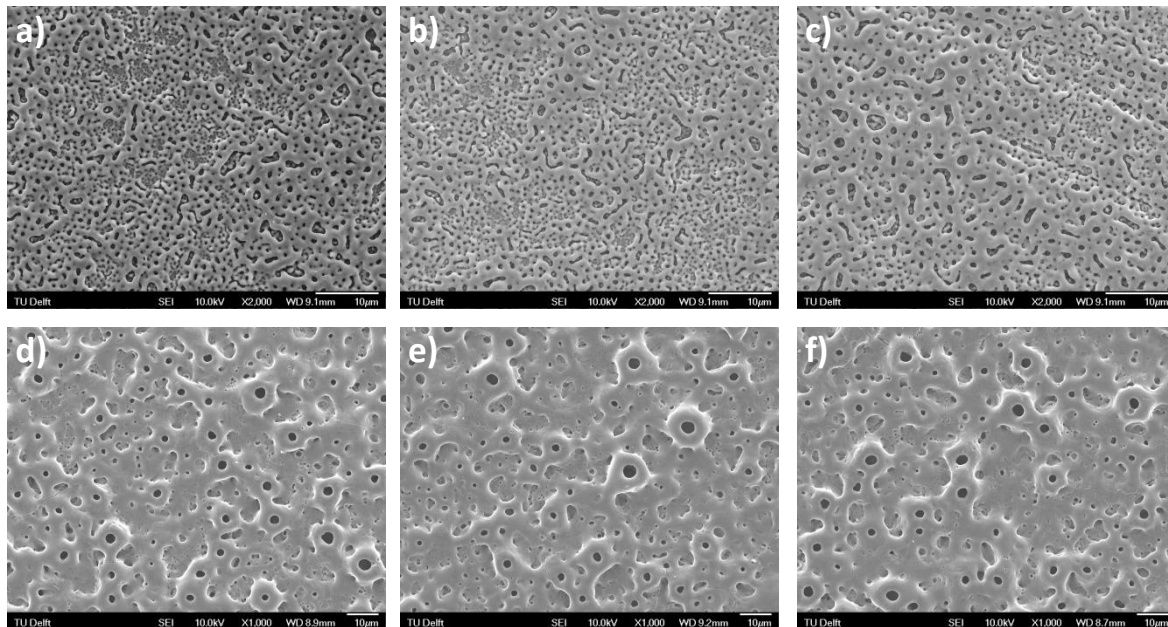


**Fig. 3.5: SEM images taken at different locations to determine porosity: (a-c) PEO1 at 2,000x magnification, (d-f) PEO5 surface at 1,000x magnification.**

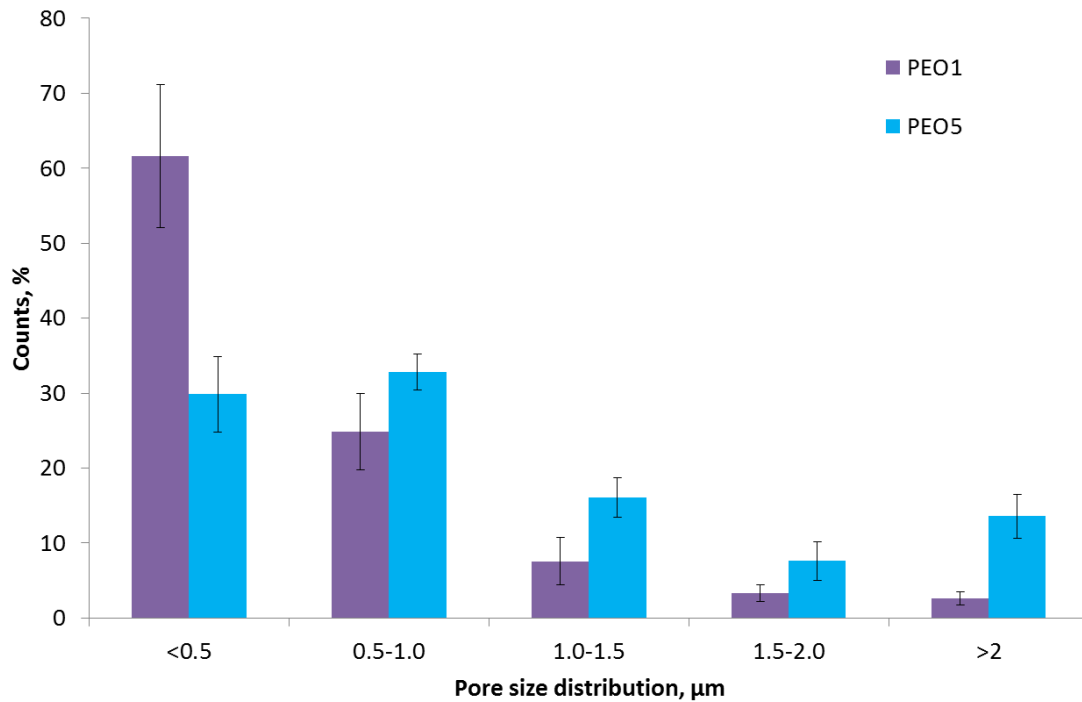


**Fig. 3.6: Pore size distribution of the two oxidized surfaces.**

The analysis of pore size distribution (Fig.3.6) indicated that about 62% of the pores on the PEO1 surface were smaller than 0.5  $\mu\text{m}$ , while the majority (63%) of the pores on the PEO5 surface were smaller than 1.0  $\mu\text{m}$ . In addition, on the PEO5 surface more pores larger than 1.5  $\mu\text{m}$  were observed. The results obtained suggest an increase in pore size with anodizing voltage and are in line with the previous studies performed on titanium in a similar electrolyte [9].

Pore density calculations (Table 3-2) confirmed the SEM observations, indicating the presence of significantly more pores on the surfaces oxidized for 1 minute, relative to the surfaces oxidized for 5 minutes. The PEO1 surface with smaller, but more numerous pores, revealed the highest surface porosity, i.e. 14.5% relative to 4.03% for the PEO5 surface. Thus, in addition to surface roughness, the pore morphology and density changed with PEO treatment time.

**Table 3-2: Porosity results for both surfaces**

	PEO1	PEO5
<b>Surface porosity, %</b>	14.5 $\pm$ 0.31	4.03 $\pm$ 0.44
<b>Pore density, pores/mm<sup>2</sup></b>	6.05 $\times$ 10 <sup>5</sup>	3.83 $\times$ 10 <sup>4</sup>
<b>Max pore size, <math>\mu\text{m}</math></b>	4.13	5.98
<b>Min pore size, <math>\mu\text{m}</math></b>	0.14	0.19
<b>Median pore size, <math>\mu\text{m}</math></b>	0.39 $\pm$ 0.07	0.98 $\pm$ 0.05

### 3.2.4 Surface chemistry

The elemental and phase composition of the surfaces after oxidation for 1 and 5 minutes were assessed by SEM/EDS and XRD, respectively. A total of 18 different EDS spectra have been acquired for each surface and Fig. 3.7 includes a typical spectrum for the PEO1 and PEO5 surfaces together with the estimates for the main elements.

The findings indicated the presence of Ti, Al, Nb from the substrate and P and Ca from the electrolyte on the oxidized surfaces. This suggests incorporation of Ca and P species in the oxide layers during the process. Furthermore, the Ca and P peaks were higher on the PEO5 surface than on the PEO1 surface, with estimated concentration of Ca of 8.7 atomic % on the PEO5 surface vs. 3.1 atomic% on the PEO1 surface and a Ca/P ratio of 2.0 on the PEO5 surface relative to almost 1.0 on the PEO1 surface (Fig. 3.7c).

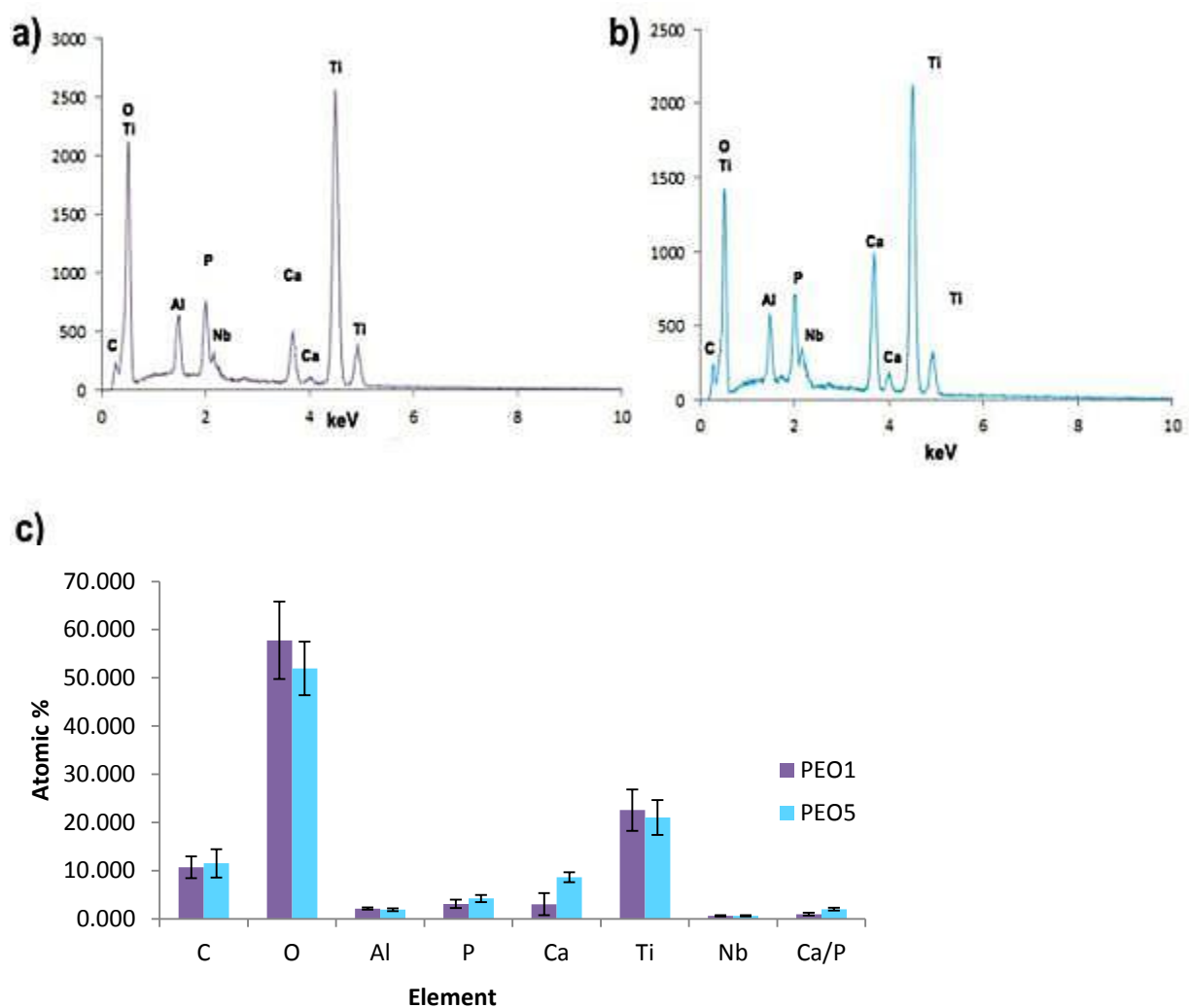
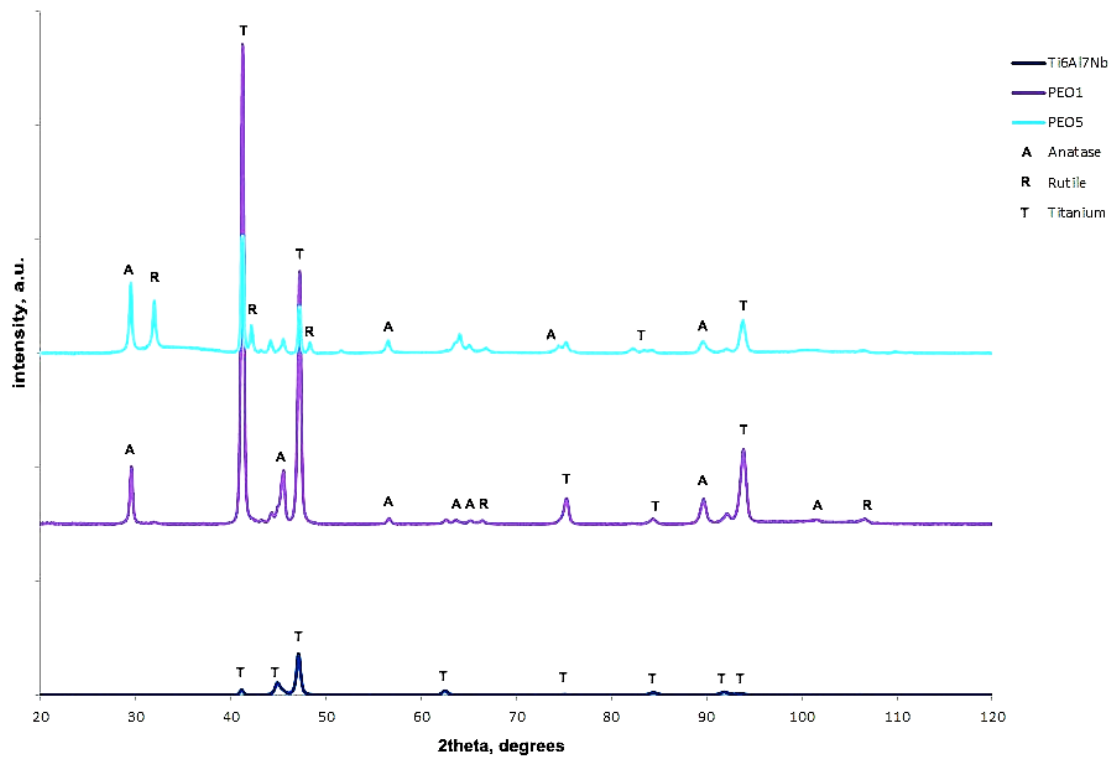


Fig. 3.7: EDS spectra for: (a) PEO1 and (b) PEO5 surface, both at 3,000x magnification; (c) the chemical composition in atomic percentages for both surfaces as estimated by SEM-EDS analysis.

The main reason for selecting Ca/P based electrolytes for PEO of titanium for biomedical applications is represented by the possibility to incorporate in the porous oxide layer Ca and P species at a stoichiometric ratio comparable to that of hydroxyapatite (1.63) present in

bone tissue, thereby creating a more suitable surface for bone apposition [31, 36]. Further, they may influence cell response [19]. Below sparking, P species enter the oxide layer by inward migration from the oxide/electrolyte interface, whereas Ca species, which are found mainly in the outer layer regions, suggests a possible local surface deposits and/or outward migration. The start of sparking is associated with increased P and Ca incorporation and the mechanism may involve plasma and thermal processes [35]. While P is distributed relatively uniform throughout the layer, Ca concentration seems to decrease with depth [9, 35].



**Fig. 3.8: Phase composition as determined by XRD for both oxidized surfaces and substrate.**

Crystalline  $\text{TiO}_2$  phases have been formed during oxidation for 1 and 5 minutes (Fig.3-8). Both anatase and some rutile were found on the oxidized surfaces, the latter being more pronounced on the PEO5 surface. With an increase in anodizing voltage, crystallinity increases and the more stable rutile phase is formed [31]. However, in the case of Ca/P electrolytes, incorporation of Ca and P in the layer influences not only the chemistry, but also the crystallinity of the oxide. It seems that P and possibly Ca suppress crystallization of the oxide as amorphous regions enriched in P and Ca have been evidenced in the outer oxide layer during PEO in Ca/P based electrolytes [31, 35].

### 3.2.5 Surface wettability and surface free energy

Increased surface wettability favors interactions of implants with the biological environment. Higher wettability is associated with enhanced surface free energy. Literature suggests that cells prefer to adhere to hydrophilic (more wettable) surfaces [37-39]. In order to determine the wettability of the surfaces, dynamic contact angles were measured in pure water and diiodomethane. The surface free energy (SFE) was calculated by the Fowkes theory (see for



details 2.2.6). In Table 3-3 and Fig. 3.9 the results of this experiment are shown for both oxidized surfaces and Ti6Al7Nb surface.

**Table 3-3: Contact angles and surface free energy for both PEO surfaces and the untreated surface.**

	Water angle, °	Diiodomethane angle, °	Polar	Dispersive	SFE, mJ/m <sup>2</sup>
<b>Ti6Al7Nb</b>	81.17 ± 6.71	66.83 ± 5.81	6.00 ± 1.51	24.64 ± 2.54	30.64 ± 4.05
<b>PEO1</b>	73.40 ± 6.43	58.48 ± 4.45	7.90 ± 2.41	29.43 ± 2.46	37.34 ± 4.79
<b>PEO5</b>	61.77 ± 3.43	66.49 ± 2.08	16.97 ± 0.81	24.85 ± 1.14	41.82 ± 1.89

The trend indicated that PEO treatment increased the wettability and the surface free energy relative to the Ti6Al7Nb surface. In addition, by extending the oxidation time, these parameters were further enhanced, although not statistically significant. In the case of surface free energy, the main contribution was from the polar component, especially for the oxide surfaces produced at extended oxidation durations.

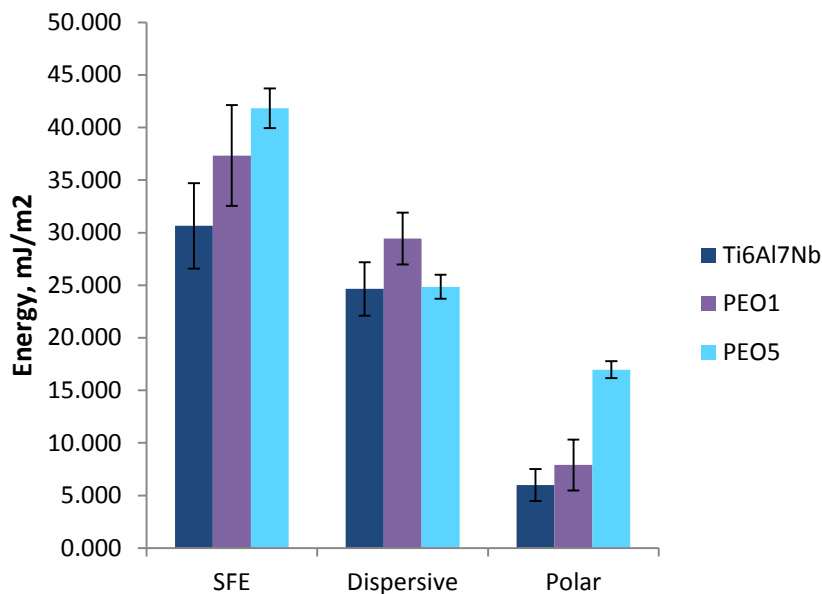


**Fig. 3.9: Surface Free Energy (SFE) and its dispersive and polar components calculated using the Fowkes theory for both oxidized surfaces and Ti6Al7Nb surface.**

These properties are affected by the chemistry and topography of the surfaces as well as the measuring conditions, such as liquids used and humidity of the surrounding environment [40]. Factors that may have contributed to the enhanced surface wettability include the change in oxide chemistry due to the PEO process and the presence of pores possibly allowing the liquid droplets to enter inside the pores [41]. The values of contact angles and the trend at increased voltage are in line with previous studies on porous anodic oxide layer on titanium [19].

### 3.2.6 Summary of the main surface characteristics of the different surfaces

In Table 3-4 the main characteristics of the PEO1 and PEO5 surfaces are summarized. It can be observed that by extending oxidation time from 1 to 5 minutes, the average roughness (Ra), maximum peak-to-valley height (Ry), pore size and Ca/P ratio of the oxide layers increased, while surface porosity and pore density decreased. Both surfaces showed pores mostly in the submicron range, a mixture of anatase and rutile oxide phases and had enhanced hydrophilicity relative to the Ti6Al7Nb surface. The response of SV-HFO preosteoblast cells on these two surfaces, from adhesion to matrix mineralization was systematically investigated and the results are presented and discussed in the next section.

**Table 3-4: Summary of the main surface characteristics for the two PEO surfaces.**

	<b>PEO1</b>	<b>PEO5</b>
<b>Average roughness</b> <b>Maximum peak-to-valley height</b>	0.19 ± 0.03 μm 1.64 ± 0.27 μm	1.43 ± 0.08 μm 10.32 ± 0.80 μm
<b>Surface porosity</b> <b>Pore density</b> <b>Median pore size</b>	14.5 % 6.05 × 10 <sup>5</sup> pores/mm <sup>2</sup> 0.39 ± 0.07 μm	4.0 % 3.8 × 10 <sup>4</sup> pores/mm <sup>2</sup> 0.98 ± 0.05 μm
<b>Ca/P atomic ratio</b>	0.99	2.02
<b>Oxide phase composition</b>	Anatase & rutile	Anatase & more rutile
<b>Contact angle in water</b> <b>Surface Free energy</b>	73.40 ± 6.43 ° 37.34 ± 4.79 mJ/m <sup>2</sup>	61.77 ± 3.43 ° 41.82 ± 1.89 mJ/m <sup>2</sup>

### 3.3 *In vitro* response of SV-HFO to oxidized surfaces

#### 3.3.1 Adhesion of SV-HFO cells (4-48 hours)

Adhesion was assessed after 4, 24 and 48 hours of incubation on both PEO surfaces and culture plastic (positive control, PC) by Fluorescence Microscopy (FM) and Scanning Electron Microscopy (SEM). The results are presented in Figs. 3.10-3.13

After 4 hours of incubation (Fig. 3.10a-c) fewer cells have been found on the oxidized surfaces than on the PC. However, the evaluation of nuclei number (Fig. 3.11) and of the multichannel images indicated that more cells attached to the PEO1 surface than to the PEO5 surface. In addition, cell spreading was only observed on the PC surface (Fig. 3.10a). The cells on the oxidized surface showed a round morphology (Fig. 3.10b-c).

With increasing incubation time from 4 to 24 hours (Fig. 3.10d-f), the number of adhering cells increased on all surfaces. Cells on the positive control showed numerous filopodia reaching from cell body to cell body. Cells that adhered to the oxidized surfaces started to spread, more pronounced on the PEO1 surface where they showed an elongated cytoskeleton relative to those on the PEO5 surface.

After 48 hours of incubation (Fig. 3.10g-i) cells on the PEO1 surface had similar morphology to those on the PC. The cells on the PEO5 surface showed a thin, small cytoskeleton and some filopodia.

The SEM investigation performed after 24 and 48 hours (Fig. 3.12) provided additional information on cell density, morphology and cell-surface interactions. The findings confirmed that the number of cells adhering to the PEO5 surface was lower than on the PEO1 surface (Fig. 3.12a-b). Furthermore, the high magnification images after 24 hours (Fig. 3.12) revealed that the cells on the PEO1 surface followed closely the topography of the oxide layer and developed protrusions that entered the pores as oppose to the cells on the PEO5 surface, which were mostly confined in the areas between the large pores and showed fewer filopodia. After 48 hours (Fig. 3.12c), most of the cells on the PEO1 surface were elongated and developed thin and extended protrusions from one cell to another (Fig. 3.12). The ragged edges of the cells on the PEO5 surface, visible on the fluorescence images (Fig. 3.11i), can be associated with the coarser porous surface of the PEO5 surface.

Adhesion represents the first phase in cell-material interactions with impact on the subsequent proliferation and differentiation stages [42]. It involves specific proteins that are expressed by the cells and are influenced by the surface characteristics. It is known that osteoblasts are anchorage dependent cells, preferring rough surfaces for attachment [43].

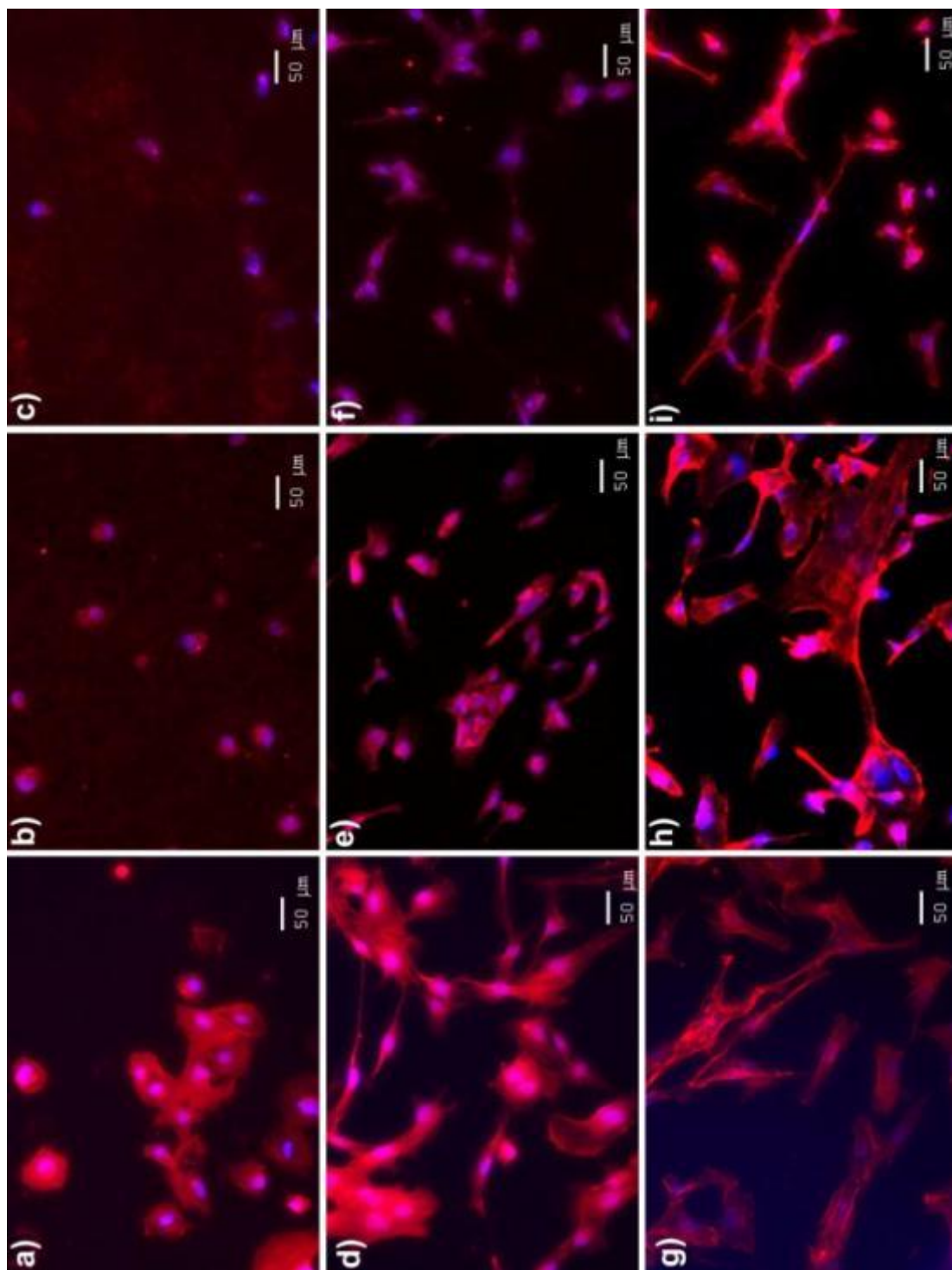


Fig. 3.10: Fluorescent images of SV-HFO cells on: PC (a,d,g), PEO1 (b,e,h) and PEO5(c,f,i) surfaces after 4 hours (a-c), 24 hours (d-f) and 48 hours (g-i) of incubation.

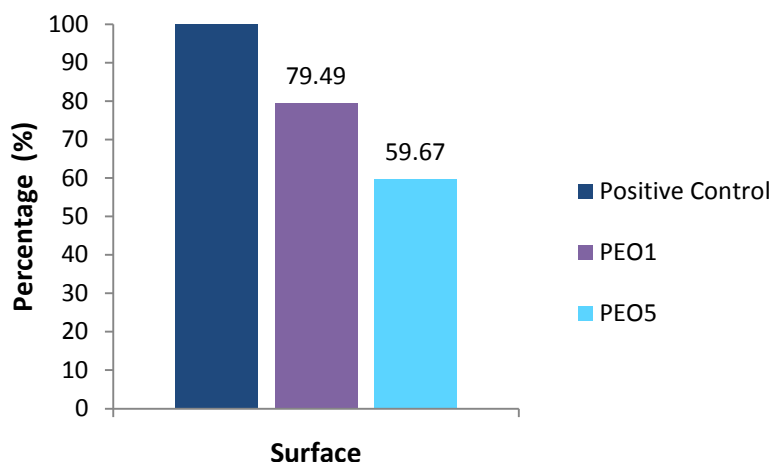


Fig. 3.11: Number of nuclei of SV-HFO cells after 4 hours of incubation, expressed as % relative to PC.

Previous studies showed that the number of SaOS-2 cells adhering to PEO-treated titanium surfaces after 1 hour of incubation, increased with surface roughness in the range 0.25-0.4  $\mu\text{m}$  [19]. However, Li et al. [9] reported a decreased number of MG63 after 3 incubations days on titanium surfaces oxidized by PEO above 300V, corresponding to surface roughness larger than 0.4  $\mu\text{m}$ . Further, Verrier et al. [28], examined the morphology of two different cells lines (hFOB and hBMSC) on anodized titanium (porous and dense surfaces with an average roughness between 0.9 – 1.2  $\mu\text{m}$ ). After 2 days of culturing both type of cells revealed a well spread morphology with long and thin pseudopodia and cell-cell contacts on the porous PEO-treated surfaces, while this morphology was only visible for the hBMSC on the dense oxidized surfaces, suggesting a higher sensitivity of hFOB1.19 to surface morphology.

The optimum surface roughness/topographies of titanium anodic oxides for osteoblast-like cell adhesion is not yet established due to the different conditions of oxidation used in different studies; cell type, incubation durations and evaluation methods, all possibly affecting the adhesion results.

In the present study, after 2 days of incubation on PEO-treated Ti6Al7Nb alloy, SV-HFO cells preferred the surface showing a finer porous structure with a larger pore density and a lower average roughness ( $0.19 \pm 0.03 \mu\text{m}$ ) for adhesion. On this surface the cells could spread and migrate easily using the pores as anchorage sites for their protrusions and showing cell-cell contacts after 48 hours. Despite the higher average roughness of PEO5 surfaces ( $1.43 \pm 0.08 \mu\text{m}$ ), the organization of roughness, namely the presence of local high pores contributing to the larger  $R_y$  value (ca. 10  $\mu\text{m}$ ), suppressed cell adhesion. The larger pores protruding from the surface acted rather as obstacles for adhesion, migration and cell-surface interactions in the first 48 hours of incubation. These findings indicate that the detailed analysis of oxides surface morphology is important in understanding surface-cell interactions during the adhesion phase. This aspect is however largely neglected in literature and may be one factor contributing to the non-conclusive results so far on roughness effects.

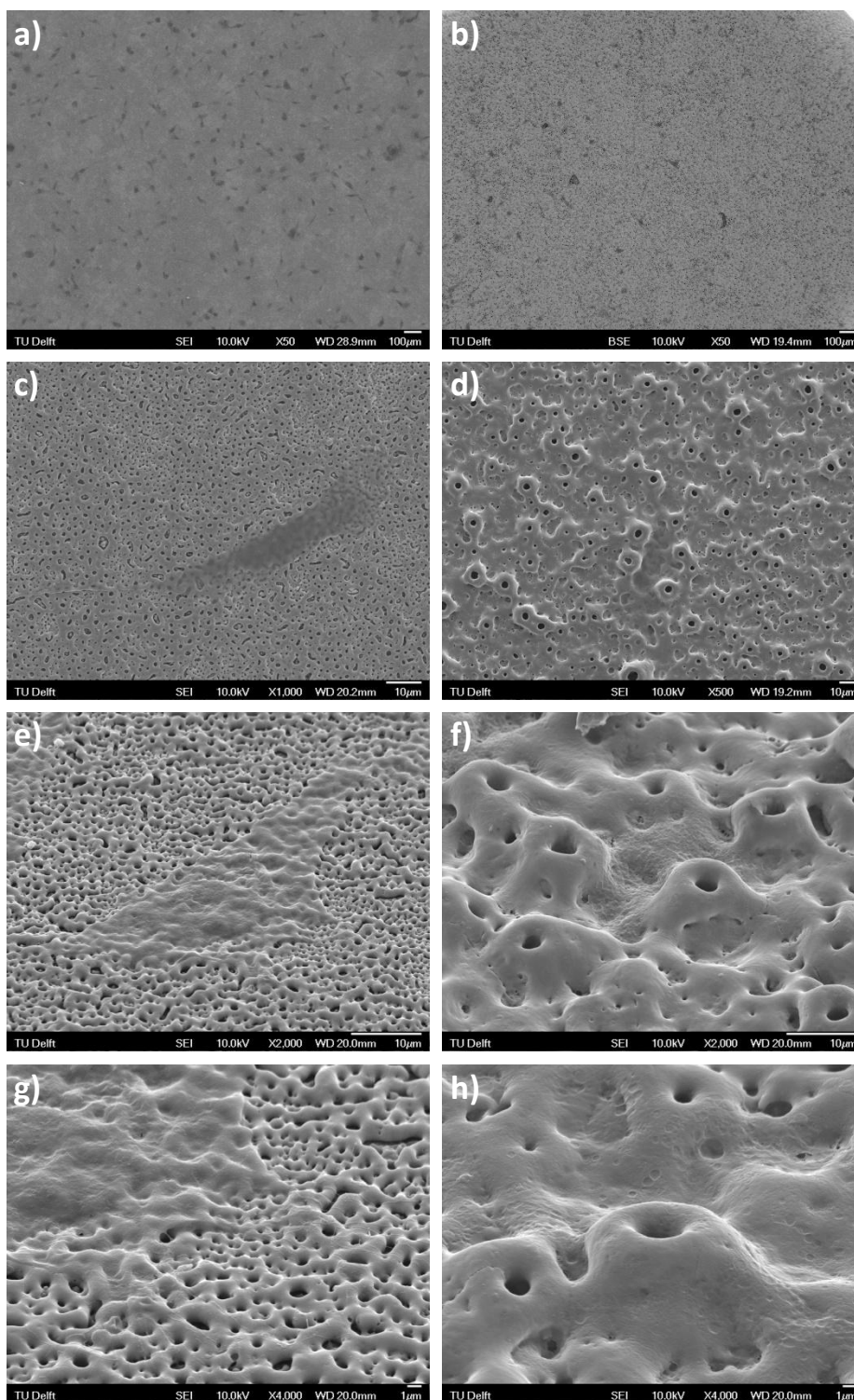


Fig. 3.12: SEM images of the cells after 24 hours of incubation on: PEO1 surface (a,c,e,g) and PEO5 surface (b,d,f,h).

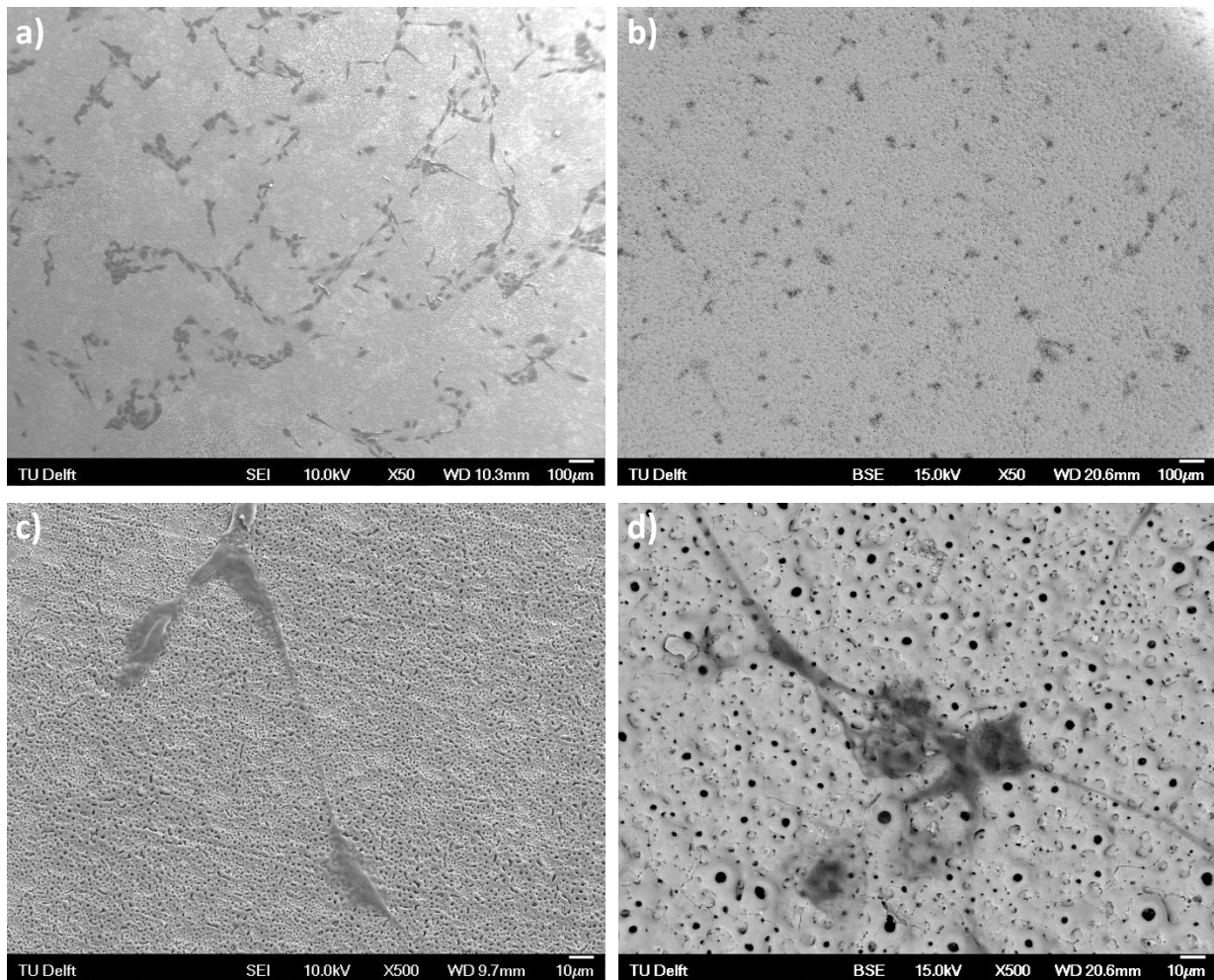


Fig. 3.13: SEM images of the cells after 48 hours of incubation on PEO1 surface (a,c) and PEO5 surface (b,d).

Apart from topography, cell response may also be influenced by surface chemistry. The release of Ca and/or P species from titanium surfaces may activate signaling pathways with favorable effects on cell adhesion and proliferation [19]. Nayab et al. [44] reported that Ca ion implantation on titanium surfaces affects adhesion of MG-63 cells in a level dependent manner. A strong inhibition of adhesion was observed on the high-Ca surfaces after 4 hours of incubation which however recovered and continued to improve after 24 hours of incubation.

The distinction between the effects of topography and chemistry becomes difficult when surface treatments are applied to titanium implants as both are often changing. In the present study, the surface showing enhanced SV-HFO cell adhesion after 48 hours of incubation, had a lower Ca concentration, suggesting that topography may have been the dominant factor influencing adhesion as also indicated by SEM investigations.

### 3.3.2 Metabolic activity of SV-HFO cells cultured on the two surfaces (1-7 days)

The metabolic activity of the SV-HFO cells was measured by Alamar Blue Test (ABT),(see 2.3.4).

The test was performed after 1, 2, 5 and 7 days of incubation on the oxidized samples and on the PC. The results were complemented with FM and SEM investigations. The findings are included in Figs. 3.14-3.16.

The fluorescence results (Fig.3-14) indicated an increase in the metabolic activity of the cells on all surfaces during 7 days of culturing. Further, after 2 days of incubation the rate of increase was higher. This could be due to the proliferative activity expected in this period and the addition of dexamethasone to the medium to stimulate osteogenic differentiation. The lower metabolic activity of the cells on the PEO5 surface may be related to the lower number of cells adhered on this surface.

The FM images depicted in Fig.3.15 show the morphology of the cells after 2, 5 and 7 days of incubation and give an indication for cell density. For all three surfaces the number of cells and cell surface coverage increased in time.

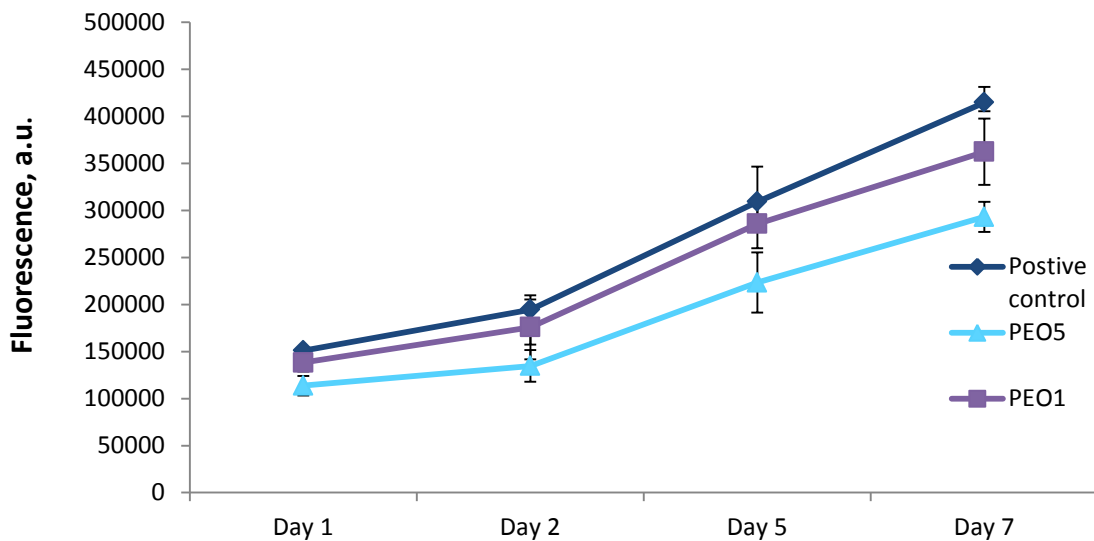


Fig. 3.14: Metabolic activity obtained with ABT for positive control and both oxidized surfaces after 1, 2, 5 and 7 days of culturing.

After 5 days of incubation the cells on the PC surface (Fig.3.15b) formed a nice monolayer covering most of the surface area, while on the PEO5 surfaces cell-free areas were visible. After 7 days of incubation most of the PEO1 surface was covered with cells, whereas on the PEO5 surface cell coverage remained lower.

Fig. 3.16 shows the SEM images of the oxidized surfaces at day 2, 5 and 7 after cell seeding. These low magnification images confirmed the FM results, namely the increase in the number of cells and cell coverage from day 2 to day 7 on both oxidized surfaces and a



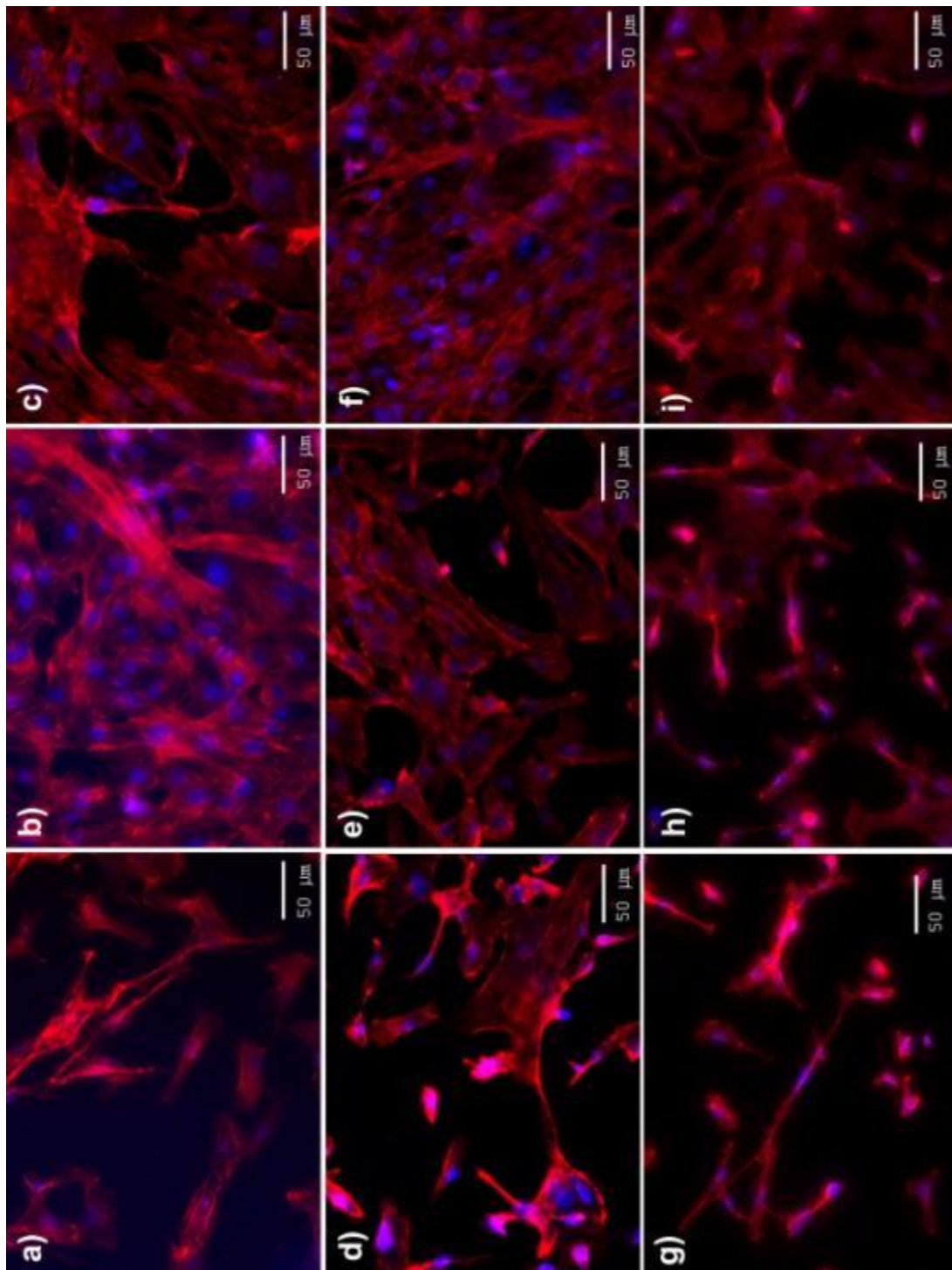


Fig. 3-.15: FMI images after 2 (a,d,g), 5 (b,e,h) and 7(c,f,i) days of incubation for the positive control (a-c), PEO1 (d-f) and the PEO5 (g-i) surface.

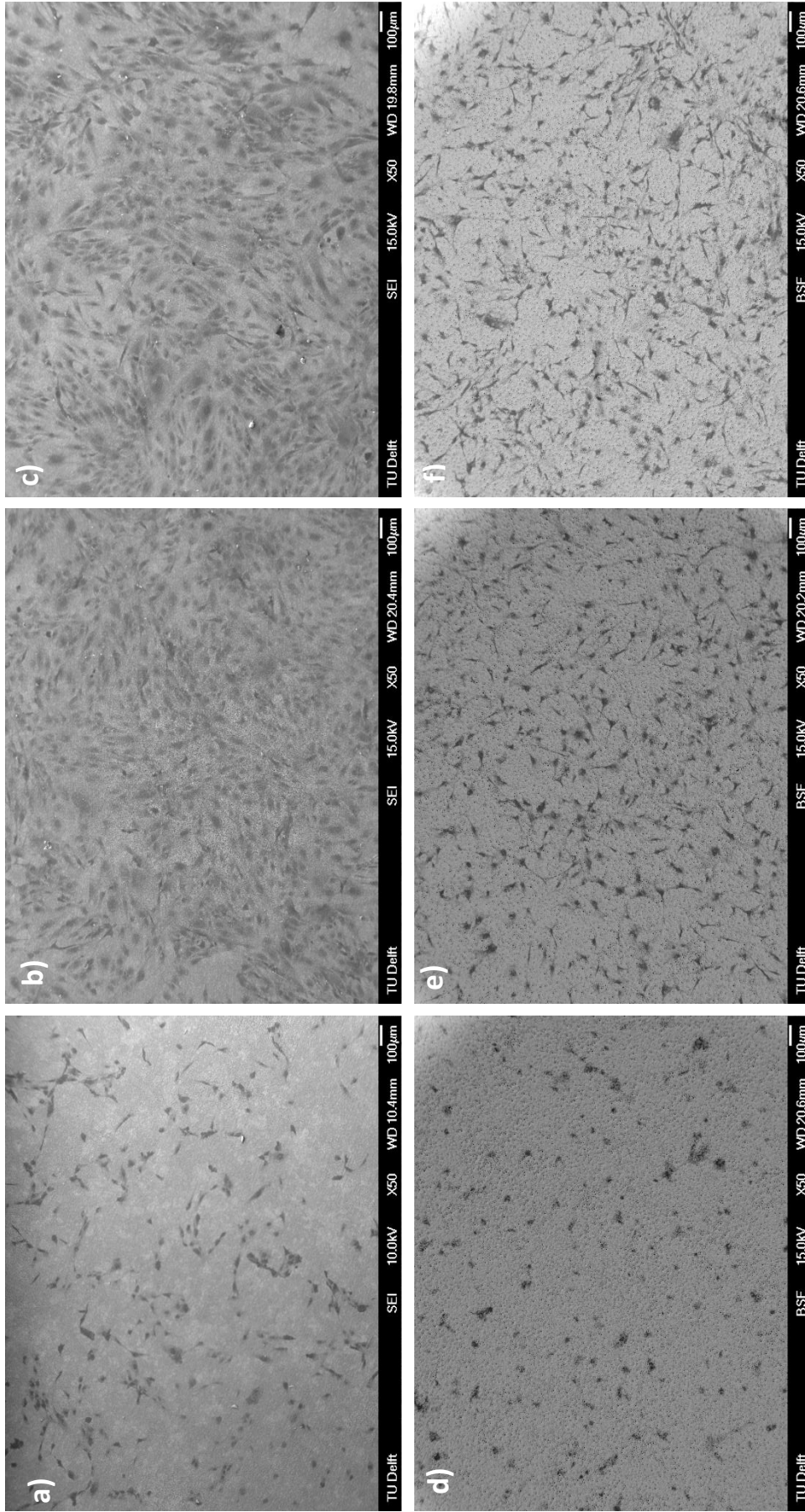


Fig. 3.16: SEM images of cells after 2 (a,d), 5 (b,e) and 7 (c,f) days of incubation on the PEO1 (a,c) and PEO5 (d-f) surface

larger cell density on the PEO1 surface. Furthermore, it was observed that the cells continued to spread and migrate easier on the PEO1 surface.

Between day 2 and day 7, SV-HFO cells are expected to proliferate and start differentiation [33]. It was previously shown that an increase in the average roughness of titanium surfaces by mechanical treatments from less than 0.2  $\mu\text{m}$  to  $\sim 0.6 \mu\text{m}$ , decreased the proliferation rates of osteoblasts by almost 40% [45]. In the case of PEO surfaces, Zhu et al. [19], observed a slightly larger number of SaOS-2 cells after 4 days on the PEO surfaces with lower Ra (0.25 vs. 0.4  $\mu\text{m}$ ) and Ca/P ratio (0.4 vs. 1.0). More recently, Whiteside et al. [27], found the highest proliferation rate of primary human osteoblast after 7 days on titanium oxide layers with a roughness of 1.29  $\mu\text{m}$  and Ca/P ratio of 0.27. The proliferation rates were relatively low on the rougher (Ra=1.67  $\mu\text{m}$ ; Ca/P=0.27), but also on the smoother (Ra=0.78  $\mu\text{m}$ , Ca/P=0.14) surfaces produced in different Ca/P based electrolytes.

When rat osteoblasts have been cultured on PEO-treated TiZrSnMoNb alloy [46], a higher metabolic activity was found after 7 days on the rougher surfaces (2.3 vs. 0.7  $\mu\text{m}$ ) with a higher Ca/P ratio (2.1 vs. 1.26). These findings suggest that proliferation of osteoblast-like cells on PEO-treated surfaces may be affected by surface roughness, surface chemistry as well as cell type. More systematic research is needed to further elucidate the effect of each factor on the growth phase of osteoblast(-like) cells. In our study, SV-HFO cells showed similar rates of metabolic activity increase on the two surfaces during 7 days of incubation.

### 3.3.3 ECM synthesis (7-21 days)

Sirius Red staining was used to evidence the collagen present in the ECM matrix after 7,14 and 21 days of culturing. The results are depicted in Fig. 3.17 and Fig. 3.18.

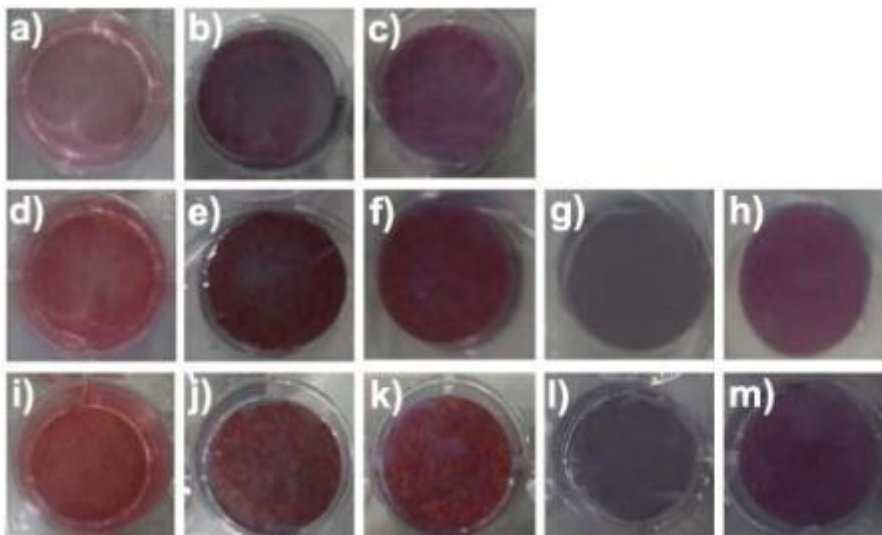
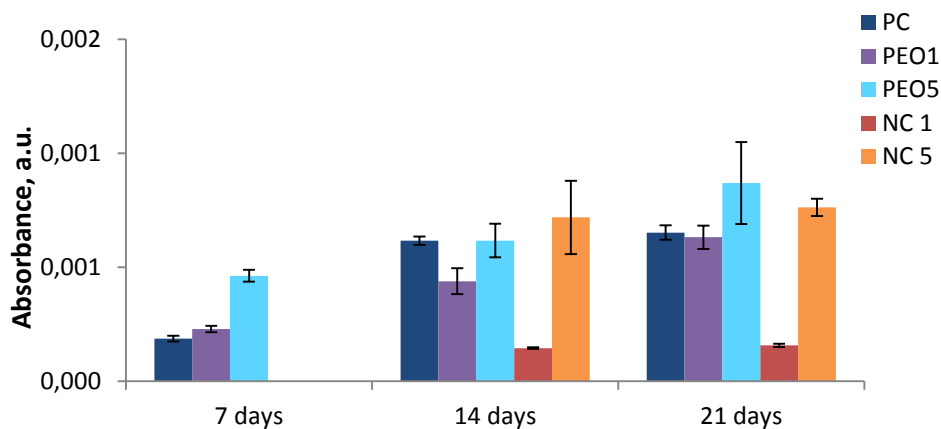


Fig. 3.17: Sirius Red staining after: 7 days (a-c), 14 days (d-h) and 21 days (i-m) on positive control (a,d,i), PEO1 (b,e,j) PEO5 (c,f,k), negative PEO1 (g,l) and negative PEO5 (h,m) surfaces.

From Fig. 3.17h,m it can be observed that the negative control of PEO5 surface, on which no cells have grown, stained pinkish-red. Elements inside the oxide layer thus interfere with the

Sirius Red staining making the identification of collagen on the PEO surfaces impossible. The results for the positive control indicated that the amount of collagen increased in time.

Next to staining, the amount of collagen was assessed by measuring the absorbance of stained surfaces at 531 nm (see 2.3.5). The results (Fig.3.18) showed that the absorbance of the negative controls was measurable. It was not possible to deduct these values from the actual samples, because the negative of the PEO5 surface gave a higher absorbance value than the actual sample. These findings indicate that alternative methods need to be used for collagen determination such as using a Sircol collagen assay or antibody labeling [27]. The Sircol collagen assay is based on Sirius red. The difference is that the collagen is first solubilized by adding 0.5 M acetic acid. This could prevent the interaction of the surface as in our protocol. Antibody labeling of the collagen with a fluorescent label circumvents any interaction with the oxidized surface, because the antibody will only bind to the collagen.



**Fig. 3.18: Absorbance of Sirius Red staining after 7, 14 and 21 days including the negative controls for the two surfaces and positive control.**

Matrix formation was also imaged by SEM. After 7 days of culturing we observed the start of ECM synthesis on the PEO1 surface (Fig.3.19a-b), which was not yet visible on the PEO5 surface (Fig. 3.20a-b). On the PEO1 surface the amount of ECM increased with time from day 7 to day 21 (Fig3.19c-h). In addition, the morphology changed from a monolayer structure to appearance of deposits protruding from the surface and formation of net-like structures which were well integrated with the porous surface. On the PEO5 surface we observed the formation of a monolayer covering all the pores during 14 days (Fig. 3.20c-d) and at day 21 a thick cell layer with white deposits was visible (Fig.3.20e-f).

The SEM images at day 21 showed areas with damaged ECM most probably caused by a too long exposure time to the SEM fixation fluid.

These findings indicate that both PEO surface provided a suitable support for ECM formation. However, the cells on the PEO1 surface started matrix deposition earlier than those on the PEO5 surface.

When cultured on plastic, SV-HFO cells start synthesizing their matrix between day 12 and 14 of incubation [33]. Only one reference was found on collagen synthesis by human

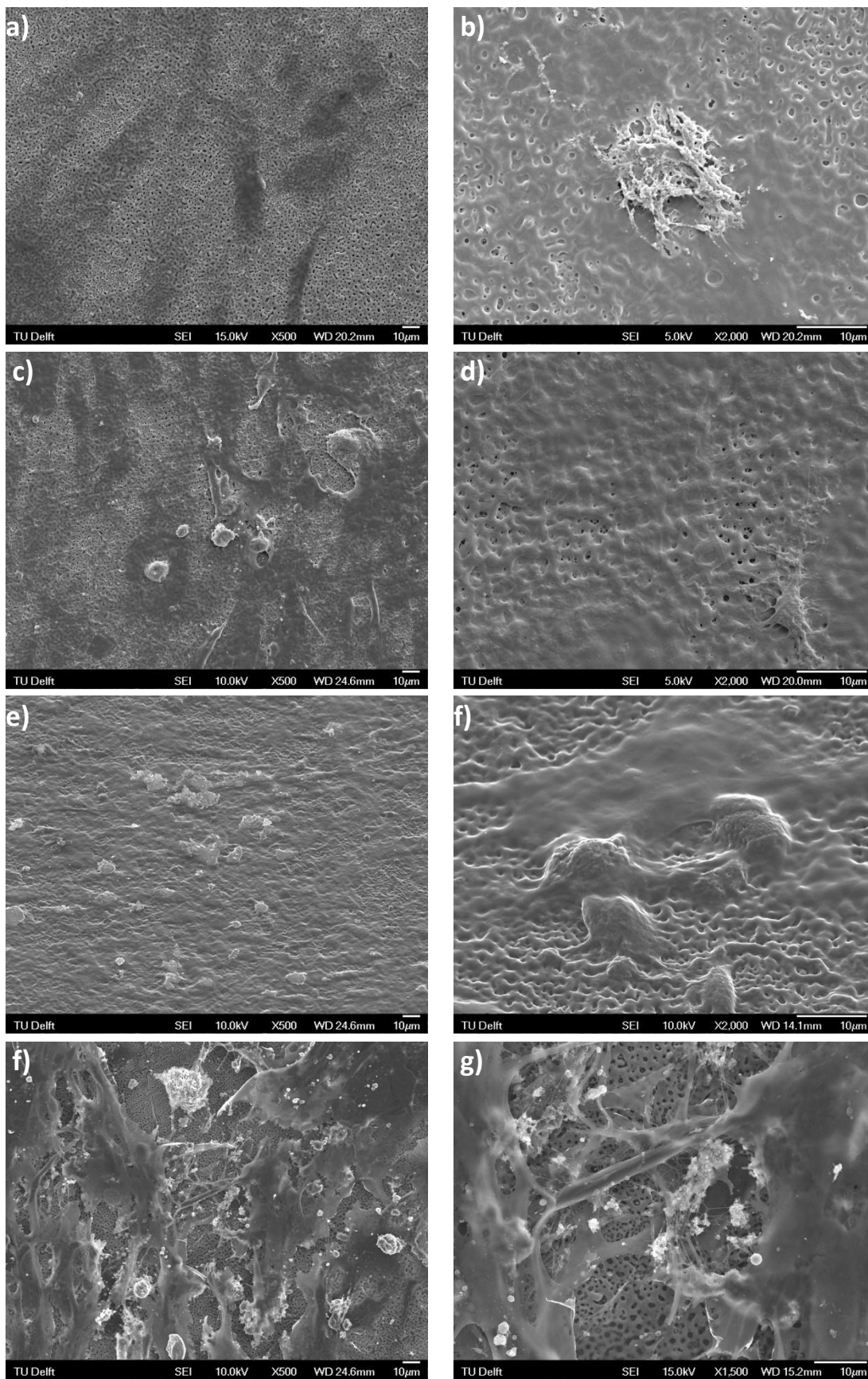


**Fig. 3.19:** SEM images of PEO1 surface after: 7 days (a-b), 12 days (c-d), 14 days (e-f) and 21 days (g-h) of incubation.

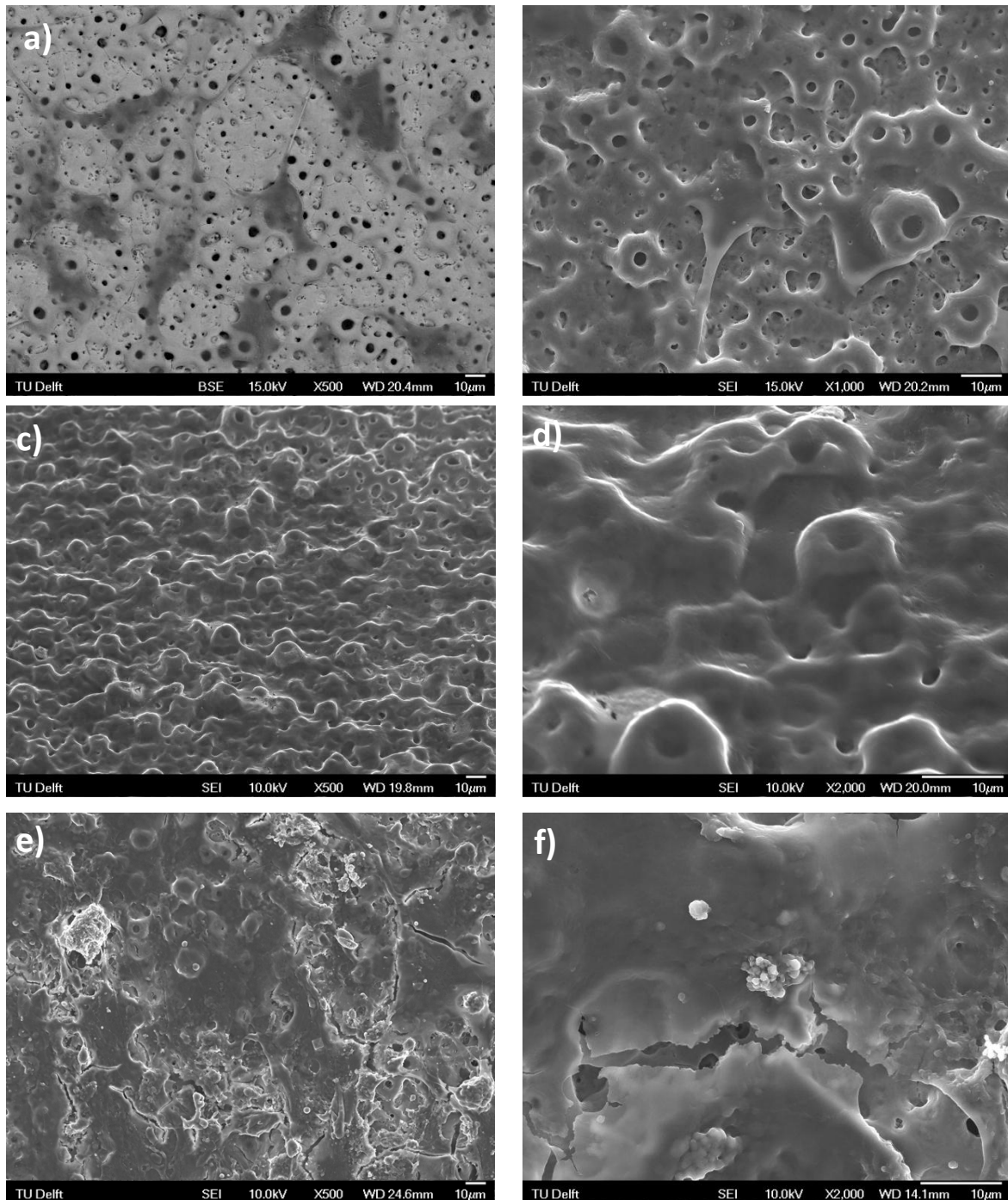


**Fig. 3.20: SEM images of PEO5 surface after: 7 days (a-b), 14 days (c-d) and 21 days (e-f) of incubation.**

osteoblast cells seeded on PEO surfaces [27]. The surfaces were produced on cp-titanium in four different Ca/P based electrolytes and the resultant surfaces differed significantly with regard to their morphology, structure and chemistry. The findings of this study showed that cells on the PEO surfaces produced more collagen after 28 days when compared to those on uncoated surfaces. This was due to an accelerated rate of synthesis after 14 incubation days on the PEO surfaces. Further, surfaces with the highest Ca/P ratio (0.46) having also the smallest average pore size (4  $\mu\text{m}$ ), highest pores density and highest roughness (2.28  $\mu\text{m}$ ) promoted collagen formation. These results suggest that collagen synthesis may be favored

by incorporation of Ca/P species in the oxide layer. Nevertheless, the effects of the other surface characteristics on collagen synthesis cannot be excluded.

For our study, it could be hypothesized that the coarser topography of the PEO5 surface, which led to lower cell adhesion and lower cell number, delayed formation of the ECM, but when the cell number is high enough, the higher Ca/P ratio may stimulate ECM synthesis. To prove this hypothesis, further research at longer incubation times with the PEO5 surface is required. In addition, the effect of Ca and P released from these surfaces on each cellular function need to be established and corroborated with the effects of the other surface features.

### 3.3.4 ECM mineralization (7-21 days)

Previous trials to evidence mineralization using Alizarin Red staining did not provide reliable data due to interference of the calcium incorporated in the oxide layers. Therefore, other methods have been checked. Xylenol orange ( $C_{31}H_{28}N_2O_{13}SNa_4$ ) is a calcium-chelating fluorochrome that labels newly calcified tissues, which makes it possible to determine the amount of mineralization of the ECM [47]. Mineralization of the extracellular matrix was observed by XO staining after 7, 14 and 21 days of culturing on the two PEO surfaces and the positive control. In addition, SEM/EDS analysis after 7, 12, 14 and 21 days of incubation were performed. The SEM findings were compared with other studies using the same method for showing morphology and mineralization of ECM [48].

After 7 days of incubation (Fig. 3.21), very few orange dots were observed on all three surfaces, but these were not numerous enough to conclude that the surfaces started to mineralize. This was also supported by the SEM/EDS analysis showing no clear Ca peaks that could be associated with these features.

After 14 days of incubation (Fig. 3.22) an increased number of nodules was found on the three different surfaces. The trend indicated the lowest number on the PEO5 surface (Fig.3.23). EDS analysis (Fig.3.24a) confirmed the existence Ca in the deposits on the PEO1 surface.

Between day 14 and 21 (Fig.3.25), the largest increase in the number of nodules was observed for the three surfaces. Interestingly, the rate of increase was higher on the PEO5 surface than on the PEO1 surface (Fig.3.23), suggesting that in this time interval matrix mineralization was faster on this surface. However, the mineralized area was more uniform on the PEO1 surface, relative to the more patchy appearance on the PEO5 surface. EDS analysis of the deposits found on the two surfaces after 21 days (Fig.3.24b-c) revealed high peaks of Ca.

These findings indicate that SV-HFO cells cultured on these two PEO surfaces could differentiate into osteoblasts which were then able to produce and mineralize the ECM. The mineralization results showed a slower matrix mineralization on the PEO5 surface up to 14 days of incubation. This could be the effect of the suppressed earlier cell adhesion on this surface, combined with the similar growth rates observed on the two surfaces which may result in more time needed for growth and differentiation of cells on this surface.

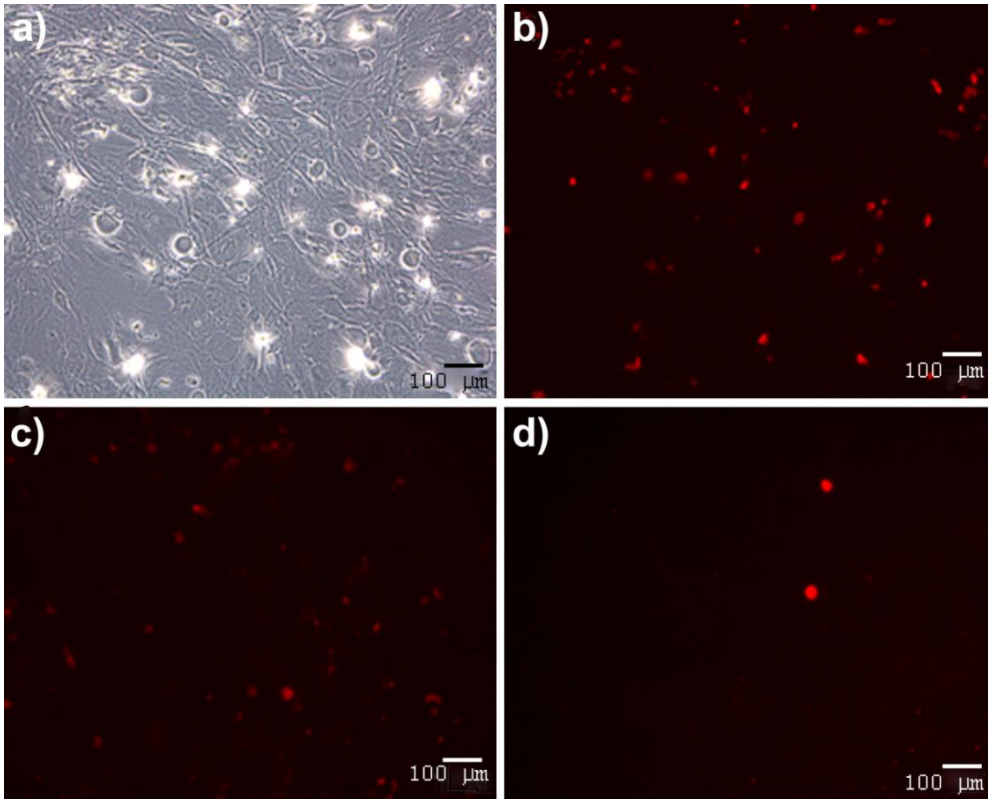


Fig. 3.21: Microscopic images of mineralisation by Xylenol Orange after 7 days of culturing. a) Positive control, brightfield image. b-d) fluorescent images of b) positive control, c) PEO1, d) PEO 5 surface. 10x magnification.μ

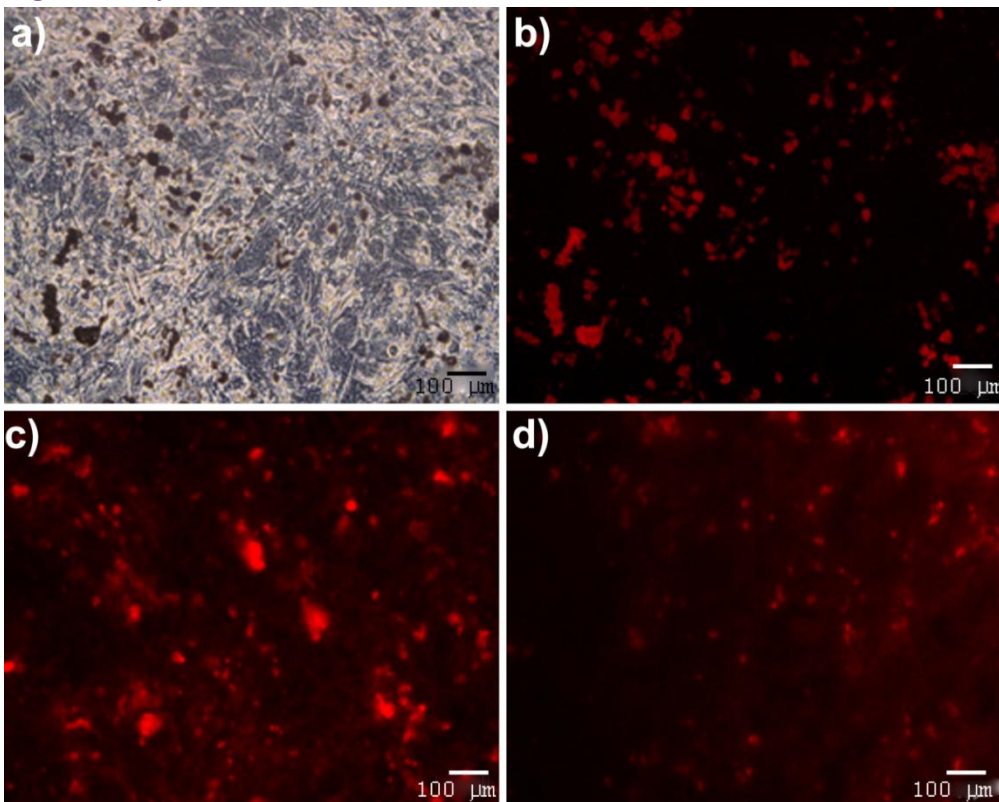


Fig. 3.22: Microscopic images of mineralisation by Xylenol Orange after 14 days of culturing. a) Positive control, brightfield image. b-d) fluorescent images of b) positive control, c) PEO1, d) PEO 5 surface. 10x magnification.



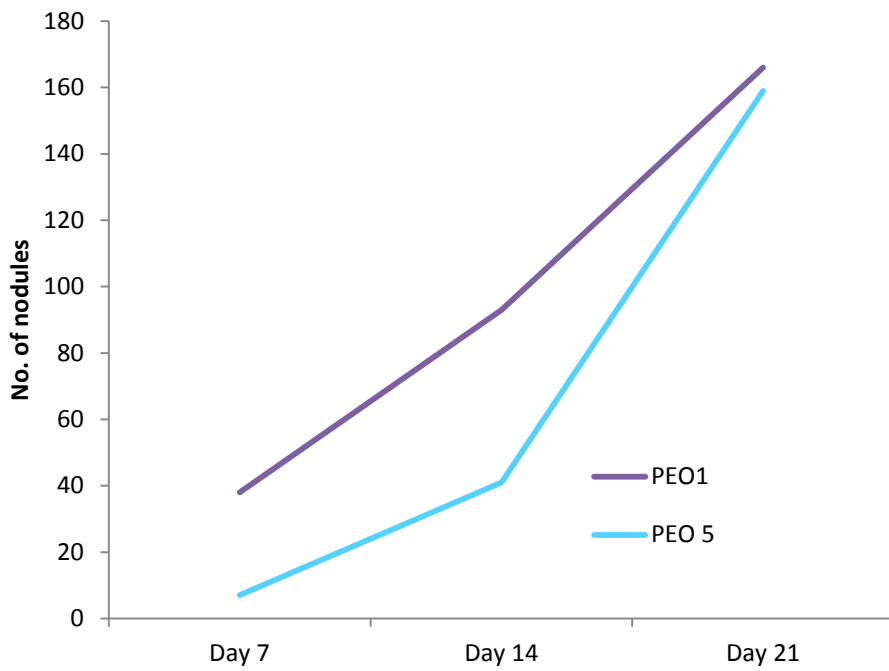


Fig. 3.23: Number of calcified nodules determined from XO images at day 7, 14 and 21.

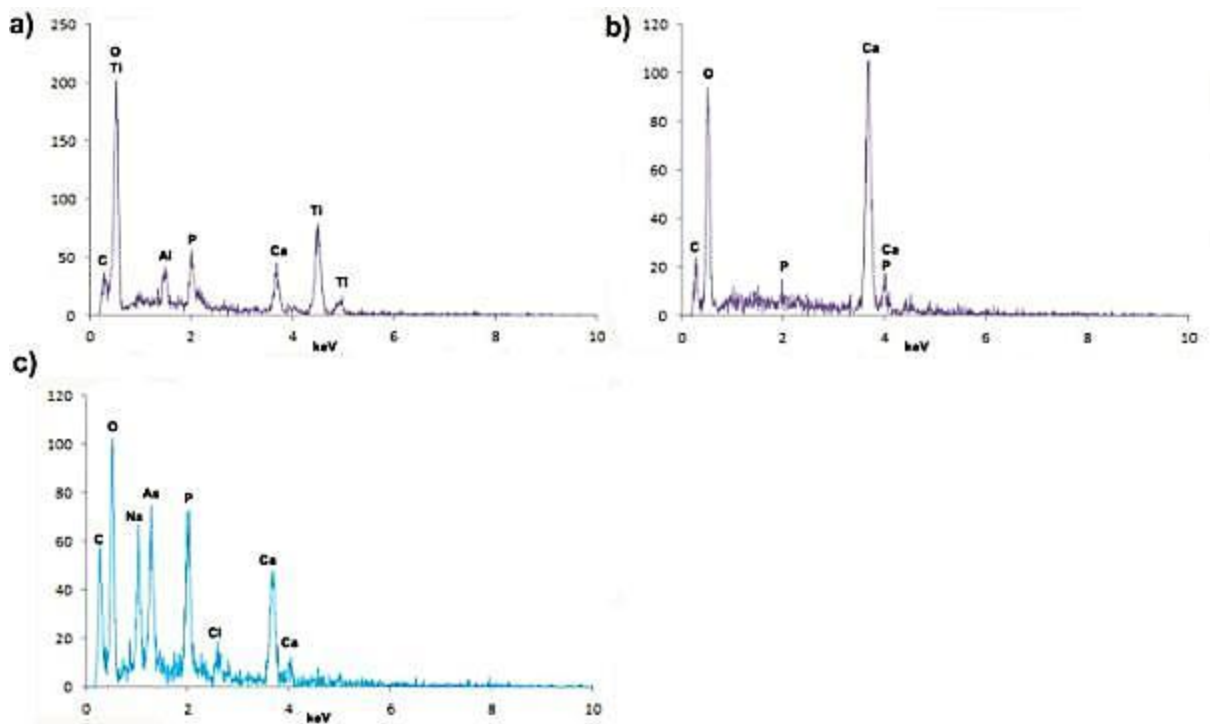
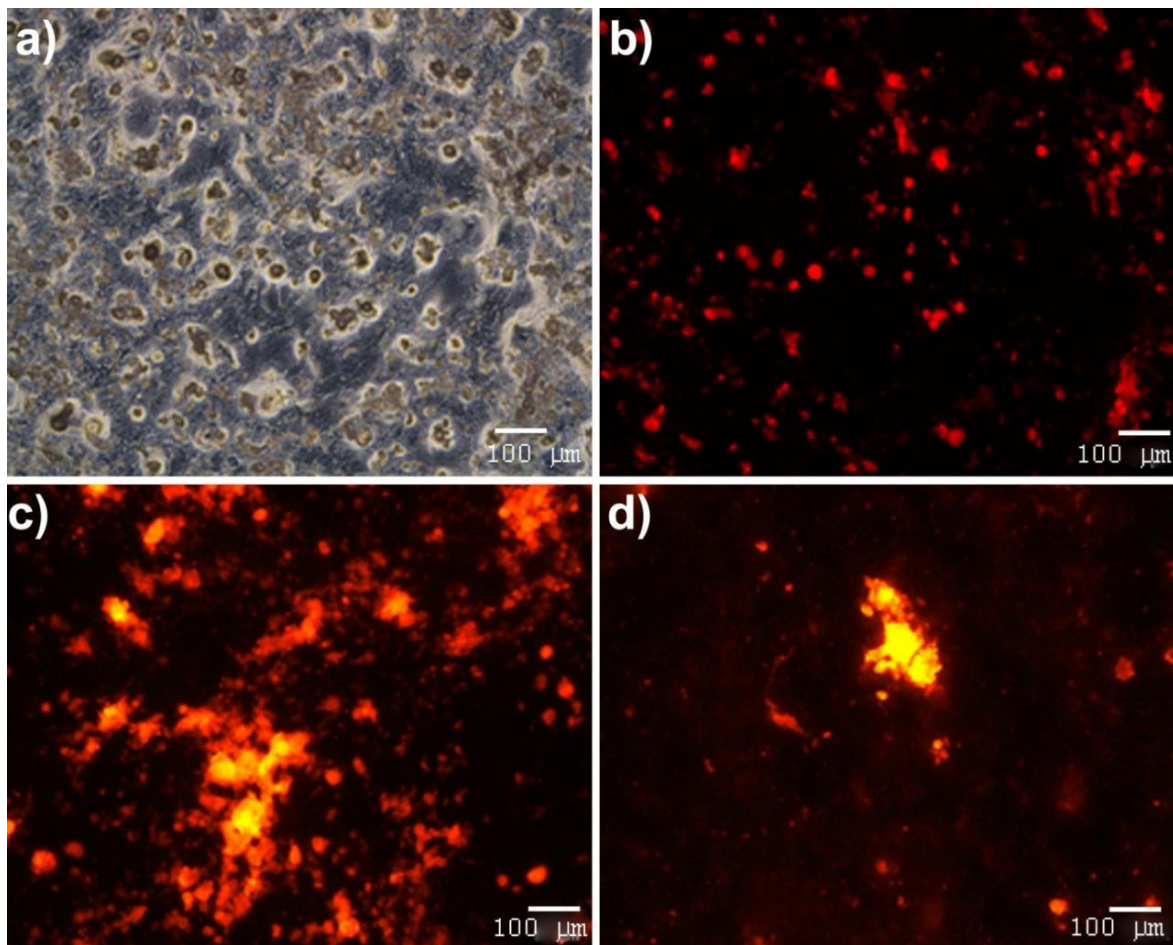


Fig. 3.24 EDS spectra after (a) 14 days of ECM on PEO1 and after 21 days (b-c) on PEO1 (b) and PEO5 (c).



**Fig. 3.25: Microscopic images of mineralisation by Xylenol Orange after 21 days of culturing. a) Positive control, brightfield image. b-d) fluorescent images of b) positive control, c) PEO1, d) PEO 5 surface. 10x magnification.**

Nevertheless, the enhanced mineralization rate observed after 14 days of incubation suggest a possible favorable effect of surface chemistry (i.e. higher Ca/P ratio) on mineralization. Further research is needed to delineate the effects of topography and chemistry of these PEO surfaces on the late cellular functions and to further understand the relationship between the earlier and later cellular response on a similar surface.

No results were found in literature on the effects of PEO oxide characteristics on matrix mineralization. Verrier et al. [28] compared hFOB1.19 and hBMSC cell response to three different titanium surfaces produced by vacuum plasma spraying, conventional anodizing and PEO (Ca/P electrolyte). Their findings showed enhanced mineralization on the PEO-treated surface after 10 and 15 incubation days, relative to the other two surfaces. However, the surfaces studied were very different and difficult to compare with regard to surface-induced effects. In addition, matrix mineralization was assessed by Alizarin Red staining, which in our previous trials showed interference from the calcium incorporated in the oxide layer during the PEO process.

### 3.3.5 Summary of the *in vitro* cellular response

In Table 3.5 the results of the *in vitro* SV-HFO response to the two oxidized surfaces are summarized.

Table 3-5: Summary of the *in vitro* response of SV-HFO cells to the oxidized surfaces

Cellular event	PEO1	PEO5
<b>Adhesion</b>	+	-
<b>Metabolic activity</b>	+ Similar growth rate	- Similar growth rate
<b>ECM synthesis</b>	+	- (delayed)
<b>ECM mineralization</b>	Larger and more uniform areas	Faster after 14 days and patchy

As can be observed both the early and late cellular responses have been influenced by the two surfaces. A schematic representation of the time-line of cellular events observed on the oxidized surfaces and the positive control is included in Fig. 3.26.

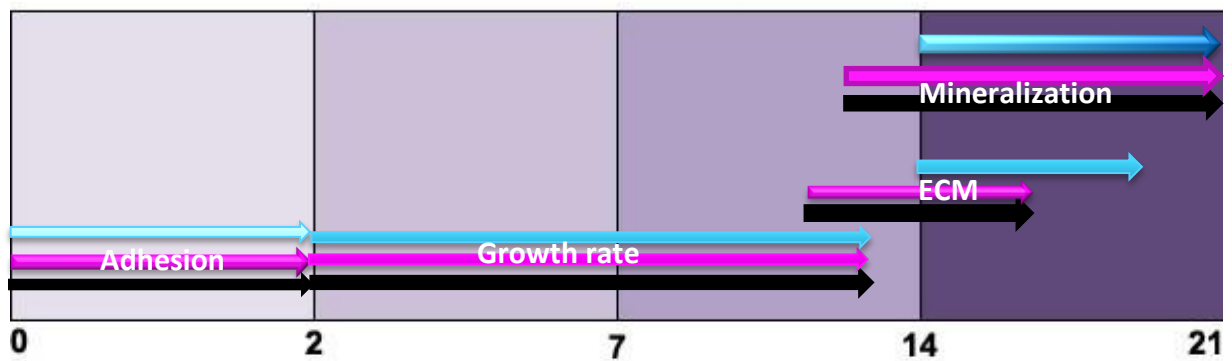


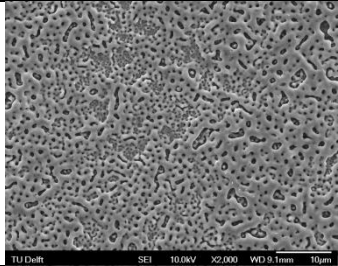
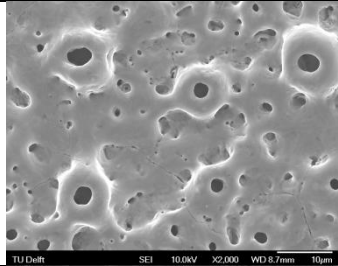
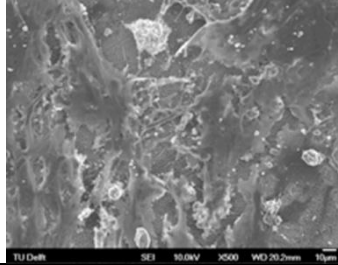
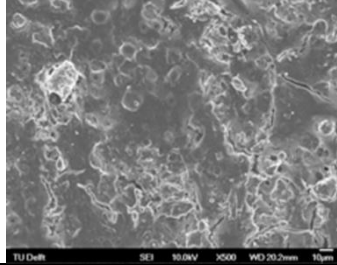
Fig. 3.26: Time-line of the SV-HFO cells response observed during the 21 incubation days on: PEO1 (pink), PEO5 (blue) surfaces and positive control (black).

The PEO1 surface follows more closely the PC, suggesting that this surface may be more beneficial in assisting surface-cell interactions leading to osteogenesis. It is believed that further studies on the effects of Ca/P on the investigated cellular functions will enable further tailoring of PEO1 surface characteristics for orthopedic implants.

## Chapter 4 Conclusions

In this study, the *in vitro* response of preosteoblast cells (SV-HFO) to Ti6Al7Nb alloy oxidized by plasma electrolytic oxidation (PEO) was systematically assessed. Two different surfaces have been generated by changing one process parameter, i.e. oxidation duration from 1 to 5 minutes. The cellular response, from adhesion to matrix mineralization was evaluated on both oxidized surfaces and on positive controls over a culture period of 21 days. A summary of the main findings of this study is included in Table 4.1.

**Table 4-1: Summary of the main surface characteristics and *in vitro* SV-HFO response to the oxidized surfaces**

Surface characteristic/ Cell response	PEO1	PEO5
<b>Average roughness</b>	0.19 ± 0.03 μm	1.43 ± 0.08 μm
<b>Maximum peak-to-valley height</b>	1.64 ± 0.27 μm	10.32 ± 0.80 μm
<b>Surface porosity</b>	14.5 %	4.0 %
<b>Pore density</b>	6.05 × 10 <sup>5</sup> pores/mm <sup>2</sup>	3.8 × 10 <sup>4</sup> pores/mm <sup>2</sup>
<b>Median pore size</b>	0.39 ± 0.07 μm	0.98 ± 0.05 μm
<b>Ca/P atomic ratio</b>	0.99	2.02
<b>Oxide phase composition</b>	Anatase & rutile	Anatase & more rutile
<b>Contact angle in water</b>	73.40 ± 6.43 °	61.77 ± 3.43°
<b>Surface Free energy</b>	37.34 ± 4.79 mJ/m <sup>2</sup>	41.82 ± 1.89 mJ/m <sup>2</sup>
<b>Morphology of the oxidized surfaces</b>		
<b>Adhesion of SV-HFO cells</b>	+	-
<b>Metabolic activity</b>	+ Similar growth rate	- Similar growth rate
<b>ECM synthesis</b>	+	- (delayed)
<b>ECM mineralization</b>	Larger and more uniform areas	Faster after 14 days and patchy
<b>Surface morphology after 21 days of incubation with SV-HFO cells</b>		

By extending the oxidation time from 1 to 5 minutes, the average surface roughness, maximum peak-to-valley height, pore size and Ca/P ratio of the oxide layers increased, while surface porosity and pore density decreased. Both surfaces (PEO1 and PEO5) had most of

the pores in the submicron range, a mixture of anatase and rutile oxide phases and their hydrophilicity improved relative to the non-oxidized surface.

During the adhesion phase (4-48 hours of incubation) SV-HFO cells preferred the smoother surface with finer pores and higher pore density. On this surface, the cells could attach and spread easily using the pores as anchorage sites for their protrusions and showing cell-cell contacts after 48 hours. The high pores protruding from the surface of the PEO5 surface acted as obstacles for cells adhesion. These findings highlighted the, largely neglected, importance of detailed morphological investigation of the PEO surfaces with respect to cellular response and showed that average roughness is not sufficient to understand the surface-cell interactions during the early adhesion phase.

Metabolic activity of the cells increased at similar rates on the two surfaces during 7 incubation days. SEM analyses showed that both PEO surfaces provided a suitable substrate for extracellular matrix formation. However, the cells on the PEO1 surface started matrix deposition earlier than those on the PEO5 surface suggesting that the surface-induced effects during adhesion and growth of the cells on this surface may have influenced subsequent matrix formation. After 21 days of incubation, net-like structures well integrated with the porous surface were visible on the PEO1 surface.

After 21 days of incubation mineralization of the matrix was evidenced on both PEO surfaces by XO staining and SEM/EDS analyses of the Ca-rich deposits. The presence of mineralized areas indicates that the surfaces assisted osteogenic differentiation of the cells which is beneficial for osseointegration. Nevertheless, the findings revealed larger and more uniform mineralized areas on the PEO1 surface at each time point, whereas an accelerated matrix mineralization above 14 incubation days and a more patchy appearance were observed on the PEO5 surface.

The PEO surfaces generated on the Ti6Al7Nb alloy under the conditions used in this study provided positive guidance for SV-HFO cells enabling them to fulfil their function from adhesion to matrix synthesis and mineralization. Nevertheless, the observed surface-induced effects indicated that PEO1 surface may be more beneficial for early osteogenesis. Follow-up studies on the effects of Ca/P incorporated in the PEO oxides on cellular functions may help in further tailoring the characteristics of this surface for this application.

## Chapter 5 Recommendations and future research

The interactions at the bio-implant interface are highly complex and difficult to control. Therefore, systematic research is needed to identify and understand the role of implant surface features in the cascade of biological events. This study evidenced that changes in the characteristics of oxide layers formed on Ti6Al7Nb alloy by plasma electrolytic oxidation may influence the early and late responses of preosteoblast cells.

Further research is required to delineate the effects of surface topography and chemistry on the observed responses. This would involve investigation of Ca and P release from the PEO surfaces during incubation and the effects of released species on cellular functions. Preliminary experiments indicated that calcium is released in the culture medium over the entire incubation period and in slightly larger concentrations from the PEO5 surfaces (23 vs. 26 mM). The experiments should be continued in the presence of cells and the results corroborated with the topography-induced effects.

Collagen staining by Sirius Red proved not to be suitable for these surfaces as staining of the negative controls (no cells) was observed indicating interference from the components of the oxide layers. Other staining methods or assays should be checked/developed. It is recommended to include negative controls in all staining procedures and assays in order to avoid possible interference from the oxide surfaces.

Follow-up molecular studies would help in unravelling and understanding the biological mechanisms involved in the observed surface-cell interactions. This would enable further tailoring of oxide surfaces to provide possible regulatory functions. Trial analyses of gene expression using qPCR indicated that the protocol has to be improved due to the very difficult harvesting of cells from the rough surfaces affecting the accuracy of the results especially at short incubation times.

The research should be extended to include other cell cultures such as mesenchymal stem cells and co-cultures in order to mimic more closely the peri-implant biological environment.

## Chapter 6 References

1. *Kunstheup deugt niet*. Available from: <http://www.rijlandorthopedie.nl/content.asp?id=143>.
2. Ratner, B.D., Schoen, F.J., Hoffman, A.S., Lemons, J.E., *Biomaterials science: an introduction to materials in medicine*. 3 ed. 2004: Academic Press.
3. Dos Santos, A., Lidizio, L.R., Santos da Cruz, T., De Sena, L.A., Damasceno, J.C., Achete, C.A., *Influence of Electrolyte Composition and Time Deposition on TiO<sub>2</sub> Films Produced by Micro-Arc Oxidation*. Key Engineering Materials, 2009. **396-398**: p. 349-352.
4. Barbosa, C., Do Nascimento, J.L., Caminha, I.M.V., Abud, I.C., *Premature failure in orthopedic implants: Analysis of three different cases*. Journal of Failure Analysis and Prevention, 2009. **9**(1): p. 67-73.
5. Geetha, M., Singh, A.K., Asokamani, R., Gogia, a.K., *Ti based biomaterials, the ultimate choice for orhopaedic implants - A review*. Progress in Materials Science, 2009. **54**(3): p. 29.
6. Ramalingam, M., Haidar, Z., Ramakrishna, S., Kobayashi, H., Haikel, Y., *Biomaterials in tissue engineering*. 2012: Wiley
7. Lavernia, C., D.J. Lee, and V.H. Hernandez, *The Increasing Financial Burden of Knee Revision Surgery in the United States*. Clinical Orthopaedics and Related Research, 2006. **446**: p. 221-226 10.1097/01.blo.0000214424.67453.9a.
8. Dorland, W.A., Dorland, D., *Dorland's Illustrated Medical Dictionary*. Vol. 29. 2010: Elsevier Health Sciences. 2087.
9. Li, L.H., Kong, Y.M., Kim, H.W., Kim, Y.W., Kim, H.E., Heo, S.J., Koak, J.Y., *Improved biological performance of Ti implants due to surface modification by micro-arc oxidation*. Biomaterials, 2004. **25**(14): p. 2867-2875.
10. Wang, Y., Wang, L., Zheng, H., Du, C., Chengyun Ning, Shi, Z., Xu, C., *Effect of frequency on the structure and cell response of Ca- and P-containing MAO films*. Applied Surface Science, 2010. **256**(7): p. 2018-2024.
11. Xie, L., Yin, G., Yan, D., Liao, X., Huang, Z., Yao, Y., Kang, Y., Liu, Y., *Structure, morphology and fibroblasts adhesion of surface-porous titanium via anodic oxidation*. Journal of Materials Science: Materials in Medicine, 2009. **21**(1): p. 259-266.
12. Wu, J., Liu, Z.M., Zhao, X.H., Gao, Y., Hu, J., Gao, B., *Improved biological performance of microarc-oxidized low-modulus Ti-24Nb-4Zr-7.9Sn alloy*. Journal of Biomedical Materials Research Part B: Applied Biomaterials, 2010. **92B**(2): p. 298-306.
13. Albrektsson, T., Johansson, C., *Osteoinduction, osteoconduction and osseointegration*. European Spine Journal, 2001. **10**: p. S96-S101.
14. Schlegel, P., Hayes, J.S., Frauchiger, V.M., Gasser, B., Wieling, R., Textor, M., Richards, R.G., *An in vivo evaluation of the biocompatibility of anodic plasma chemical (APC) treatment of titanium with calcium phosphate*. Journal of Biomedical Materials Research Part B: Applied Biomaterials, 2008. **90B**(1): p. 26-34.
15. Sul, Y.T., Johansson, C.B., Röser, K., Albrektsson, T., *Qualitative and quantitative observations of bone tissue reactions to anodised implants*. Biomaterials, 2002. **23**(8): p. 1809-1817.
16. Sul, Y.T., Johansson, C.B., Petronis, S., Krozer, A., Jeong, Y., Wennerberg, A., Albrektsson, T., *Characterization of the surface oxides on turned and electrochemically oxidized pure titanium implants up to dielectric breakdown: the oxide thickness, micropore configurations, surface roughness, crystal structure and chemical composition*. Biomaterials, 2002. **23**(2): p. 491-501.
17. Park, K.H., Heo, S.J., Koak, J.Y., Kim, S.K., Lee, J.B., Kim, S.H., Lim, Y.J., *Osseointegration of anodized titanium implants under different current voltages: a rabbit study*. Journal of Oral Rehabilitation, 2007. **34**(7): p. 517-527.
18. Matykina, E., Montfort, F., Berkani, A., Skeldon, P., Thompson, G.E., Gough, J., *Characterization of Spark-Anodized Titanium for Biomedical Applications*. Journal of The Electrochemical Society, 2007. **154**(6): p. C279-C285.

19. Zhu, X., *Effects of topography and composition of titanium surface oxides on osteoblast responses*. *Biomaterials*, 2004. **25**(18): p. 4087-4103.
20. Le Guehennec, L., Soueidan, A., Layrolle, P., Amouriq, Y., *Surface treatments of titanium dental implants for rapid osseointegration*. *Dental Materials*, 2007. **23**: p. 11.
21. Barrère, F., Mahmood, T.A., de Groot, K., van Blitterswijk, C.A. , *Advanced biomaterials for skeletal tissue regeneration: Instructive and smart functions*. *Materials Science and Engineering R*, 2008. **59**(1-6): p. 38-71.
22. Jungner, M., Lundqvist, P., Lundgren, S., *Oxidized titanium implants (Nobel Biocare TiUnite) compared with turned titanium implants (Nobel Biocare mark III) with respect to implant failure in a group of consecutive patients treated with early functional loading and two-stage protocols*. *Clinical Oral Implants Research*, 2005. **16**(3): p. 308-312.
23. Necula, B.S., Fratila-Apachitei, L.E., Zaat, S.A.J., Apachitei, I., Duszczyk, J., *In vitro antibacterial activity of porous TiO<sub>2</sub>-Ag composite layers against methicilin-resistant Staphylococcus Aureus*. *Acta Biomaterialia*, 2009. **5**(9): p. 3573-3580.
24. Matschegewski, C., Staehlke, S., Loeffler, R., Lange, R., Chai, F., Kern, D.P., Beck, U., Nebe, B.J., *Cell architecture–cell function dependencies on titanium arrays with regular geometry*. *Biomaterials*, 2010. **31**(22): p. 5729-5740.
25. Le Guehennec, L., Lopez-Heredia, M.-A., Enkel, B., Weiss, P., Amouriq, Y., Layrolle, P., *Osteoblastic cell behaviour on different titanium implant surfaces*. *Acta Biomaterialia*, 2008. **4**(3): p. 535-543.
26. Takebe, J., Ito, S., Champagne, C. M., Cooper, L. F., Ishibashi, K., *Anodic oxidation and hydrothermal treatment of commercially pure titanium surfaces increases expression of bone morphogenetic protein-2 in the adherent macrophage cell line J774A.1*. *Journal of Biomedical Materials Research Part A*, 2007. **80A**(3): p. 711-718.
27. Whiteside, P., Matykina, E., Gough, J.E., Skeldon, P., Thompson, G.E., *In vitro evaluation of cell proliferation and collagen synthesis on titanium following plasma electrolytic oxidation*. *Journal of Biomedical Materials Research Part A*, 2010. **94A**(1): p. 38-46.
28. Verrier, S., Peroglio, M., Voisard, C., Lechmann, B., Alini, M., *The osteogenic differentiation of human osteoprogenitor cells on Anodic-Plasma-Chemical treated Ti6Al7Nb*. *Biomaterials*, 2011. **32**(3): p. 672-680.
29. Seriwatanachai, D., Krishnamra, N., Van Leeuwen, J.P.T.M., *Evidence for direct effects of prolactin on human osteoblasts: inhibition of cell growth and mineralization*. *Journal of Cellular Biochemistry*, 2009. **107**(4): p. 677-685.
30. Semlitsch, M., Staub, F., Weber, H., *Titanium-Aluminium-Nionium alloy, development for biocompatible, high strength surgical implants*. *Biomed Technik*, 1985. **30**: p. 5.
31. Zhu, X., Kim, K.H., Jeong, Y., *Anodic oxide films containing Ca and P of titanium biomaterial*. *Biomaterials*, 2001. **22**: p. 2199-2206.
32. *Surtronic3+ Manual*.
33. Eijken, H.J.M., *Human osteoblast differentiation and bone formation: growth factors, hormones and regulatory networks*. 2007, Erasmus University: Rotterdam. p. 157.
34. Teh, T.H., Berkani, A., Mato, S., Skeldon, P., Thompson, G.E., Habazaki, H., Shimizu, K., *Initial stages of plasma electrolytic oxidation of titanium*. *Corrosion Science*, 2003. **45**: p. 2752-2768.
35. Matykina, E., Arrabal, R., Skeldon, P., Thompson, G.E., *Transmission electron microscopy of coatings formed by plasma electrolytic oxidation of titanium*. *Acta Biomaterialia*, 2009. **5**(4): p. 1356-1366.
36. Ishizawa, H., Fujino, M., Ogino, M., *Mechanical and histological investigation of hydrothermally treated und untreated anodic titanium oxide films containing Ca and P*. *Journal of Biomedical Materials Research*, 1995. **29**(11): p. 1459-1468.
37. Göransson, A., Arvidsson, A., Currie, F., Franke-Stenport, V., Kjellin, P., Mustafa, K., Sul, Y. T., Wennerberg, A., *An in vitro comparison of possibly bioactive titanium implant surfaces*. *Journal of Biomedical Materials Research Part A*, 2009. **88A**(4): p. 1037-1047.



38. Wei, D., Zhou, Y., Yang, C., *Structure, cell response and biomimetic apatite induction of gradient TiO<sub>2</sub>-based/nano-scale hydrophilic amorphous titanium oxide containing Ca composite coatings before and after crystallization*. Colloids and Surfaces B: Biointerfaces, 2009. **74**(1): p. 230-237.
39. Takebe, J., Itoh, S., Okada, J., Ishibashi, K. , *Anodic oxidation and hydrothermal treatment of titanium results in a surface that causes increased attachment and altered cytoskeletal morphology of rat bone marrow stromal cells in vitro*. Journal of Biomedical Materials Research 2000. **51**(3): p. 398-407.
40. Weirauch, D.F., Strong, R.L., Wallace, R.M., Chandra D., *An evaluation of the sessile drop technique for the study of (Hg, Cd)Te surfaces*. Semicond. Sci. Technol., 1993. **8**: p. 916-922.
41. Bico, J., Thiele, U., Quéré, D., *Wetting of textured surfaces*. Colloids and Surfaces A: Physicochemical and Engineering Aspects, 2002. **206**: p. 41-46.
42. Anselme, K., *Osteoblast adhesion on biomaterials (review)*. Biomaterials, 2000. **21**(7): p. 667-681.
43. Das, K., Bose, S., Bandyopadhyay, A., *Surface modifications and cell-materials interactions with anodized Ti*. Acta Biomaterialia, 2007. **3**(4): p. 573-585.
44. Nayab, S.N., Jones, F.H, Olsen, I., *Effects of calcium ion implantation on human bone cell interaction with titanium*. Biomaterials, 2005. **26**: p. 4717-4727.
45. Linez-Bataillon, P., Monchau, F., Bigerelle, M., Hildebrand, H.F., *In vitro MCT3 osteoblast adhesion with respect to surface roughness of Ti6Al4V substrates*. Biomoleculair Engineering, 2002. **19**: p. 133-141.
46. Zhao, L., Wei, Y., Li, J., Han, Y., Ye, R., Zhang Y., *Initial osteoblast functions on Ti-5Zr-3Sn-5Mo-15Nb titanium alloy surfaces modified by microarc oxidation*. Journal of Biomedical Materials Research Part A, 2010**92A**(2): p. 432-440.
47. Rahn, B.A., Perren, S.M, *Xylenol orange, a fluorochrome useful in polychrome sequential labeling*. Stain Technology, 1971. **46**(3): p. 125-130.
48. Morra, M., Cassinelli, C., Cascardo, G., Mazzucco, L., Borzini, P., Fini, M., Giavaresi, G., Giardino, R., *Collagen I-coated titanium surfaces: Mesenchymal cell adhesion and in vivo evaluation in trabecular bone implants*. Journal of Biomedical Materials Research Part A, 2006. **78A**(3): p. 449-458.

The SEM image on the front of the report shows the SV-HFO cells after 1 day of incubation on the PEO5 surface.

## Appendix 1: Additional calculations

### 6.1 Surface roughness

Roughness for 1 min PEO				Roughness for 5 min PEO			
Sample	Ra in $\mu\text{m}$	Ry in $\mu\text{m}$	Sm in $\mu\text{m}$	Sample, mea	Ra in $\mu\text{m}$	Ry in $\mu\text{m}$	Sm in $\mu\text{m}$
1,1	0,16	1,5	34	1,1	1,4	9,7	40
1,2	0,18	1,4	36	1,2	1,44	10,2	38
1,3	0,18	1,4	41	1,3	1,46	9,8	39
1,4	0,18	2,2	42	1,4	1,44	10,8	42
1,5	0,18	1,5	47	1,5	1,5	10	40
1,6	0,2	2	45	1,6	1,48	11,1	37
1,7	0,2	1,8	42	1,7	1,42	10,7	37
1,8	0,2	1,7	36	1,8	1,42	10,6	39
1,9	0,2	1,6	35	1,9	1,38	10,1	35
1:10	0,18	1,4	40	1:10	1,51	11,2	39
2,1	0,18	1,4	36	2,1	1,42	9,5	38
2,2	0,2	1,8	44	2,2	1,36	9,1	35
2,3	0,18	1,6	41	2,3	1,32	10,7	37
2,4	0,16	1,7	40	2,4	1,4	9,4	40
2,5	0,18	1,6	37	2,5	1,32	9,7	36
2,6	0,18	2,4	38	2,6	1,32	8,6	35
2,7	0,26	1,5	40	2,7	1,36	9	39
2,8	0,18	1,7	39	2,8	1,52	10,5	42
2,9	0,3	1,4	38	2,9	1,52	11,2	38
2:10	0,18	1,4	40	2:10	1,52	10,2	41
3,1	0,18	1,4	47	3,1	1,42	10,2	37
3,2	0,18	1,6	47	3,2	1,36	10,1	36
3,3	0,18	1,7	43	3,3	1,54	10,6	42
3,4	0,18	1,4	47	3,4	1,3	9,8	34
3,5	0,18	1,4	43	3,5	1,52	11,4	38
3,6	0,2	1,6	41	3,6	1,32	10,3	35
3,7	0,18	1,5	37	3,7	1,48	12,2	39
3,8	0,18	2,2	50	3,8	1,42	11	41
3,9	0,18	1,7	50	3,9	1,38	10,4	37
3:10	0,18	1,4	38	3:10	1,58	11,5	40

Average for 1 min PEO surface			
	Ra in $\mu\text{m}$	Ry in $\mu\text{m}$	Sm in $\mu\text{m}$
Average	0,1893333	1,63	41,13333
St.dev.	0,0271564	0,266717	4,423552

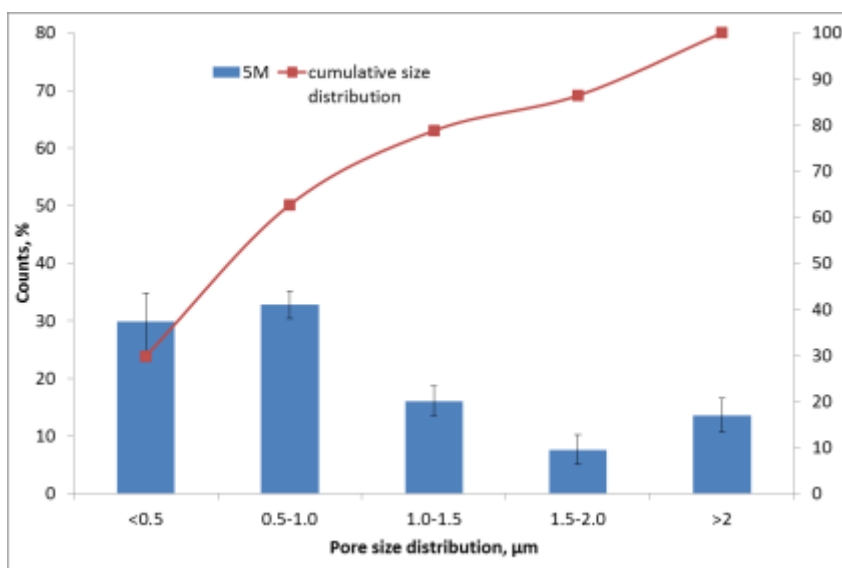
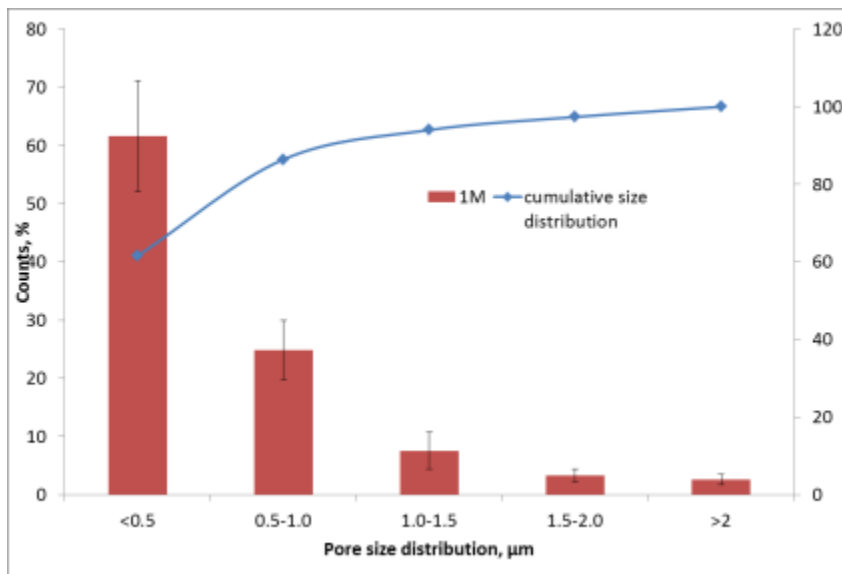
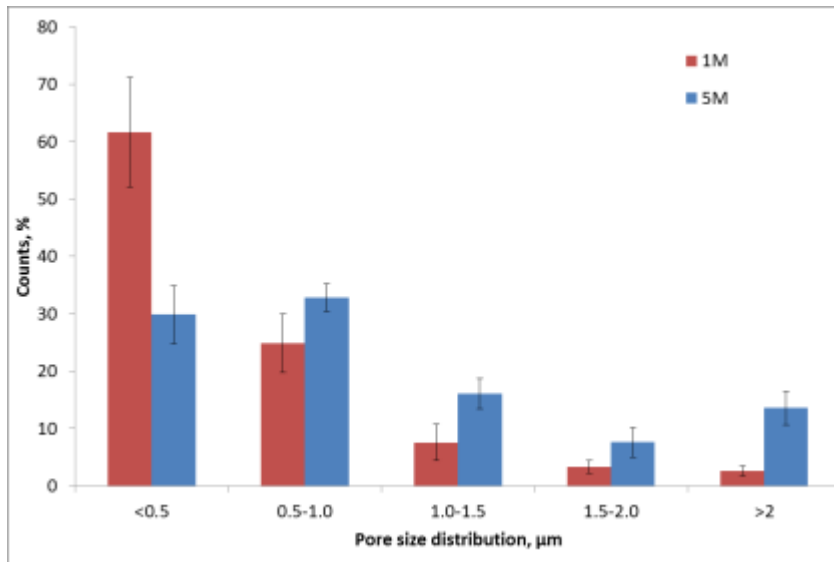
Average for 5 min PEO surface			
	Ra in $\mu\text{m}$	Ry in $\mu\text{m}$	Sm in $\mu\text{m}$
Average	1,427667	10,32	38,2
St.dev.	0,076909	0,802754	2,280351

T-test		T-test		T-test	
Ra	5 min	Ry	5 min	Sm	5 min
1 min	2,933E-36	1 min	1,148E-30	1 min	4,002E-03

#### Conclusion:

There is a significant difference in Ra, Ry and Sm values obtained from the two different surfaces.





### 6.3 Surface chemistry

Chemical composition for 1 min PEO									
Element	C	O	Al	P	Ca	Ti	Nb	Ca:P	
sample1	7,79	64,91	2,11	2,7	2,24	19,76	0,49	0,82962963	
sample1	11,33	46,4	2,18	4,37	4,92	29,83	0,97	1,125858124	
sample1	9	60,2	2,4	3,17	1,95	22,57	0,71	0,615141956	
sample 1	9,85	52,4	2,5	4,02	3,43	27,13	0,68	0,853233831	
sample 1	9,54	58,96	2,04	2,34	4,18	22,95		1,786324786	
sample 1	8,88	59,37	2,26	3,37	2,67	22,84	0,61	0,792284866	
sample2	7,38	63,28	2,08	3,37	3,36	19,91	0,62	0,997032641	
sample2	7,62	62,26	2,28	2,81	2,39	22,07	0,47	0,850533808	
sample2	6,47	66,46	1,78	3,05	3	18,5	0,74	0,983606557	
sample2	8,35	53,56	2,11	4,28	5,07	25,93	0,7	1,184579439	
sample2	9,83	57,77	2,09	3,64	4,2	21,78	0,69	1,153846154	
sample2	11,16	59,42	2,09	3,11	2,48	21,11	0,62	0,797427653	
sample3	14,52	48,73	2,38	1,95	2,43	29,98		1,246153846	
sample3	13,25	54,21	2,08	3,79	4,29	21,68	0,71	1,131926121	
sample3	13,16	62,25	1,99	1,64	1,95	19,01		1,18902439	
sample3	16,89	55,59	2,36	2,89	2,08	19,7	0,47	0,719723183	
sample3	14,36	52,75	2,63	3,21	2,34	24,22	0,49	0,728971963	
sample3	13,68	61,47	1,19	2,6	2,18	17,49	0,78	0,838461538	

Chemical composition for 5 min PEO									
Element	C	O	Al	P	Ca	Ti	Nb	Ca:P	
sample1	11,8	51,91	1,92	4,44	9,91	19,45	0,58	2,231981982	
sample1	14,35	43,37	1,92	4,33	7,99	27,24	0,8	1,845265589	
sample1	9,78	58,86	1,91	2,96	5,98	19,8	0,71	2,02027027	
sample 1	16,18	42,34	2,06	4,23	8,1	26,34	0,74	1,914893617	
sample 1	11,38	48,76	1,74	5,76	12,28	19,51	0,58	2,131944444	
sample 1	10,28	61,6	1,7	3,36	7,33	15,28	0,45	2,181547619	
sample2	11,34	51,75	1,57	5,15	11,5	18,14	0,54	2,233009709	
sample2	10,44	49,53	1,89	4,8	10,69	21,39	0,71	2,227083333	
sample2	10,3	52,26	2,14	3,62	8,2	22,67	0,83	2,26519337	
sample2	12,05	48,79	1,93	4,54	10,52	21,55	0,63	2,317180617	
sample2	10,73	60,74	1,83	2,73	6,28	17,14	0,55	2,3003663	
sample2	10,8	50,74	1,79	5,47	10,88	19,75	0,57	1,989031079	
sample3	8,99	58,48	2,32	3,31	4,6	21,49	0,79	1,389728097	
sample3	17,38	28,94	2,38	5,24	12,04	33,19	0,83	2,297709924	
sample3	9,87	56,66	1,81	4,11	8,08	18,91	0,57	1,96593674	
sample3	10,43	60,47	1,6	3,87	6,75	16,28	0,59	1,744186047	
sample3	11,1	53,56	2,02	4,31	6,56	21,78	0,67	1,522041763	
sample3	10,22	56,08	1,84	4,43	7,96	18,87	0,59	1,796839729	

Average for PEO surfaces									
	C	O	Al	P	Ca	Ti	Nb	Ca:P	
1 min	10,726	57,777	2,142	3,128	3,064	22,581	0,650	0,990	
St.dev	2,968	5,550	0,312	0,741	1,044	3,636	0,136	0,275	
5 min	11,523	51,936	1,909	4,259	8,647	21,043	0,652	2,021	
St.dev	2,236	8,038	0,217	0,848	2,270	4,303	0,112	0,276	

Statistics									
Element	C	O	Al	P	Ca	Ti	Nb	Ca:P	
p-value	0,184408	0,00796	0,00697	7,687E-05	2,25E-11	0,127419	0,484744	2,79991E-13	

**Conclusion:**  
 There is a significant difference in the atomic percentage of O, Al, P and Ca and in the Ca:P ratio.

## 6.4 Surface wettability and surface free energy

Contact angle										
	water 1	water 2	water 3	diido 1	diido 2	diido 3	SFE	dispersive	polar	
1 min 1	100,2	101,7	83,6	78,1	79,5	79,9	20,78	17,92	2,85	
1 min 2	84,8	77,7	83,5	67,9	65,1	65,1	30,52	25,11	5,41	
1 min 3	77	78,3	78	76	88	87,5	27,78	15,56	12,31	
	water 1	water 2	water 3	diido 1	diido 2	diido 3	SFE	dispersive	polar	
5 min 1	80,6	85,9	75,7	64,3	79,4	76,8	31,44	21,16	10,28	
5 min 2	74,2	76,3	73,7	73	79,9	72,7	31,48	20	11,48	
5 min 3	82,8	71,8	78,9	69,5	71,7	64,6	31,56	23,64	7,92	
Average for surfaces										
	water	diidometha	SFE	dispersive	polar					
1 min	84,978	76,344	26,360	19,530	6,857					
St.dev	9,522	8,734	5,023	4,974	4,893					
5 min	77,767	72,433	31,493	21,600	9,893					
St.dev	4,638	5,705	0,061	1,859	1,811					
<b>t-test</b>			<b>t-test</b>			<b>t-test</b>				
water angle	5 min		diido angle	5 min		SFE	5 min			
1 min	0,02726		1 min	0,36564		1 min	0,216705			
<b>t-test</b>			<b>t-test</b>							
dispersive	5 min		polar	5 min						
1 min	0,644817		1 min	0,501497						

## 6.5 Metabolic activity day 1 and day 2

Proliferation in time using fluorescence:									
Fluorescence: average of triplicates									
Day 1					Day 2				
Sample	PC	1 min	5 min	NC	Sample	PC	1 min	5 min	NC
Run 1	160432	144184	133255	12170	Run 1	237577	201702	151308	10319
	160599	144913	129768	11996		238341	202954	150904	10418
	162630	143314	132934	12092		236010	202051	150774	10144
	162021	139436	110327			224646	216422	141325	
	156801	139079	108885			221420	235157	138911	
	158652	139684	108768			220087	212601	140092	
	163584	152596	12042			230038	200256	155848	
	163218	153919	12071			229251	197083	155707	
	162383	152650	11978			236234	199962	154597	
Run 2	85585	48277	28895	9268	Run 2	140786	86443	95361	
	93905	43075	28363	9411		137917	85092	93544	
	104774	45430	28035	8738		135306	83568	92652	
	103409	18937	77680	8476		139388	114375	23794	
	88868	19306	77386	9762		135242	112034	23444	
	92620	19675	80117	10622		136085	111246	23399	
	91308	26338	12471	10775		139622	9330	10295	
	86121	25962	12581	10277		138079	9165	10148	
	80704	26272	12788	9876		137877	9186	10102	
Run 3	143129	129145	114586	9568	Run 3	166197	147880	134958	9116
	141924	129675	119178	9531		159916	145854	131148	9562
	142044	128011	108683	9677		160126	146218	129388	9311
	144828	126105	110502	9679		158268	141958	125885	9874
	140701	124322	109269	9609		155721	134024	120675	9894
	141154	125070	109600	9746		155847	134436	119094	9829
	138754	139191	103438	9497		155540	154018	106828	9838
	137234	138540	103386	9350		161865	143783	109606	9956
	136612	137830	102866	10910		154657	146321	107510	9835
Average	150928	138204	113696	10049	Average	194541	175704	134698	9841
Stdev	10790	9535	10355	1032	Stdev	37307	34112	16937	376

## 6.6 Metabolic activity day 5 and day 7

Day 5					Day 7				
Sample	PC	1 min	5 min	NC	Sample	PC	1 min	5 min	NC
Run 1	315846	311506	205654	9526	Run 1	415456	398828	293426	11417
	318189	304127	203058	9266		412990	397171	293826	11509
	316914	304885	202014	9034		412868	395608	291773	11436
	308313	310041	218931	9542		410848	385774	316082	11169
	305202	306237	222415	9846		419327	382857	309080	11215
	304850	310195	218604	9900		403994	380263	310730	11259
	306096	289774	197454			418814	383440	307383	
	306614	284769	197714			410239	375919	308202	
	308317	283188	197933			410158	382733	306983	
Run 2	291477	179747	10291	12181	Run 2	360418	19245	10848	9755
	284767	173468	10237	12328		354288	19455	10808	9601
	283512	174779	10130	12128		374896	19776	11257	9557
	289272	54576	14645			352615	27126	38289	
	280704	52578	14102			356284	27946	37690	
	277649	53091	14285			369489	28394	38897	
	312700	30172	37861			361083			
	306889	30006	37102			361216			
	301869	29224	36724			372000			
Run 3	337905	236681	191578	8947	Run 3	425225	298560	201534	14743
	334406	232185	189712	9005		412632	287655	194955	15008
	336402	231807	190127	9025		410960	289540	194145	15306
	322670	284933	247169	8901		404573	360286	271039	24383
	313611	279807	243209	8906		404617	357113	269706	30167
	313573	285562	268089	8779		399496	358767	269751	21892
	325361	297139	278521	8882		431459	358931	284141	29589
	323548	295015	275684	8860		431427	360936	282308	29873
	319364	293518	271010	8793		428463	365368	281177	29633
Average	309112	285632	223271	9147	Average	414641	362208	293040	17084
Stdev	16494	26005	32047	377	Stdev	9486	35147	16123	8054



## 6.7 ECM mineralization

Xylenol orange				Number of nodes and area covered									
After 7 days				After 14 days				After 21 days					
Surface	No. of noc	Area of noc	Area in %	Surface	No. of noc	Area of noc	Area in %	Surface	No. of noc	Area of nodes	Area in %		
1M1	68,00	4189,00	0,87	'1M1_1.j	133,00	12149,00	2,53	'1M1-1)	7,00	577,00			
1M2	27,00	2643,00	0,55	'1M1_2.j	81,00	4695,00	0,98	'1M1-2)	5,00	347,00	0,12		
1M3	45,00	3712,00	0,77	'1M1_3.j	45,00	3790,00	0,79	'1M1-3)	7,00	480,00	0,07		
1M4	32,00	3432,00	0,72	'1M1_4.j	66,00	5129,00	1,07	'1M1-4)	127,00	41690,00	0,10		
1M5	20,00	1066,00	0,22	'1M1_5.j	122,00	9761,00	2,03	'1M1-5)	10,00	595,00	8,69		
5M1	7,00	1084,00	0,23	'1M1_6.j	69,00	5707,00	1,19	'1M1-6)	258,00	356486,00	0,12		
5M2	6,00	868,00	0,18	'1M2_1.j	79,00	11471,00	2,39	'1M2-1)	420,00	113371,00	74,27		
5M3	6,00	491,00	0,10	'1M2_2.j	103,00	18980,00	3,95	'1M2-2)	197,00	24923,00	23,62		
5M4	8,00	1788,00	0,37	'1M2_3.j	125,00	23263,00	4,85	'1M2-3)	411,00	41936,00	5,19		
5M5	7,00	728,00	0,15	'1M2_4.j	110,00	11413,00	2,38	'1M2-4)	403,00	144561,00	8,74		
				'1M2_5.j	73,00	13259,00	2,76	'1M2-5)	312,00	89774,00	30,12		
				'1M2_6.j	115,00	13895,00	2,89	'1M2-6)	459,00	177561,00	18,70		
				'5M1_1.j	9,00	277,00	0,06	'5M1-1)	10,00	4683,00	36,99		
				'5M1_2.j	9,00	257,00	0,05	'5M1-2)	21,00	3263,00	0,98		
				'5M1_3.j	10,00	332,00	0,07	'5M1-3)	22,00	2086,00	0,68		
				'5M1_4.j	31,00	660,00	0,14	'5M1-4)	62,00	13124,00	0,43		
				'5M1_5.j	32,00	1964,00	0,41	'5M1-5)	15,00	908,00	2,73		
				'5M1_6.j	58,00	3031,00	0,63	'5M1-6)	38,00	5942,00	0,19		
				'5M2_1.j	22,00	860,00	0,18	'5M2-1)	194,00	17869,00	1,24		
				'5M2_2.j	18,00	461,00	0,10	'5M2-2)	424,00	154783,00	3,72		
				'5M2_3.j	14,00	1315,00	0,27	'5M2-3)	672,00	97715,00	32,25		
				'5M2_4.j	71,00	12652,00	2,64	'5M2-4)	170,00	32385,00	20,36		
				'5M2_5.j	78,00	12868,00	2,68	'5M2-5)	126,00	28499,00	6,75		
				'5M2_6.j	149,00	23529,00	4,90	'5M2_6)	154,00	26755,00	5,94		
				'5M3_1.j	9,00	1013,00	0,21						5,57
				'5M3_2.j	99,00	8392,00	1,75						
				'5M3_3.j	20,00	2761,00	0,58						
				'5M3_5.j	42,00	4880,00	1,02						
				'5M3_6.j	21,00	2309,00	0,48						

Day7	nodes
1 min	38,40
5 min	6,80

Day14	nodes
1 min	93,42
5 min	40,71

Day21	nodes
1 min	218,00
5 min	159,00